NOISE GENERATION IN THE GAS WIPING PROCESS

NOISE GENERATION IN THE GAS WIPING PROCESS

By

David Arthurs, B. Eng.

A Thesis

Submitted to the School of Graduate Studies

In Partial Fulfillment of the Requirements

for the Degree

Master of Applied Science

McMaster University

MASTER OF APPLIED SCIENCE (Mechanical Engineering)

McMaster University Hamilton, Ontario

TITLE: Noise Generation in the Gas Wiping Process

AUTHOR: David Arthurs, B. Eng. (McMaster University)

SUPERVISOR: Dr. Samir Ziada

NUMBER OF PAGES: xviii, 148

ABSTRACT

This thesis investigates the characteristics of noise generation in the gas wiping process, including the effects of the various parameters manipulated in the process and countermeasures used to reduce noise levels. The process of gas wiping is used in many industrial applications such as drying of pulp and paper, photograph production and some high performance cooling applications. One of the most important industrial applications of gas wiping is the production of hot-dipped galvanized sheet steel. Gas wiping is a very efficient and reliable process to control coating thickness and uniformity of galvanized steel products, and can be used for very high line speeds and production rates. Changing the various process parameters such as the jet to strip distance (z), the jet slot width (h), plenum pressure (P) and jet inclination angle (α) allows manufacturers to control the coating thickness and quality of the finished product.

The gas wiping process is also responsible for the generation of very high levels of noise, which can be a factor in limiting the overall production rates and indirectly increase production costs for manufacturers. To maintain a constant coating thickness as the line speed and production rate is increased, the plenum pressure supplied to the jets and thus the incident jet velocity must be increased, or the jet-to-strip distance must be decreased. Noise production in the gas wiping process is acknowledged to be proportional to the incident jet velocity and inversely proportional to the jet-to-strip distance. Thus, for a given coating thickness, as the production rates increase, the noise generated by the process must also increase. Ergonomic restrictions in the workplace,

which limit the exposure to high sound pressure levels and audible acoustic tones, may indirectly limit the maximum line speed for a steel sheet with a given coating thickness. This limitation is particularly relevant to the production of high quality automotive sheet steels, which often have very thin coating thicknesses and have higher than normal coating uniformity tolerances, which necessitate the use of high plenum pressures and small jet-to-strip distances.

At present, the state of knowledge for noise generation in the gas wiping process is very limited. Only two previous investigations have been devoted to this problem, and the experiments for these studies have only modeled specific individual cases, with no attempt at a comprehensive modeling of noise in this process. For the current study, measurements have been performed in both an actual manufacturing environment and on a scaled galvanizing simulator in a laboratory environment. A comprehensive set of experiments over a wide range of gas wiping parameters was performed in order to provide a broad overview of noise generation in the gas wiping process and allow for process optimization to reduce noise and allow higher production rates and efficiency. The creation of noise maps, modeling the overall sound pressure level and tone intensity for gas wiping as function of the various operating parameters of the process, as well as a set of equations and models to determine the frequency of discrete acoustic tones are presented. A full analysis of the frequency response, as well as the acoustic modes generated in various jet impingement regions has also been provided.

ACKNOWLEDGEMENTS

I would like to thank Dr. Samir Ziada for his invaluable advice and encouragement throughout my studies at McMaster. I would also like to thank my parents, John and Barbara Arthurs for their love and support.

I would also like to express my gratitude to Dr. Hrymak, Dr. McDermid and Dr. Ching for their advice and assistance with my research, as well as Dave Schick, Ron Lodewyks, Jimmy McLaren, Joe Verhaeghe and Mark MacKenzie for their assistance with the technical aspects of my work.

Finally, I would like to acknowledge the generous support of NSERC and McMaster University, as well as ILZRO for funding the research and the participating manufacturers for access to their facilities.

Most importantly, I would like to thank Clare O'Connor for her continued love, support and encouragement throughout my studies.

NOMENCLATURE

C	Power fit constant
D	Microphone distance from impingement point [m]
D_{EB}	Edge Baffle distance [mm]
D_j	Jet-jet impingement region length [mm]
f	Acoustic frequency [Hz]
f_j	Primary jet-jet mode frequency
f_{j2}, f_{j3}	Secondary jet-jet stage mode frequencies
f_p	Jet-sheet/jet plate mode frequencies
h	Jet slot width [mm]
k	Exponent constant for frequency fit
L_j	Jet length [mm]
M	Mach number
P	Plenum pressure [psi or (Bar)]
P_{ref}	Acoustic reference pressure (20 μPa)
P_{rms}	RMS acoustic pressure [Pa]
Re	Reynolds number
SPL	Sound pressure level [dB, P_{ref} = 20 μPa]
St	Strouhal number
t	Sheet thickness [mm]
TI	Acoustic tone intensity [dB]
V	Jet velocity [m/s]
V_i	Isentropic jet velocity [m/s]
V_s	Sheet velocity [m/s]
w	Steel sheet width [m]
W_c	Coating weight [g/m^2]
We	Weber number
z	Impingement distance [mm]
α & β	Jet inclination angle of Jet #1 and Jet #2 respectively [degrees]
γ	Jet-shifting angle ($\gamma = \alpha - \beta$).

δ_c	Coating thickness [μm]
Δy	Jet offset [mm]
θ	Microphone measurement angle (from horizontal) [degrees]
ρ_g	Density of working gas [kg/m^3]

TABLE OF CONTENTS

LIST OF FIGURES

LIST OF TABLES

Chapter 1 – INTRODUCTION

1.1 – MOTIVATION

The objective of the study is to identify, understand and characterize the noise sources mechanisms of noise generation within the gas wiping process and thereby provide producers and manufacturers with additional tools to manage and reduce noise in the gas wiping process. Much of the current knowledge of noise generated in this process at a manufacturing level consists of qualitative rules and observations; there is currently very little quantitative knowledge of the noise behavior of this process. No formal attempt has been made to quantify the noise characteristics as a function of the various process parameters, and there are currently no rules or guidelines available to manufacturers to minimize noise and its impact on production efficiency. There is clear need to perform noise measurements over a wide range of typical operating parameters for the process in order to understand and quantify the trends of noise generated by gas wiping, and to develop rules and guidelines for manufacturers to reduce the impact of noise in gas wiping.

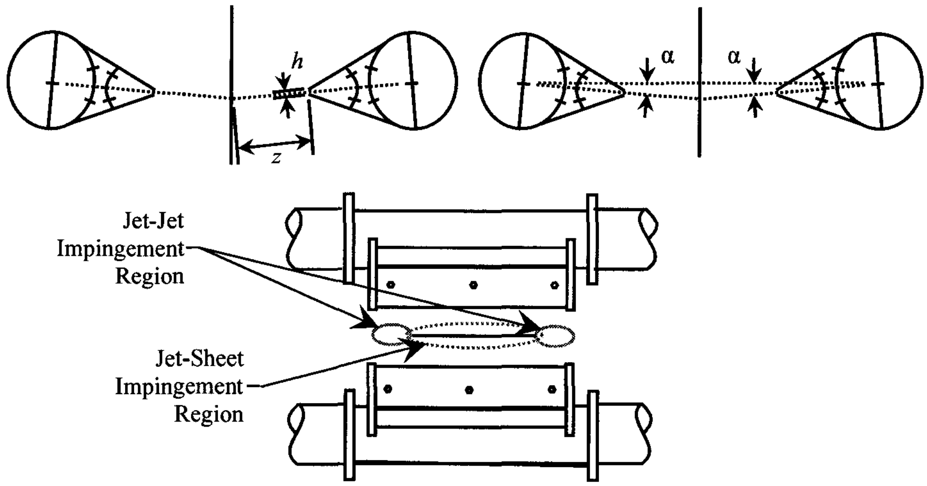

Figure 1-1: Basic schematic showing jet impingement length *z*, jet slot width *h*, and jet inclination angle *α* as well as the jet-jet and jet-sheet impingement regions.

The basic physical layout of the gas wiping process as well as the fundamental process parameters and the two impingement regions are shown in Figure 1-1. The two opposing jets impinge symmetrically on the steel sheet being drawn between them with at a jet-to-strip impingement distance z, and a jet slot width of h. The jets are generally inclined a small amount downwards towards the approaching sheet, typically at jet inclination angles between α = 1° and 12°. The two resulting impingement regions: the jet-jet and jet-sheet regions are shown in the bottom portion of Figure 1-1. Figure 1-2 shows various countermeasures frequently used to reduce noise levels associated with the gas wiping process including edge baffles, jet-shifting and vertical jet offset configurations. Edge baffles generally consist of rigid flat plates inserted into the jet-jet impingement region to eliminate the collision of the two opposing jets and noise associated with this region. Jet-shifting and vertical jet offset are both forms of jet-incidence asymmetry which are also used to reduce noise levels. Jet-shifting uses a difference in jet inclination angle between the two jets, while vertical jet offset uses a vertical shift in the overall jet position of one jet with respect to the other. Both geometries are used to introduce asymmetric impingement lengths for each of the two jets.

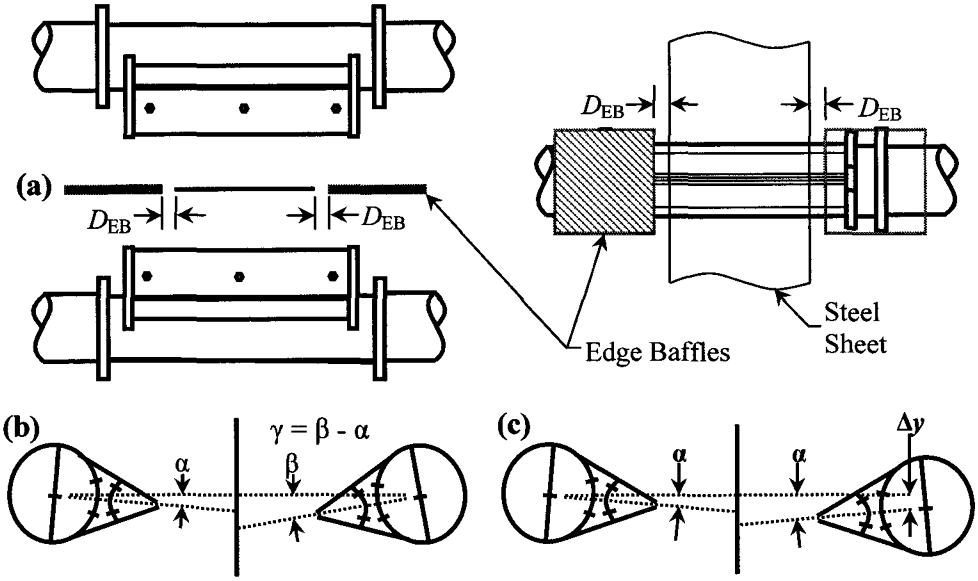

Figure 1-2: Basic schematic of various countermeasures employed to reduce noise intensity including edge baffles (a), jet-shifting (b) and vertical jet offset (c) configurations.

1.2 – Objectives

The objective of this thesis is to characterize the noise generated by the gas wiping process for a frequently utilized range of process parameters. A commonly used baseline gas wiping configuration was chosen with the input of several steel manufacturers, and a test program was developed to investigate the effect of various parameters such as plenum pressure (P), the dimensionless jet impingement ratio (z/h), and jet inclination angle (α) on the overall sound pressure level, tone intensity and spectral content of the noise. In addition, the effect of some conventional countermeasures has been investigated including edge baffles, and two types of jet incidence asymmetry: jet-shifting and vertical jet offset. A complete list of the objectives of the study is outlined in the following:

1. Characterize the nature of the noise, including any transient effects of frequency and amplitude of discrete acoustic tones.
2. Develop noise maps to illustrate the behavior of the noise generated by the baseline gas wiping configuration.
3. Characterize the different acoustic tones generated by the two different impingement regions of the baseline gas wiping configuration.
    a. Develop models to predict the frequency of acoustic tones based on process parameters.
    b. Identifying process configurations at risk of developing significant acoustic tones.
4. Using the baseline configuration as a starting point, examine the effect of jet inclination angle on the acoustic response of the gas wiping process.
5. Determine the effect of edge baffles as a passive countermeasure on the noise production of the process. The effect of edge baffle distance (D_{EB}), impingement ratio (z/h) and plenum pressures (P) has been investigated.
6. Examine the effect of jet incidence asymmetry on noise production of gas wiping, including:
    a. Vertical jet offset (Δy) – Offsetting one jet vertically with respect to the other jet.

   b. Jet-shifting (γ) – Introducing a different inclination angle for each of the two jets.

7. Develop strategies for process optimization to minimize the production of noise for a given process output.

1.3 – Thesis Layout

The layout of this thesis consists of 8 chapters and 2 appendices. Chapter 1 contains the introduction to the work, including the motivation and objectives of the study. Chapter 2 provides the reader with background information and details of the industrial process as well as a brief literature review of the noise in the gas wiping process, as well as other related subject matter. Chapter 3 contains details of the experimental apparatus, equipment used for the measurement of its performance, and a brief description of the testing methods and procedures utilized for all measurements. Chapter 4 presents and compares results of measurements performed on an industrial galvanizing line and on a scaled galvanizing simulator, validation of the in-lab galvanizing simulator, and noise and equipment characterization measurements and analysis. Chapter 5 presents the acoustic response of the baseline configuration, while Chapter 6 examines the acoustic response of jet-plate impingement, and the effect of plate inclination on the formation of acoustic tones. Chapter 7 examines the effect of changing the jet inclination angle as well as the effect of jet incidence asymmetry. Finally, Chapter 8 includes guidelines for process optimization, as well as discussion, conclusions and suggestions for future work.

Appendix A contains technical information regarding the various equipment and materials used in the course of this study. Appendix B contains miscellaneous measurements and results referred to in the text.

Chapter 2 - PROCESS DESCRIPTION AND LITERATURE REVIEW

2.1 – BASIC PROCESS DESCRIPTION AND OUTPUTS

The process of gas wiping is used in the production of galvanized sheet steels to maintain Zinc coatings of a desired thickness and uniformity. The production of these sheet steels occurs on continuous steel mills, where the sheet at its finished thickness and width is fed into a molten Zinc bath and withdrawn vertically. The sheet is then drawn through a pair of opposing planar gas wiping jets or air knives, which impinge on the sheet and entrained molten Zinc coating, and act to control the coating thickness and uniformity on the strip. The combined action of gravity, and the stagnation pressure and shear stress profiles of the impinging jets strip away excess molten Zinc, causing it to run back into the molten Zinc bath. The finished coating then solidifies as it advances down the line past the wiping jets, eventually proceeding to annealing (where applicable) and coiling. The gas jets utilize either compressed air or Nitrogen as the working fluid and in most cases, the jets are aligned such that they impinge symmetrically at the same position on either side of the steel strip in an aligned jet configuration. However, in some cases a small amount of misalignment may be intentionally introduced. Figure 2-1 shows a basic schematic of the gas wiping process, showing approximate positions of the strip, Zinc pot and wiping jets.

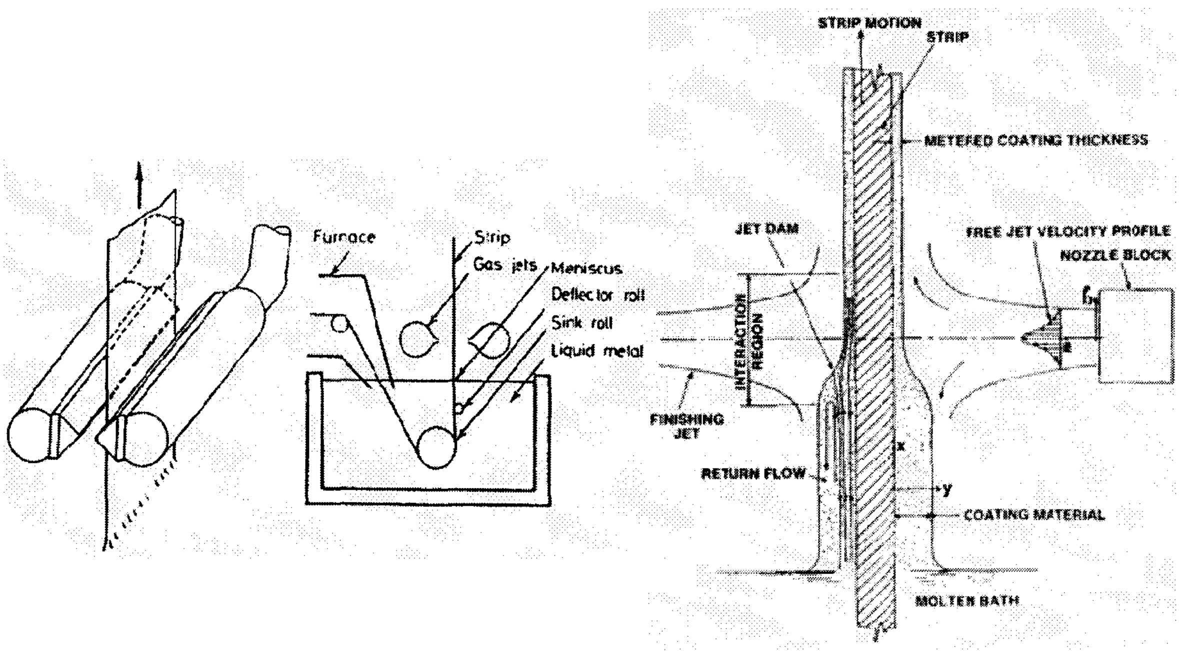

Figure 2-1: Schematic of the gas wiping process showing the relative location of the wiping jets, steel sheet, and Zinc bath. (Ellen & Tu, 1984, Left, Thornton & Graff, 1976, Right)

The main parameters which are manipulated to control the thickness and quality of the coating are the impingement distance (z), the jet slot width (h), and the plenum pressure (P). The impingement distance is often referred to in its dimensionless form, the impingement ratio (z/h), which is simply the impingement distance, z, non-dimensionalized by the jet slot width, h. The main outputs of the process are the coating thickness (δ) and the speed at which the sheet is drawn through the air knives, the sheet speed, V_S. In general, if a manufacturer wishes to decrease the coating thickness, either the plenum pressure must be increased, the impingement ratio must be decreased, or some combination of the two. If a manufacturer wishes to maintain the same coating weight, but increase the sheet speed, the plenum pressure must be increased or the impingement ratio must be decreased. Many researchers have formulated coating weight models using experimental, empirical and numerical techniques to predict coating weight thickness based on the various input parameters of the process. A brief summary of the work in this area is given in section 2.3 of this thesis. A brief description of each of the gas wiping parameters, and their effect on the process, is given in the sections below.

2.2 - PROCESS PARAMETERS

2.2.1 – PLENUM PRESSURE

Plenum pressure, P, is varied by manufacturers in the gas wiping process to modulate the resultant coating thickness. Increasing the plenum pressure results in an increase in incident gas jet velocity, V_i, which in turn leads to larger stagnation pressures and larger shear stresses acting on the surface of the molten Zinc coating. The increased pressures and shear stresses act to strip away more molten Zinc as the sheet is fed through the air knives, and a decrease in the resultant thickness is realized. The plenum pressure supplied to the jets typically varies between P = 1.0 and 6.0 psi (0.07 Bar $\leq P \leq$ 0.41 Bar) for gas wiping process. In some specialized applications, the pressures can be much higher, with as high as 40.0 psi (2.72 Bar) reported in some cases. In the steel making industry, plenum pressures are almost universally reported in pounds per square inch (psi), whereas many other process parameters, such as coating weight and jet slot width are measured using metric units. In order to be consistent with industry conventions, plenum pressure will be reported in pounds per square inch (psi), and the equivalent pressure in Bar will also be provided in brackets. Furthermore, Table 7 on page 75 shows a complete list of all tested plenum pressures in psi, and the equivalent pressure in Bar.

2.2.2 – GAP PROFILES

The jet slot width and slot width profiles used in the gas wiping process vary considerably from manufacturer to manufacturer, with many different techniques developed to deal with problems arising in the gas wiping process. The most basic jet slot profile is a flat profile, where the jet slot width (h) is constant over the span of the jet (L_j), as shown in Figure 2-2. Edge overcoating, where coating thickness increases near the edge of the steel strip, is a persistent problem for manufacturers, and can result in significant difficulties during coiling of the sheet after the manufacturing process is complete. In addition, inadequate galvannealing near the strip edge may occur (Park, 2001). The phenomenon of edge overcoating is caused by surface tension effects near the edge of the strip and several different techniques, which can be utilized separately or together, have been developed to combat edge overcoating, including the use of bowtie jet slot profiles. Bowtie profiled air knives increase the jet slot width near the edge of the sheet, compared to the sheet center, to increase the momentum of the impinging flow in the area where edge overcoating typically occurs. The additional flow momentum results in excess molten Zinc being stripped from the sheet and results in a more uniform coating thickness. Figure 2-2 shows a basic schematic of edge overcoating and typical dimensions and profile of a bowtie air knife profile taken from an industrial site. The dimensions and design of the nozzle profile differ somewhat between facilities, but the basic shape of bowtie profiled air knives is relatively similar.

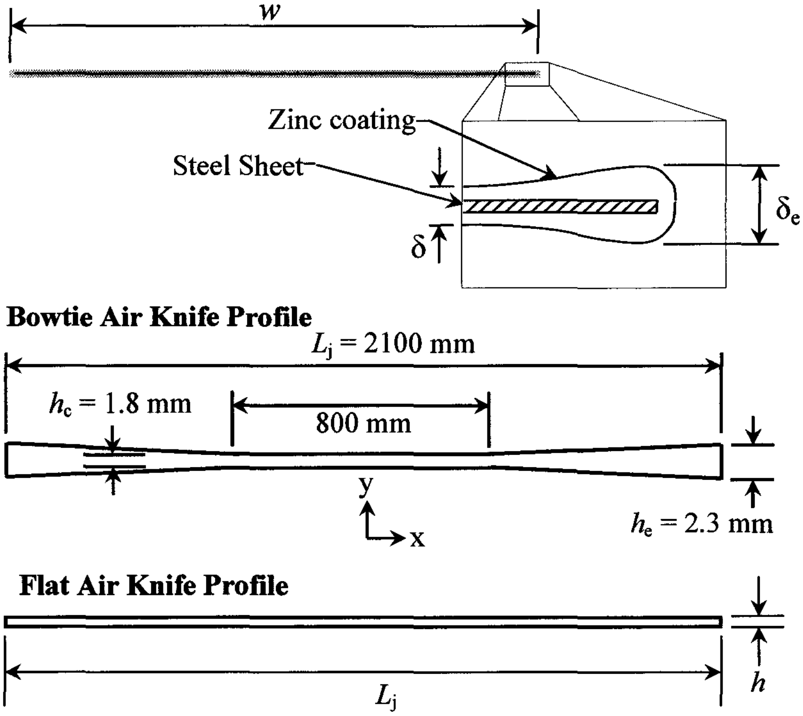

Figure 2-2: Basic schematic showing steel strip with edge overcoating and bowtie air knife profile.

2.2.3 – IMPINGEMENT RATIO

The dimensionless impingement ratio, z/h, is a ratio of the jet to strip distance, z, and jet slot width, h. Impingement ratios typically used in gas wiping range from $z/h \approx 5$ up to $z/h \approx 30$, and cover the range of the potential core, transition and fully developed regions of turbulent jet flow. For gas wiping jets with a constant jet slot width h, impingement ratios will be constant over the span of the jet, however, in jets with non-constant jet slot widths, such as in bowtie configurations, the impingement ratio will vary over the span of the jet. As impingement ratio of the incident jet is decreased, the coating thickness will also decrease, due to higher jet velocities and shear stresses at jet impingement on the coating surface.

2.2.4 – JET INCLINATION ANGLE

Another parameter which is manipulated by manufacturers in the gas wiping process is the jet inclination angle (α), which is measured in degrees downwards from the horizontal as shown in Figure 2-3. Typically, jet inclination angles used in the gas wiping process vary between $\alpha = 0°$ and $\alpha = 12°$, however in certain specialized cases, jet inclination angles of up to $\alpha = 30°$ have been used. For low inclination angles typically used in gas wiping, jet inclination does not have a significant impact on the stagnation pressure or surface shear stress profiles of the impinging jets, and thus does not significantly affect the coating thickness of the gas wiping process (Hrymak et al., 2004).

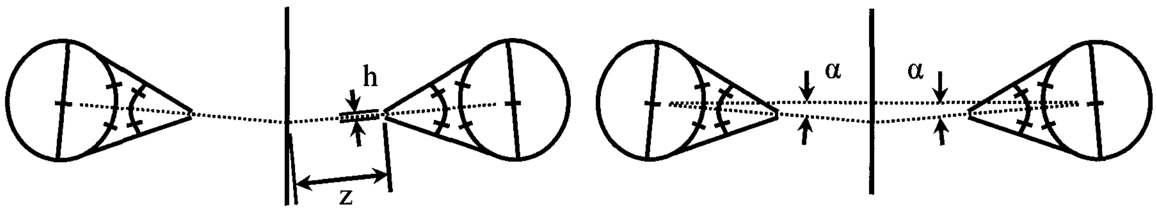

Figure 2-3: Basic schematic of the gas wiping process showing the impingement distance (*z*), the jet slot width (*h*) and the jet inclination angle (α).

The inclination angle of the jets is a critical parameter in determining the maximum line speed which can be obtained without the onset of coating splashing. Splashing is a phenomenon where droplets of liquid Zinc are ejected from the coating surface due to a liquid film instability induced by the impingement of the two gas wiping jets on the molten Zinc coating. Splashing is generally initiated at the strip edges at some critical sheet speed, and quickly spreads inwards to the sheet center. At the onset of this instability, the wiping efficiency decreases drastically, and the resultant coating thickness increases considerably. Splashing also results in inconsistent coating quality and can result in jet nozzle blockage and streaks in the finished coating, due to liquid droplets landing and solidifying on, the air-knife nozzle. Several different studies such as Dubois et al. (1995) and Dubois et al. (2004) have concluded that increasing the jet inclination angles from normal impingement $\alpha = 0°$ to $30°$ can delay the onset of splashing significantly and allow increases of the sheet speed of up to 20-30%, depending on the coating thickness and other wiping parameters. In practice, inclination angles of 30° are uncommon due to difficulties in the physical setup of such configurations; however the use of inclination angles in the range of 1-12° is much more widespread.

2.2.5– SHEET SPEED

The speed at which the continuous steel sheet is drawn through the air knives, or sheet speed (V_S), typically ranges between 50 m/min and 150 m/min (0.8 m/s $\leq V_S \leq 2.5$ m/s). Because higher sheet speeds mean higher rates of production and greater efficiency, manufacturers tend to produce a given steel product at the highest possible sheet speed to reduce production costs. As a manufacturer increases sheet speed, keeping all other parameters equal, the coating weight of the steel strip will increase. This is due to the pressure and shear stress fields of the impinging jets having less time to act on and strip away excess Zinc coating. Thus, as a manufacturer wishes to increase the sheet speed, a decrease in the impingement ratio or an increase in the plenum pressure supplied to the jets will be necessary, or some combination of the two.

2.2.6 – Edge Baffle Distance

Edge baffles, as shown in Figure 2-4, are frequently used by manufacturers to reduce noise levels in the gas wiping process. These baffles generally consist of rigid flat plates inserted into the jet-jet impingement region in order to prevent the collision of the opposing jets and interrupt the formation of any discrete acoustic tones. Edge baffles were originally designed to reduce edge overcoating by maintaining constant stagnation pressure and shear stress profiles on the surface of the molten zinc coating near the edge of the strip. The main parameter manipulated with edge baffles in the gas wiping process is the edge baffle distance (D_{EB}), the distance in mm from the edge of the coated steel strip to the edge baffle. It is generally recognized that the smaller the edge baffle distance, the lower the overall noise level and the level of any acoustic tones. However, manufacturers are often limited in the proximity of the baffles to the sheet by variance in the process such as wander of the sheet on the mill rolls, which may cause the baffles to contact the sheet, causing damage to the sheet and coating.

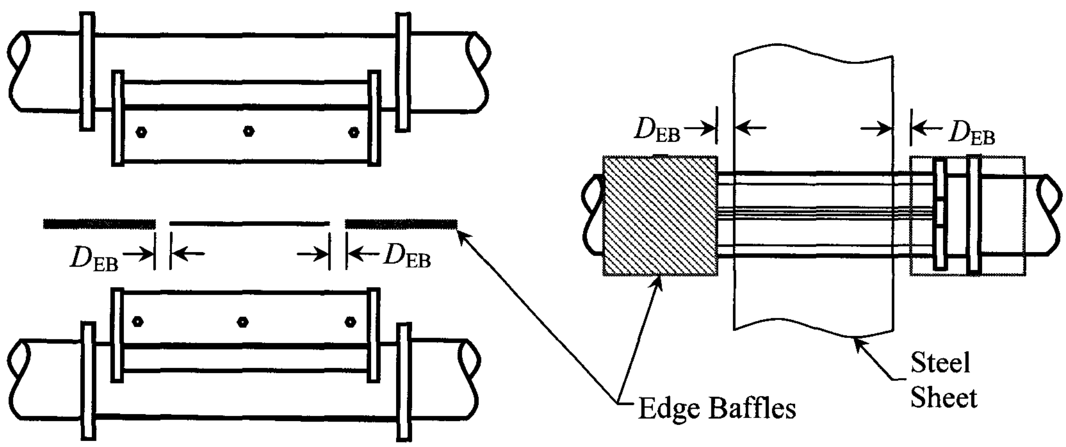

Figure 2-4: Simplified schematic of the gas wiping process with edge baffles, showing edge baffle distance, D_{EB}.

2.3 – Coating Weight Models

Numerous authors have undertaken theoretical, experimental, empirical and numerical approaches in order to develop models to predict the coating weight of the finished steel sheet as a function of the various process parameters. These models vary in complexity greatly, but all current models use a series of simplifying assumptions which ultimately limits their applicability to specific ranges of operating parameters. These models, by necessity, must capture the basic parameters of the process such as those listed above, however several models are quite complex, accounting for the surface quality of the steel sheet, sheet flatness and distortion, and non-uniform jet slot width profiles such as bowtie air knives. A brief description of some of the more common and frequently used coating weight models is summarized below.

Thornton & Graff (1976) developed a theoretical coating weight model which supplemented the gravitational body force on the coating with the imposed pressure profile of the impinging gas jet. Stagnation pressure profiles were determined experimentally, and the model was verified empirically for low sheet speeds ($V_s < 1$ m/s) and relatively high coating weights ($W_c < 300$ g/m^2). The model assumes fully self-similar velocity profiles for the jets, even at relatively close impingement ratios ($z/h < 8$), where the velocity profiles are not self similar. More importantly, this model neglected the effects of shear stress due to impinging gas stream at the surface of the molten Zinc coating. The studies of Ellen & Tu (1984) and Tu (1995), improved on the previous model by including shear stress effects at the coating surface, and as a result, the model offered significantly more accurate predictions of coating weight than previous models which neglected shear stress effects. This model, like the previous model by Thornton & Graff, utilized a self-similar velocity profile assumption, which resulted in poor predictions for relatively small impingement ratios inside the potential and transition regions of the plane jet.

The studies of Hrymak et al. (2002, 2004) utilized computational methods using the k-ε model in Fluent® to improve predictions for small impingement ratios by modeling the velocity, pressure and shear stresses directly, and the resulting model yielded very good predictions, typically within 8% of actual coating weight compared with industrial line data for low coating weights (W_c < 75 g/m^2). For higher coating weights, the model is less accurate in determining actual coating thickness, due in part to the model neglecting the inertial effects of the entrained molten coating, which becomes significant as the coating thickness increases. This coating model was also the first to model the effects of slot width profile, e.g. bowtie profiled air knives. It also incorporates a lumped heat transfer model with convective and radiation heat transfer effects. In addition, the model takes into account the effects of common types of sheet deformation such as gutter and cross bowing, and a full sensitivity analysis to optimize operating conditions for a targeted coating weight.

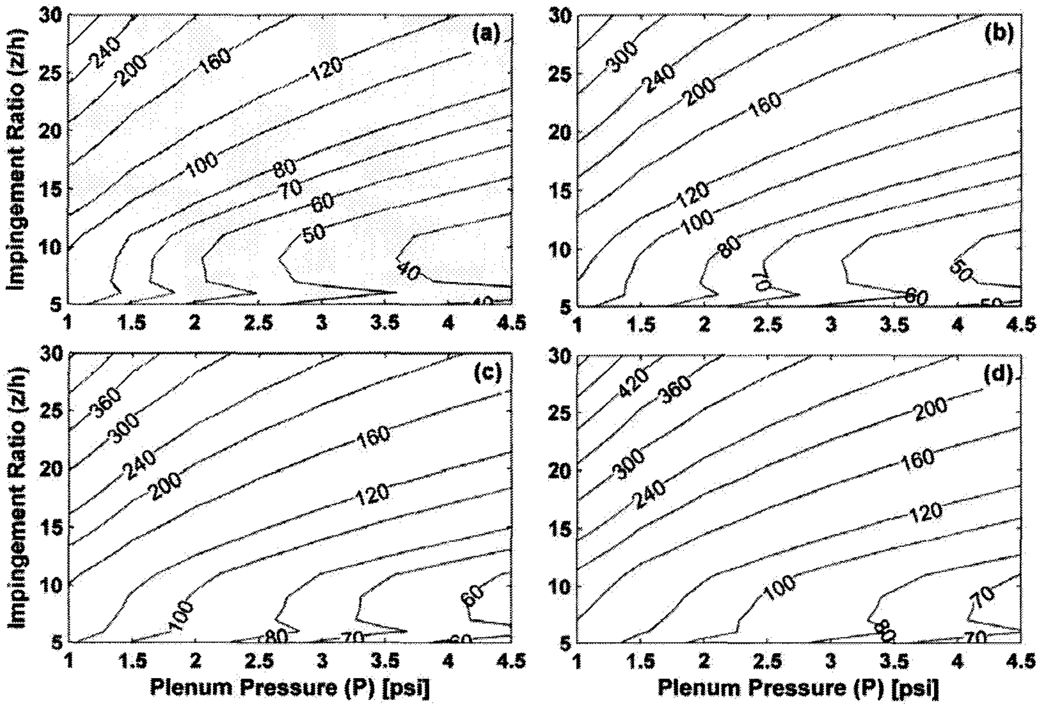

Figure 2-5: Coating weight model predictions for coating weight model of Hrymak et al. (2004) showing iso-coating weight lines in g/m^2 for line speeds of (a) 1 m/s, (b) 1.5m/s, (c) 2.0 m/s and (d) 2.5 m/s.

Figure 2-5 shows predictions of the Hrymak et al. (2004) model for varying line speeds between V_s = 1.0 m/s and 2.5 m/s for a range of plenum pressures from P = 1.0 psi (0.068 Bar) and 4.5 psi (0.306 Bar) and a range of impingement ratios from z/h = 5 up to 30. In later sections of this thesis dealing with process optimization and noise reduction of the gas wiping process, these coating weight models and isocoating maps will be explored further.

2.4 – Related Areas of Research

There are a multitude of other research topics associated with gas wiping such as strip vibration, parameters affecting sheet distortion and flatness, as well as work in designing new and innovative jet designs and control systems to control coating thickness and uniformity more accurately. Although the subject of gas wiping has been subject to intense research effort in the previously reviewed areas, the area of noise in the gas wiping process has been largely ignored. In the following section, previous studies on noise in gas wiping will be reviewed.

2.5 – Noise and the Gas Wiping Process

The gas-wiping process is, first and foremost, a process to control and regulate coating quality. The noise generated by this process is an undesired side effect of the impingement of the jets, however any techniques or configurations developed to reduce noise intensity must not adversely affect the coating quality or production rates. To date, only three separate studies have investigated noise in the gas wiping process, and of the three, only two focus significantly on noise, and only one study contains significant spectral analysis of the noise. As ergonomic restrictions pertaining to allowable noise levels in the workplace continue to be tightened, noise in the gas wiping process will continue to play an increasing role in the production efficiency of galvanized steel goods. As of July 1, 2007, Ontario lowered the allowable A-weighted sound pressure level from 90 dBA to 85 dBA and changed the exchange rate from 5 dBA to 3dBA. As a result, the maximum A-weighted sound pressure level that a worker can be exposed to for only 15 minutes fell from 115 dBA to 100 dBA. Only Quebec has not adopted the 85 dBA criterion level, and all but four provinces have implemented the more stringent 3 dBA exchange rate. Table 1 shows the allowable noise exposure levels for Ontario under both the pre-July 1st regulations with a 5 dBA exchange rate, and the new noise regulations with the 3 dBA exchange rate.

Table 1: Noise regulations implemented in the Ontario Health and Safety Act as of July 1st, 2007. (http://www.e-laws.gov.on.ca/html/source/regs/english/2006/elaws_src_regs_ R06565_e.htm)

Maximum Exposure	*Old OHSA Regulations (Pre-July 1st, 2007)*	*New OHSA Regulations (July 1st, 2007 onward)*
8 hrs.	90 dBA	85 dBA
4 hrs.	95 dBA	88 dBA
2 hrs.	100 dBA	91 dBA
1 hr.	105 dBA	94 dBA
30 min.	110 dBA	97 dBA
15 min.	115 dBA	100 dBA

Thornton & Graff (1976) reported that changing the working gas used in gas wiping from superheated steam to compressed air lowered the overall A-weighted sound pressure levels by 5dBA, and commented that over 90% of the product line produced at the production facility where the study was conducted could now be finished at 90 dBA or less. However, the line speeds were considered quite low by modern standards ($V_s <$ 1m/s) and the coating weights were also relatively high ($W_c <$ 300 g/m^2). In addition, no specific measurements of noise and associated gas wiping configurations were given in the study. Increasing line speeds and decreasing coating weights would certainly result in much greater noise production.

A subsequent study performed by Park (2001) focused more heavily on noise production in gas wiping, with a variety of noise measurements performed for specific gas wiping configurations. No frequency spectra of the noise are provided, nor did the author comment on the qualitative nature of the noise or indicate whether any audible discrete tones were present. The study did however utilize narrow band frequency spectra measurements and the author did provide the "main noise frequency" in Hz, and a main noise level of the dominant acoustic tone is also provided. The measurements of this study were performed on an actual industrial continuous galvanizing line, with measurements being performed at three separate microphone locations. Table 2 shows the results of the noise measurements for this study.

Table 2: Results of noise study of Park (2001), showing the overall SPL's and main noise frequencies.[1]

	3·9 m front centre			1·5 m front centre			1·5 m front edge		
	Total noise level, dBA	Main noise level, dBA	Main noise frequency, Hz	Total noise level, dBA	Main noise level, dBA	Main noise frequency, Hz	Total noise level, dBA	Main noise level, dBA	Main noise frequency, Hz
Variation with strip width, mm: without edge baffles, nozzle to nozzle distance 25 mm, wiping angle 80°, nozzle air pressure 24·5 kPa									
900	108·4	95·1	1550	116·1	101·7	1450	115·8	101·7	1550
1200	105·6	94·4	1440	112·8	97·7	1510	113·0	100·1	1610
Variation with nozzle angle (front, rear): without edge baffles, nozzle to nozzle distance 30 mm, strip width 900 mm, nozzle air pressure 25·0 kPa									
85°, 85°	105·3	88·7	1390	114·1	98·3	1340	...	...	...
80°, 80°	107·1	92·1	1205	113·9	97·5	1226	...	...	...
70°, 70°	106·4	88·3	2000	114·6	98·3	1985	...	...	...
70°, 80°	93·6	73·2	827	100·8	84·9	422	...	...	...
80°, 70°	92·2	75·4	165	99·2	79·2	188	...	...	...
80°, 75°	98·2	87·8	969	104·0	88·3	970	...	...	...
As function of nozzle air pressure, kPa: without edge baffles, nozzle to nozzle distance 30 mm, strip width 900 mm, wiping angle 80°									
15	102·9	89·1	970	109·3	95·9	1060	...	...	...
20	104·9	92·5	1085	112·1	101·2	1085	...	...	...
25	106·8	93·6	1205	114·3	98·7	1200	...	...	...
30	109·8	95·7	1320	116·0	101·2	1320	...	...	...
Effect of edge baffles: nozzle to nozzle distance 20 mm, wiping angle 80°, nozzle air pressure 25 kPa, baffle to strip distance 20 mm									
No baffles	106·7	92·5	2036	116·9	103·7	1930	114·4	99·1	2007
Baffles	98·0	83·9	2090	106·1	91·3	1920	106·0	92·3	2040

From his measurements, the author concluded that the majority of the noise generated in the gas wiping process was produced at the strip edges, in the region of jet-jet impingement, and attributed the noise production in this area to increased turbulence due to the impingement of the opposing jets. This conclusion was reached by altering the

[1] Inclination angle in this study is defined as the angle between the sheet and the incident jet, not relative to the horizontal as in other studies. In this case an inclination angle of 90° would represent normal jet impingement.

width of the steel sheet from w = 900 mm to 1200 mm, thus changing the jet-jet impingement length, D_j. The increase in jet-jet impingement length resulted in a significant increase of 3.5 dBA in sound pressure level. In addition, the study also confirmed the effect of incident jet velocity on the amplitude of the overall sound pressure level and the frequency and sound pressure level of discrete tones.

The effect of jet inclination angle was investigated for angles between 5° and 15°, and it was found that altering the inclination angle of the two jets resulted in relatively little change in the overall sound pressure level and the sound pressure level of acoustic tones, although increasing inclination angles did have a significant effect on the frequency of such tones. Furthermore, the author also investigated the effect of introducing jet incidence asymmetry through a technique known as jet-shifting, as a means to combat the formation of discrete acoustic tones and lower overall sound pressure levels. Jet-shifting involves changing the inclination angle of one jet with respect to the other, in order to create asymmetry in jet impingement. The author found that such techniques were very effective in suppressing acoustic tones, but commented that "... this is not practicable in production". Finally, the author investigates the effect of edge baffles for a single gas wiping configuration and a single edge baffle distance, and observed 8.7 dBA and 8.6 dBA reductions in overall and peak sound pressure levels respectively.

The measurements performed by Park are quite useful in evaluating many of the basic trends and behaviors of noise within the gas wiping process. However, a more comprehensive investigation is required in order to be able to aid manufacturers and process engineers obtain meaningful reductions in noise for this process. Dubois (2001a, 2001b) performed a more comprehensive set of measurements in his two part study, and was able to characterize some aspects of the spectral behavior of noise in gas wiping. Dubois' reports were presented at the annual Galvanizers Association Meeting held in 2001, and the documents are an internal report generated for ILZRO (International Lead Zinc Research Organization) and its members. The study is composed of measurements performed in both a laboratory environment, as well as in a production environment, with more measurements being performed over a greater range than the work of Park (2001). The measurements performed in this study include examining the effects of plenum pressure (P) impingement ratio (z/h), inclination angle (α), and the effects of edge baffles and edge baffle distance (D_{EB}). Edge baffles are a point of particular focus for this study, especially their effects in combination with other parameters, such as jet inclination angle (α). The study also investigates the effects of jet-shifting and other forms of jet-incidence asymmetry. Furthermore, the study presents a thorough analysis of the spectral content of all measurements, focusing on the frequency response of the various modes and acoustic tones generated during gas wiping. Schlieren photography has also been performed as basic flow visualization.

2.6 – Impinging Jet Noise

The topic of impinging jets is an important fluid dynamic system with wide ranging applications and as a result has been widely studied in the literature. Noise generated by gas jets impinging on solid surfaces has been the subject of a number of experimental studies, although most have focused on axisymmetric jets and the subject of planar jet impingement has received far less attention. Petrie (1974) experimentally investigated noise generated by an axisymmetric gas air jet impinging on a flat surface for flow velocities between $V = 82$ and 213 m/s for nozzle diameters between $d = 19$mm and 38mm. The author reported that the sound pressure level was in general inversely proportional to jet impingement ratio z/d, and for specific distances, increases of more than 27 dB above the noise of a free jet were produced, with a "distinct tonal character" of the noise being reported. Some basic spectral measurements were performed; however the author did not provide any information regarding the behavior of the acoustic tone as a function of flow velocity, jet diameter (d) or impingement distance (z). The author also examined the sensitivity of these acoustic tones to jet-plate impingement angle, starting with a normally impinging jet, and slowly inclining the plate to the axis of the jet. For inclination angles of $\varepsilon = 30°$, a decrease in peak SPL of over 10dB was observed, and further reductions were observed for jet-surface inclination angles up to $\varepsilon = 60°$.

Ho & Nosseir (1981, 1982) focused on the noise generation and feedback mechanism of an axisymmetric jet impinging normally on a flat plate. The authors concluded that a feedback mechanism existed for axisymmetric jets impinging on a flat surface for impingement ratios of less than $z/d < 7.5$. The feedback mechanism consisted of coherent structures generated within the jet shear layer which travel downstream impinging on the flat surface. The impingement of these structures resulting in pressure fluctuations and distortion to the vorticity field. These fluctuations propagate upstream to the nozzle lip, exciting subsequent perturbations in the shear layer, completing the feedback cycle and causing large acoustic tones to be generated. The coherent structures and upstream travelling fluctuations were observed to be phase locked at the nozzle outlet, and the frequency of the tone generated was observed to be a function of the convection speed of the coherent structures, and the speed of sound.

Research performed on planar impinging jet geometries has been less frequent in the literature compared to axisymmetric jets. Some specialized geometries utilizing plane jets such as jet-edge and jet-slot configurations (Ziada, 1995) have been examined, as well as some research on confined planar jets impinging on flat surfaces (Varieras et al., 2007 & Pavageau et al., 2006). Most studies which have been performed on plane jets impinging on flat surfaces have focused on steady state characteristics of the flow field (Maurel & Solliec, 2001) such as heat transfer characteristics and mean velocity profiles and have ignored the unsteady characteristics of the flow, or the studies have been performed for very low Reynolds number, typically less than $Re_h < 2000$ (Sakakibara et al., 2001).

Studies performed on jet-jet impingement using plane jets are even less common than studies detailing jet-plate impingement, with most studies being performed for highly specialized geometries used in industrial applications. To the author's knowledge, the only studies dealing with this geometry have been performed by Nosseir et al (1987) and Nosseir & Behar (1987), which studied the impingement of opposing low aspect ratio plane jets in a highly confined channel. Due to the nature of this highly specialized geometry, this study has no real practical relevance to the application at hand; however it is interesting to note that the authors detected a strong flapping mode of the opposing jets which generated low frequency noise.

Chapter 3 – EXPERIMENTAL SETUP

3.1 - EXPERIMENTAL FACILITIES

The work presented in this thesis consists of measurement performed both in an in-plant, manufacturing environment and in a lab on a scaled galvanizing simulator. The same measurement equipment and measurement techniques were used for both environments, however the measurements locations relative to the jets vary and are detailed in the appropriate results sections of this thesis. It should be noted that measurements performed in the actual manufacturing environment took place in production conditions with little or no provisions being made to reduce or eliminate noise from processes other than gas wiping. The manufacturing environment is filled with a myriad of noise sources other than gas wiping including but not limited to, fans, large rollers and drive motors, gas furnaces, overhead cranes and many, many others. Measurements of noise in the gas wiping process were made within close proximity of jet impingement and gas wiping is the major contributor to noise at this location, however, the noise measured is understood to be a result of gas wiping as well as all previously mentioned sources.

A scaled galvanizing simulator shown in Figure 3-1 has been used for all in-lab measurements. The simulator consists of a steel frame with a series of steel rollers mounted a various locations around its perimeter. A continuous stainless steel loop with a thickness of t = 0.18 mm used to simulate the steel sheet in the gas wiping process is mounted on the perimeter rollers. The sheet tension of the steel loop is adjusted by a series of draw and lead screws mounted to each of the perimeter rollers mounted on the steel frame. An articulating arm was used to hold the microphone used for acoustics measurements in the desired location. In initial measurements performed to investigate the effect of noise directionality, the microphone position was measured via x and y coordinates from some reference point on the galvanizing frame. For repeated measurements at a single location, the microphone position was set using a series of jigs constructed to place the microphone accurately and ensure repeatability. The microphone articulating arm is shown in the inset of Figure 3-1.

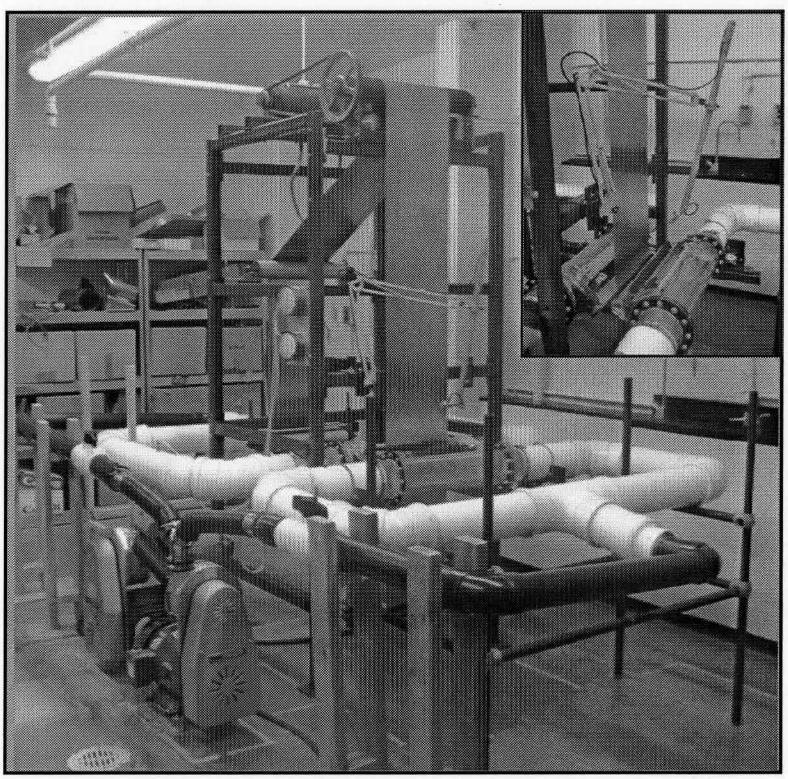

Figure 3-1: Scaled galvanizing simulator used for all in-lab measurements of gas wiping. Inset: Opposing gas wiping jets and articulating microphone arm.

The air knives used in the study are constructed of Aluminum and clear Acrylic and have been constructed as a scale replica of jets used at various galvanizing facilities. The interior of the knives have a series of internal baffles upstream of the nozzle outlet which are used to uniformly distribute plenum pressure across the jet span, ensuring even flow velocities at all points across the jets width. Previous work and measurements have been performed to ensure even flow across the jet span (Hrymak et al., 2004). These baffles are a key feature used in the wiping jets used at many manufacturing facilities. All internal dimensions of the scaled jet reflect the dimensions of the full sized wiping jet except for the overall jet length L_j. In addition, the jets have an adjustable slot width (0mm $\leq h \leq$ 7.5mm). Figure 3-2 shows a scale schematic of the jets including in the internal baffles and a photograph of the jet-jet and jet-sheet impingement regions of gas wiping on the scaled galvanizing simulator.

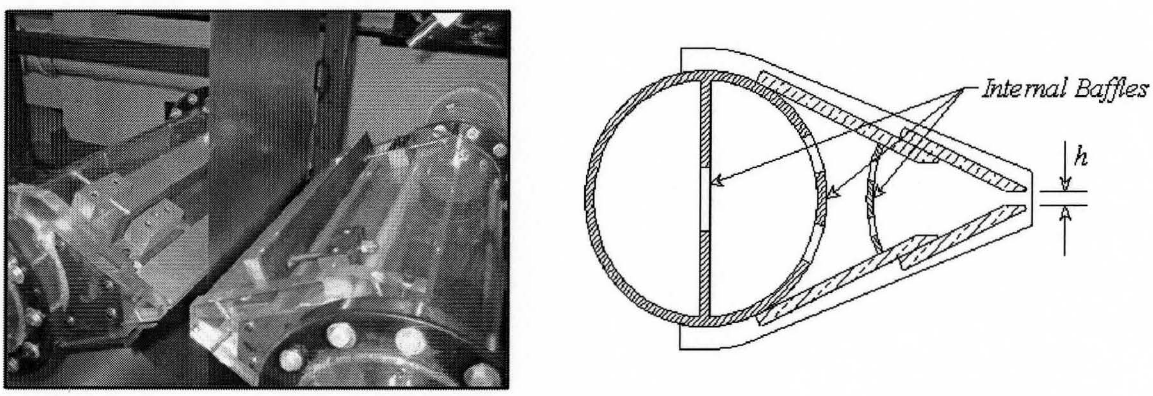

Figure 3-2: Close up of jet-jet and jet-sheet impingement regions (left) and scale drawing of gas jets showing the internal baffles (right).

The air knives are mounted in a pair of steel cradles located at either end of the air knife designed to allow the adjustment of both the angle of inclination of the jet α, as well as impingement distance z. The cradles support the jets by their supply pipes in a semicircular support plate made of ¼” plate steel and the supply pipes are held securely in place with a steel, worm drive support strap. The support plate is bolted to a steel slide, milled flat on its sliding surface. The angle of inclination of the jet can be manipulated by rotating the jet with respect to its supply pipe at the slip joint connecting the two assemblies. A T-bolt clamp is used to secure the air knife once the angle of inclination of the jet has been set to the desired specifications. The impingement distance of the jet is adjusted using a set of lead screws mounted on each jet support plate and slide assembly, and measured with a dial indicator accurate to 0.001” (0.025 mm), which is mounted directly to the support plate. The lead screw contacts the frame of the galvanizing simulator, and the impingement distance of the jet can be changed by rotating the lead screw. The complete jet cradle and slide assembly can be seen in Figure 3-3.

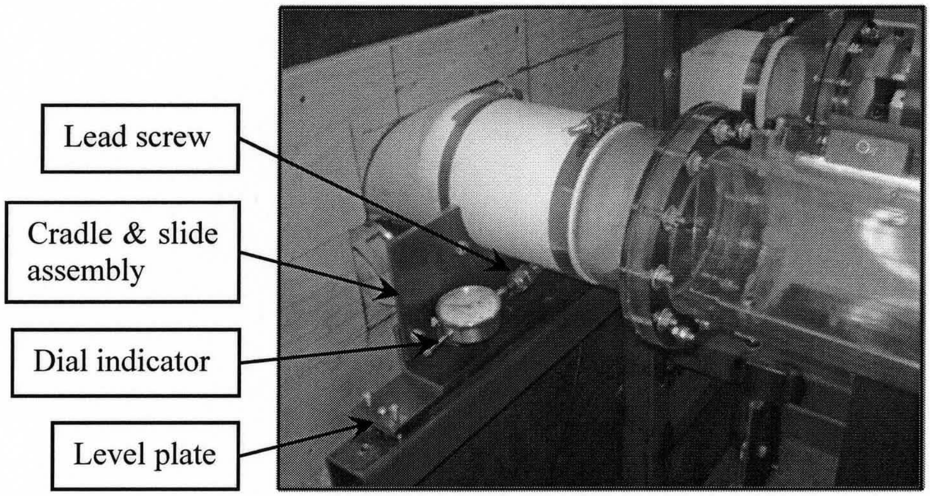

Figure 3-3: Jet cradle and slide assembly showing dial indicator and lead screw used to adjust impingement distance, *z*.

The two air knives and slide mechanisms are mounted on four individually adjustable mounting pads which are bolted to the frame of the simulator. Each mounting pad has adjustable height and can be leveled relative to the horizontal, in order to accurately position the jets with respect to one another. The height of each of the four mounting pads can be set to within +/-0.1 mm using a 40" machinist straight edge and a 12" master precision level accurate to +/-0.05 mm/m. In addition, the level of each of the four jet mounting pads is set using a 12" master precision level accurate to 0.05mm/m.

The jets are supplied with pressurized air via a piping system constructed of 5" I.D. PVC pipe. The two jets are supplied with pressurized air from each end using the piping system shown in Figure 3-1 and Figure 3-5. Several flow conditioning devices such as screens and honeycomb sections are located at various positions upstream of the jet, to alleviate the presence of large scale turbulent structures from migrating to the nozzle outlet which could cause unsteady flow at the nozzle outlet. The pressure supplied to the jets is controlled by a globe valve located at the start of the PVC air supply system.

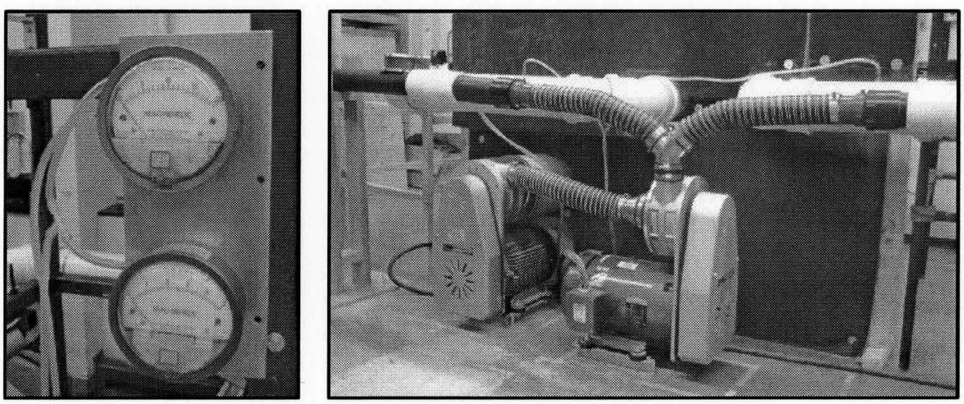

Figure 3-4: Plenum pressure gage setup (left) and series configuration centrifugal blowers used for pressurization.

The pressurized air supplied to the jets is produced by a pair of Sonic Air Systems 700 series centrifugal blowers. The two blowers are plumbed in series to increase the pressure capabilities of the apparatus to P = 4.5 psi (0.306 Bar). Technical specifications of the blowers including performance curves have been included in Appendix A of this thesis. Measurements at lower plenum pressures ($P \leq 0.170$ Bar) have been performed using only one blower, whereas measurements at higher pressures (0.204 Bar $\leq P \leq$ 0.306 Bar) have been performed using both blowers. Using two blowers for measurements performed at low pressures was not feasible due to high levels of heat associated with restricting the outlet of the two blowers with globe valves used to throttle the jets. In some cases these high temperatures would exceed the maximum working temperature of the polymers used to construct the jet and piping system. The plenum pressure supplied to the jets was measured by a pair of Magnahelic® mechanical pressure gauges. The absolute pressure of Jet #1 was monitored in psi to within 0.05 psi (0.003 Bar), and the differential pressure between the two jets was measured using a separate pressure gauge accurate to 0.004 psi (0.0003 Bar). Both pressure gauges were calibrated using a standard pressure calibrator to ensure accuracy.

Edge baffle configurations were tested using a pair of adjustable edge baffles consisting of rectangular 1/8" thick aluminum plates measuring 260 mm x 160 mm which were inserted into each of the jet-jet impingement regions. The edge baffle distance (D_{EB}) is adjustable between D_{EB} = 0 mm (no clearance) and 48mm (fully withdrawn), and the edge baffle distance was measured using a pair of Mitutoyo® digital calipers to within +/- 0.05mm.

An acoustic baffling system has been constructed to help minimize the effects of ambient and blower noise in the lab, as well as minimize the effect of acoustic reflection and reverberation effects and ensure that all acoustic measurements are performed in the acoustic near field. The acoustic baffling was constructed using 3/8" plywood and 2" thick mineral fiber insulation. The NRC acoustic ratings of the insulation have been included in Appendix A – Equipment Specifications. The configuration of the baffles is shown in photographs of Figure 3-5.

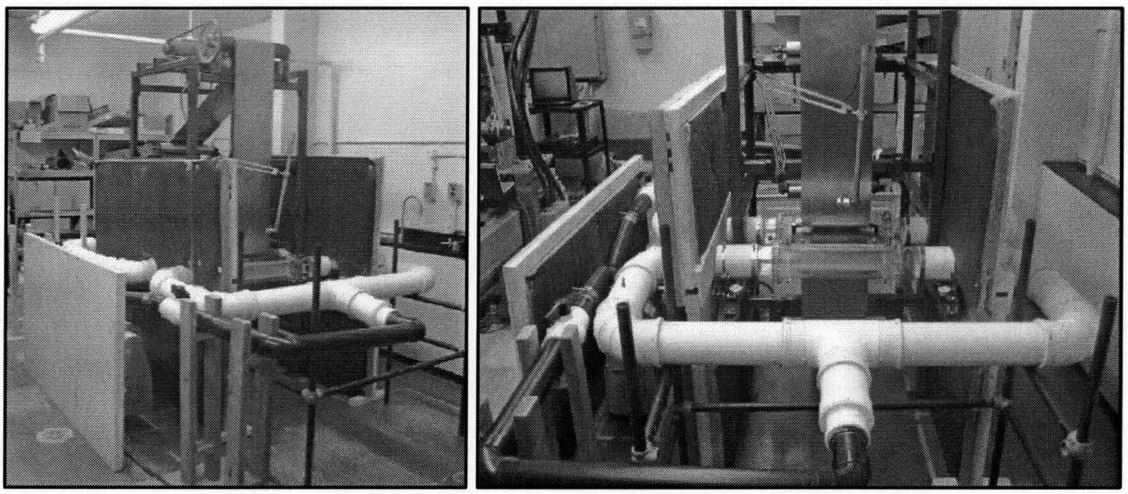

Figure 3-5: Gas wiping setup with acoustic baffles in place.

Measurements of jet-plate impingement, shown in Figure 3-6, were performed using the same jet used for gas wiping, and a ¼" Aluminum plate mounted to a three axis manual traverse accurate to +/- 0.001" (0.025 mm). The microphone was held in position by the same articulating microphone arm used in the gas wiping portion of the experiments and was mounted to the traverse to maintain the microphone position with respect to the jet impingement point. Plate inclination was achieved by inclining the plate about a hinge at its midpoint for span-wise inclination, or rotating the jet about the slip joint between the jet and the supply piping system, for stream-wise inclination.

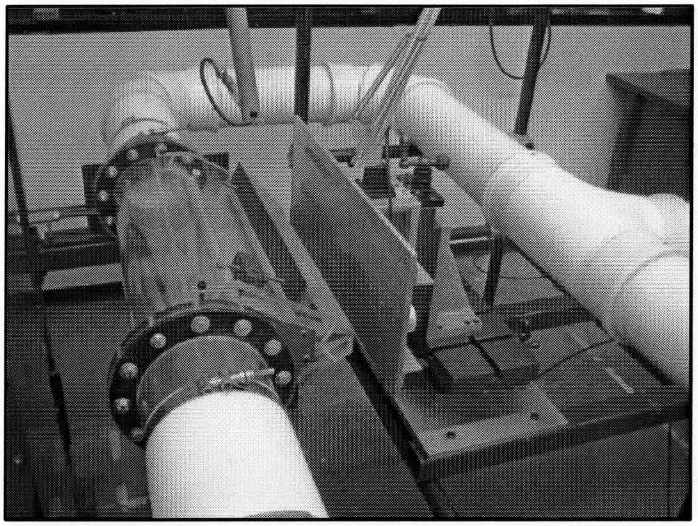

Figure 3-6: Jet-plate impingement setup showing planar jet, ¼" Aluminum plate and 3-axis manual traverse.

A ½" GRAS pressure microphone has been used for all testing in conjunction with a National Instruments 9233 USB based data acquisition card with 24 bit resolution and a hardware based anti-aliasing filter. All data was collected using LabView® in the form of amplitude spectra, power spectra and power spectral density at a sample rate of 25,000 Hz. Data was averaged using a linear averaging scheme for a total of 50 one second averages. In addition, an integrated peak-hold type SPL meter was used to determine the maximum overall sound pressure level. Microphone calibration was performed using a G.R.A.S. Type 42 AB pressure calibrator prior to each day of measurements and the calibration was re-checked at the conclusion of a measurement set to ensure no drift had occurred.

Chapter 4 – Validation of the Scaled Galvanizing Simulator

4.1 - In-Plant Measurements

In order to characterize the noise field in the industrial environment, acoustics measurements were performed at two separate galvanizing facilities, referred to here as Site #1 and Site #2. Measurements were obtained in the form of both time signal and frequency spectra in order for comparison against measurements performed on the scaled galvanizing simulator. The objective was to characterize the noise generated and validate the in-lab apparatus to allow the problem to be further studied more efficiently on the in-lab facility. The various gas wiping process parameters were recorded for each configuration prior to all measurements, so that the configurations could be reproduced in the laboratory as closely as possible. The goal of performing these in-plant tests was to obtain measurements of the actual noise field at the manufacturing facilities, as well as identify trends both in the spectral content and in the overall sound pressure levels. Because of the extremely harsh environment and high temperatures associated with this process and its proximity to the molten Zinc bath, directly measuring the various process parameters was often not possible. Where direct measurement of the parameters was not feasible, measurements were obtained from the process control equipment, the process engineer or from the operator. In some cases, only an estimate could be given for a particular process parameter. For process parameters obtained by estimate or other indirect means, an estimate by the process engineer of the relative uncertainty has been provided.

4.1.1 – In-Plant Measurement Techniques

Due to the particularly harsh environment in which gas wiping is performed, special care was required when performing acoustics measurements of manufacturing lines. The microphone and data acquisition equipment used for in-plant measurements was the same as that used for all in-lab measurements, however for the in-plant measurements a 30 foot telescopic boom was used in order to position the microphone from a safe distance. The microphone was held in place by hand during all measurements, as it was not possible to setup any mechanical holding device in the immediate vicinity of the Zinc pot. Additionally, direct measurements of microphone position were not possible for the in-plant measurements. An estimate of microphone position was assessed visually for each case.

Data for all in-plant measurements was obtained at a sample rate of 10 kHz in the form of both microphone time signal and various frequency spectra. All spectral measurements utilized a Hanning window and resulting spectra with a frequency range of 0 Hz to 5kHz with a 1Hz resolution were constructed with the spectra being averaged 50 times using 50 blocks of data of 10,000 samples each.

4.1.2 – Measurement Results: Site #1

Measurements at Site #1 were performed for only one wiping configuration; the impingement distance, angle, nozzle slot width and other physical parameters were not changed. The facility of Site #1 was not equipped with edge baffles, but an acoustic enclosure was built around the gas jets and jet impingement region. Only a small gap of approximately 15-20 cm between the top of the molten zinc and bottom of the enclosure and a slot opening at the top of the enclosure approximately 15 cm wide to allow the removal of the continuous steel sheet. Figure 4-1 shows a basic schematic of the wiping jet configuration and baffle system surrounding the gas wiping process.

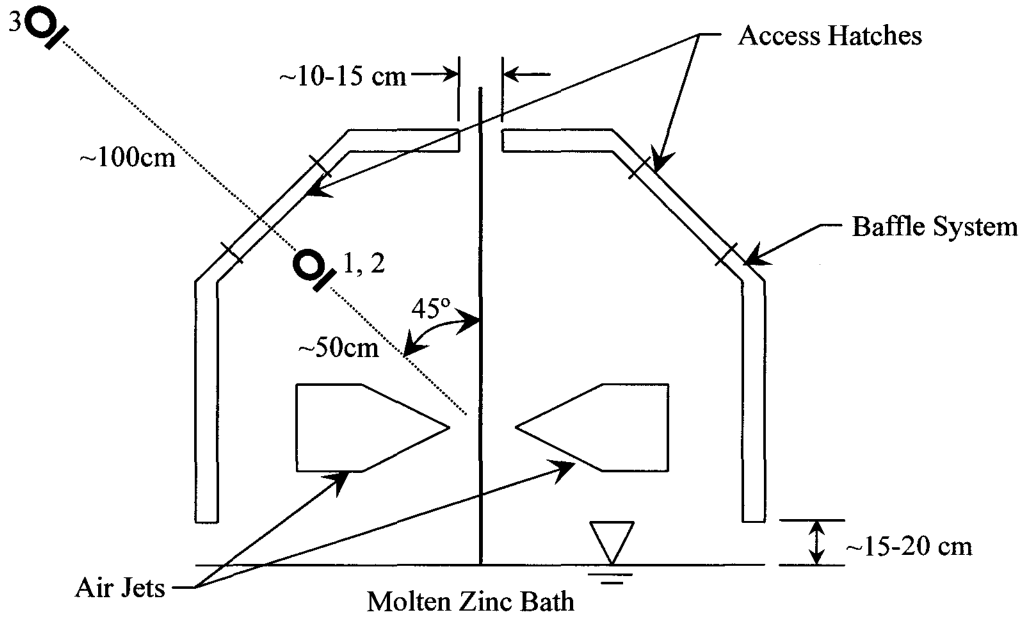

Figure 4-1: Side view of Zinc pot and gas wiping area of Site #1 galvanizing facility.

The plenum pressure supplied to the jets was regulated by a closed loop controller which monitored the coating thickness approximately 700 meters downstream of the wiping area, and continuously adjusted the pressure to meet the desired coating thickness. The current measurements were performed at a nominal plenum pressure of P = 6.4 psi (0.44 Bar) +/- 0.1 psi and an impingement distance of $z \approx$ 14mm (+/- 1.9mm). A bowtie jet profile was used with a center jet width of h_c = 1.5 mm and an edge jet width of h_e = 2.0mm. The jet impingement angle was normal to the sheet for both jets (α = 0°), and the jets were in an aligned configuration, with no vertical jet offset (Δy = 0mm). Acoustics measurements were performed at five different positions surrounding the zinc pot area to assess any directionality effect in the noise field. Figure 4-2 illustrates the microphone positions used for the various measurements taken at Site #1, relative to the jets and Zinc pot.

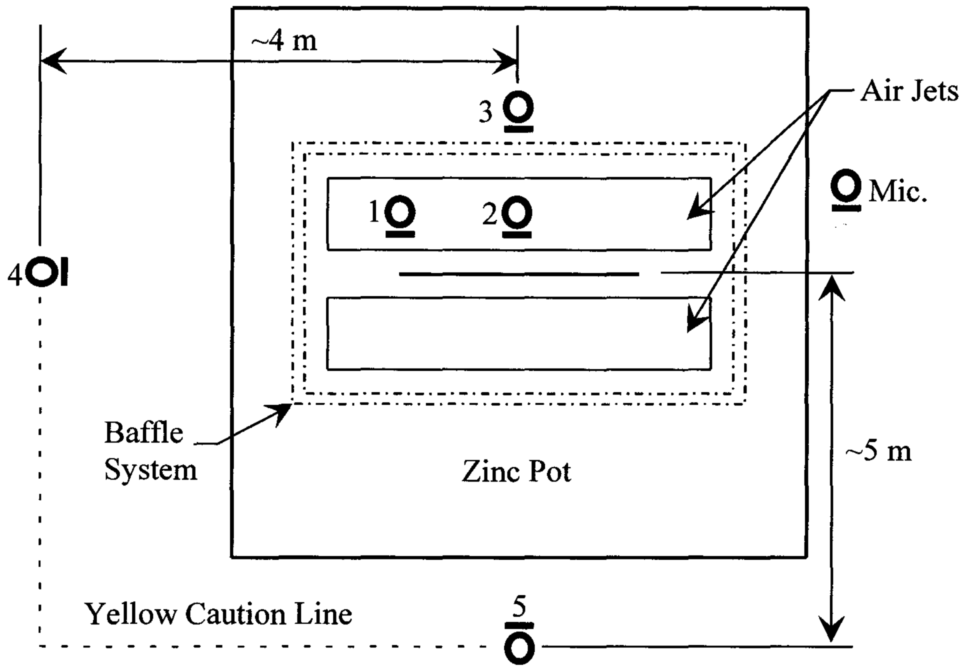

Figure 4-2: Plan view of Zinc pot and gas wiping area of Site #1 galvanizing facility and microphone measurement locations.

The results of the noise measurements for the five different microphone positions are shown in

Figure 4-3 in the form of frequency spectra plots and overall sound pressure levels. The overall sound pressure levels of the process for this configuration are quite high, over 126 dB in regions closest to the jet. The frequency spectra for the five positions show a strong spectral peak at approximately 1500 Hz for the measurements at all five positions. This spectral peak behavior is consistent with measurements performed in previous investigations by Park (2001) and Dubois (2001a, 2001b), who reported that an audible tone was generated in the region of jet-jet impingement, near the edge of the strip. Comparing the resulting spectra and sound pressure levels at positions 1 and 2, at the edge and center of the steel strip respectively, we can see that the overall SPL as well as the magnitude of the acoustic tone is larger near the strip edge by approximately 5 dB, which is again consistent with previous findings that the majority of noise as well as any tones were generated in the jet-jet impingement region. This observation confirms earlier findings of other investigations that the majority of the noise generated in this frequency range is produced by the impingement of the opposing jets rather than by jet-sheet impingement. The directionality of the noise field in an industrial setting also appears to be negligible, as the overall spectral distribution of acoustic energy is relatively constant.

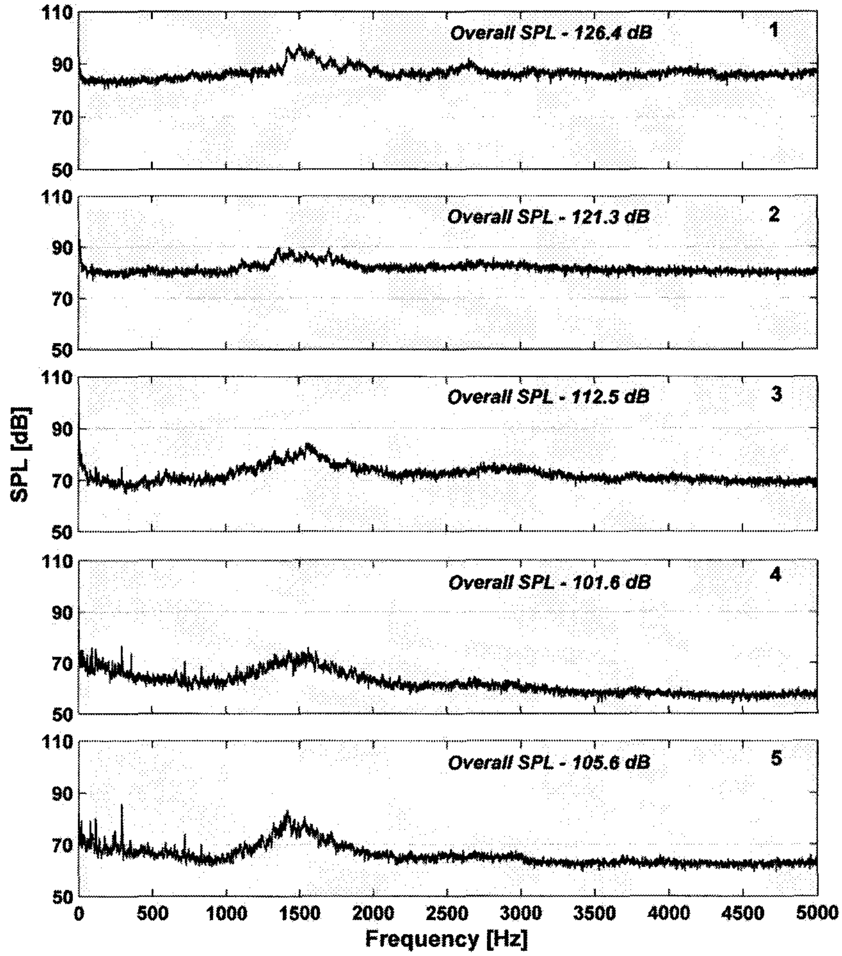

Figure 4-3: Frequency spectra of the gas wiping process for microphone positions 1 through 5 for Site #1 manufacturing facility.

4.1.3 – Measurement Results: Site #2

Measurements at Site #2 were performed for a variety of process configurations including varying plenum pressure, jet alignment, as well as the presence of edge baffles. Having established that there was no significant directionality of the noise field from the measurements performed at Site #1, all measurements were performed at a single microphone location, but at various operating conditions, to observe some basic behavior of the effect of process parameters on noise generation of the process. The microphone was positioned at a distance of approximately $D \approx 1.0$ m and at angle of $\theta = 30°$ from the horizontal from the impingement point on the sheet at the center of the sheet width. Figure 4-4 shows a schematic of the side and plan views of the microphone position.

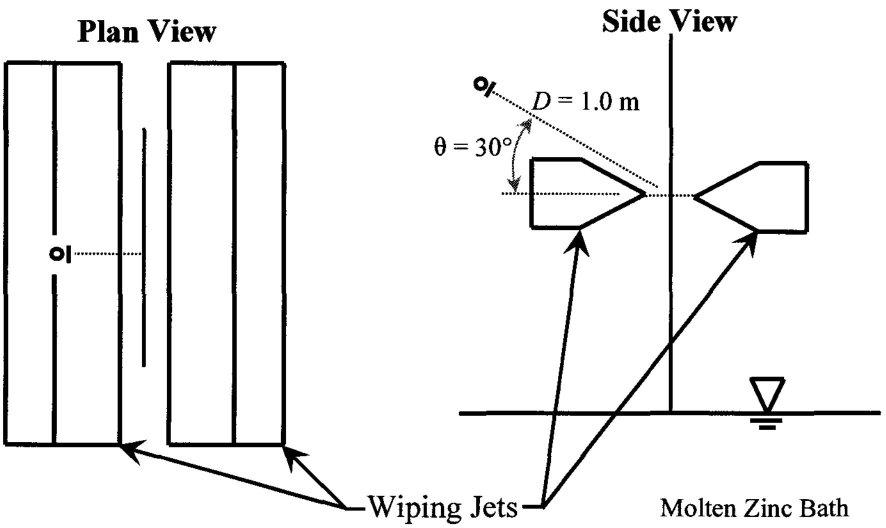

Figure 4-4: Plan and side views of microphone position for acoustics measurements at Site #2.

Figure 4-5 shows the effect of both varying plenum pressure and the effect of edge baffles on noise generated in a misaligned gas wiping case in an industrial environment. The fixed process parameters for these measurements is a jet inclination of $\alpha = 3°$ (+/- 1°), an impingement distance of $z = 11$mm (+/- 1.2mm) and a bowtie jet slot profile was used with an edge gap of $h_e = 2.3$mm and a center gap of $h_c = 1.8$mm. A vertical jet offset of $\Delta y = 3$mm (+/- 0.5 mm) was used and when in use, the edge baffle distance was set to $D_{EB} = 13$mm (+/- 3.0 mm). When the edge baffles were not in use they were completely retracted from the jet-jet impingement region. Figure 4-5 (a), (b) & (c) show a case with edge baffles present and plenum pressures of $P = 6.0$ psi, 4.5 psi and

3.5 psi (0.41 Bar, 0.31 Bar & 0.24 Bar) respectively. The content of the frequency spectra does not change appreciably between the three cases, although there is a broadband increase in acoustic pressure level as the plenum pressure is increased. The overall sound pressure level for these cases is given in Figure 4-6 and shows that as the plenum pressure is increased, the overall sound pressure level increases as well. Parts (d), (e) and (f) of this figure shows the effect of removing the baffle plates for plenum pressures of P = 6.0 psi, 4.5 psi and 3.5 psi, respectively. Comparing cases of with and without baffle plates in the figure, it is clear that the presence of baffle plates causes a broadband reduction in sound pressure level of noise in the gas wiping process, as well as a significant reduction in overall sound pressure level. Reductions in overall sound pressure level as much as 5 dB are measured for the highest plenum pressure tested with the use of edge baffles. In addition, cases with edge baffles tend to suppress any small spectral peaks occurring in cases without edge baffles, because the opposing jets do not impinge on one another.

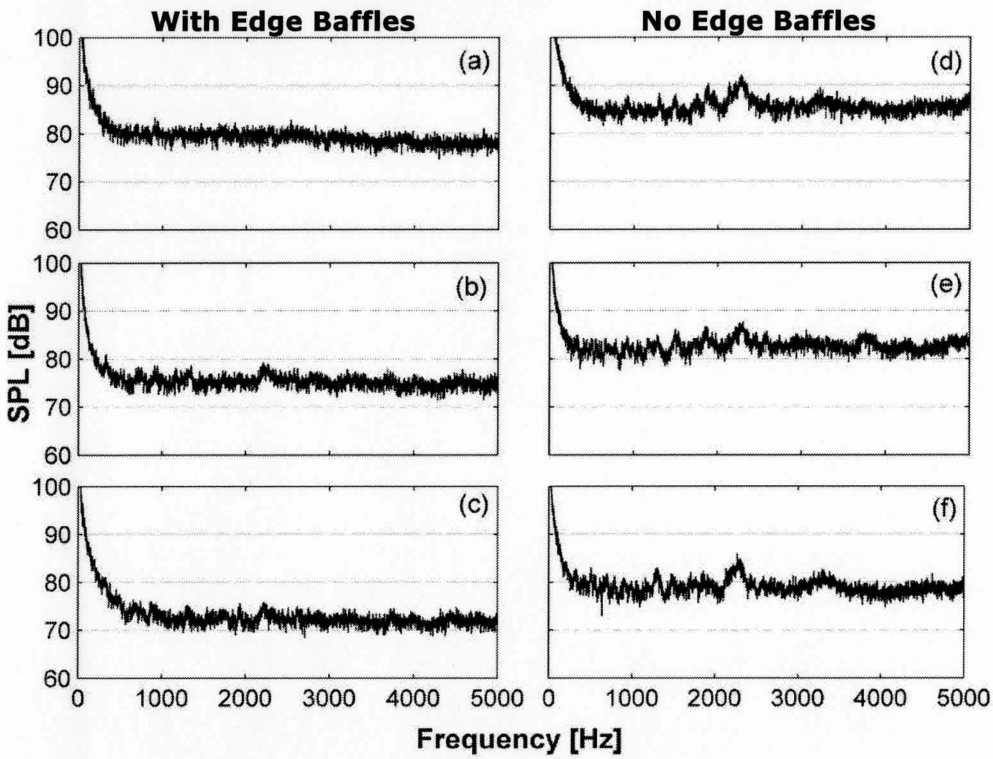

Figure 4-5: Frequency spectra showing the effect of edge baffles on noise production at various plenum pressures. With edge baffles: $P = 6.0$ psi (a), 4.5 psi (b), 3.5 psi (c). No edge baffles: $P = 6.0$ psi (d), 4.5 psi (e), 3.5 psi (f).

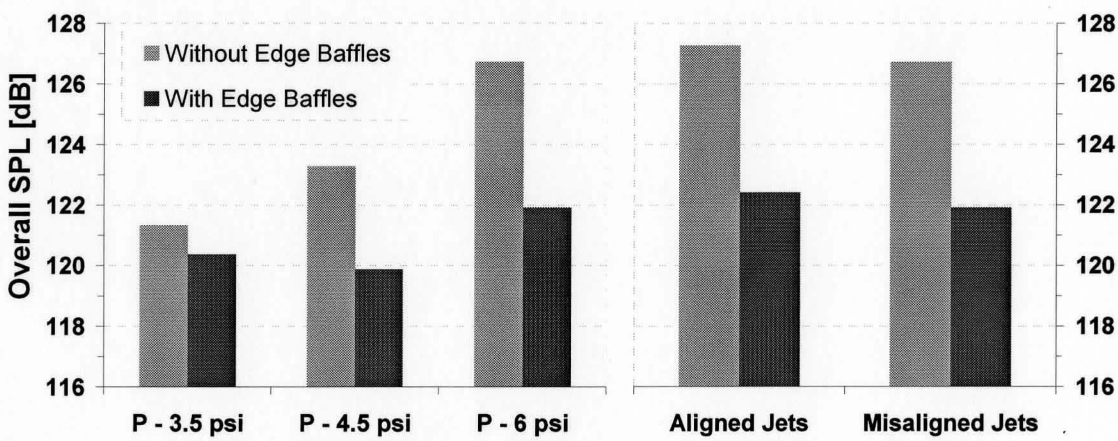

Figure 4-6: Effect of Edge Baffles and jet alignment on the overall sound pressure level for various plenum pressures.

The effect of jet alignment was also investigated at Site #2, with measurements being performed at plenum pressures of 6.0 psi (0.41 Bar) for aligned and misaligned jet cases both with and without edge baffles. The fixed process parameters outlined earlier remain unchanged for these measurements, however the vertical jet offset was changed from Δy = 3mm to Δy = 0mm (+/- 0.5mm) for the misaligned and aligned jet cases respectively. Figure 4-7 shows the combined effect of edge baffles and jet alignment. Parts (a) and (c) showing aligned and misaligned jet cases respectively, both being without edge baffles, illustrates the strong dependence on jet alignment of acoustic tone formation in the jet-jet region reported by Dubois (2001a, 2001b). Aligned jet cases have been shown to generate much stronger audible acoustic tones for a variety of gas wiping configurations. Strong audible tones generated in the gas wiping process have the effect of increasing the perceived sound pressure levels by workers in the immediate vicinity of the process, due to increased annoyance caused by the tones. Figure 4-6 shows the overall sound pressure levels of both the aligned and misaligned jet cases, with and without edge baffles. This figure indicates that edge baffles used in aligned jet cases have similar reductions in overall sound pressure levels; however, Figure 4-7 shows that the reduction of the acoustic tone in the aligned jet case with edge baffles is minimal if at all.

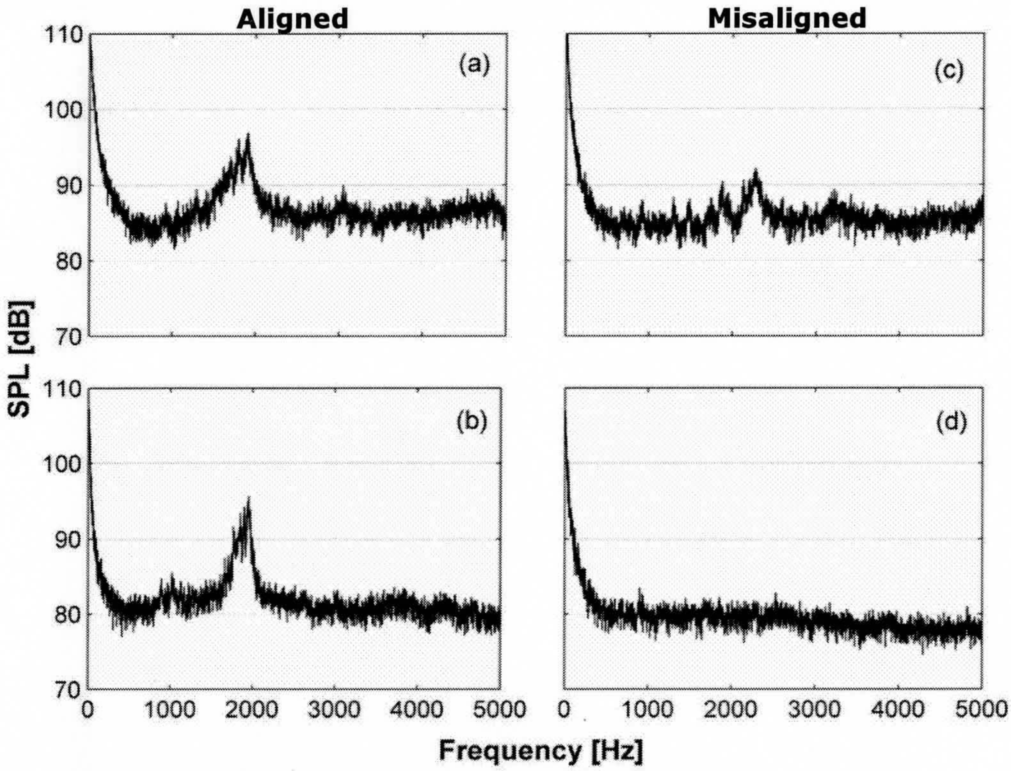

Figure 4-7: Frequency spectra showing the effect of jet alignment for cases with and without edge baffles. Aligned jet case: No edge baffles (a), with edge baffles (b). Misaligned jet case: No edge baffles (c), with edge baffles (d).

The results of these in-plant measurements have shown that there is no strong directionality component of the noise, and that the frequency content of the noise does not change appreciably with measurement position. The overall noise level has been shown to scale with the plenum pressure supplied to the jets and the majority of the noise production has been shown to emanate for the jet-jet impingement region, which agrees with the observations of some previous investigations. The effect of edge baffles at a single edge baffle distance was also investigated and found to be effective in reducing overall sound pressure levels, but relatively ineffective in suppressing acoustic tones.

Furthermore, the acoustic tone generation has been shown to be strongly dependant on the jet alignment.

4.2- INITIAL IN-LAB MEASUREMENTS

Measurements were performed on the scaled galvanizing simulator in similar configurations to those tested in the manufacturing environment, in order to recreate the acoustic response and noise production of the actual process in a controlled laboratory environment. Differences in scale between the in-plant and in-lab facilities, as well as difficulty manipulating and measuring process parameters accurately in a production environment prevent the measurements from being directly compared. However, comparisons in the frequency content and overall sound pressure levels and overall trends between the two sets of measurements are a valid comparison, and will allow the validation of like behavior between the two cases. A brief assessment of various in-lab and in-plant measurements will be presented in order to confirm the accuracy of utilizing the galvanizing simulator as a method to study gas wiping in an industrial environment.

4.2.1 – IN-LAB VS. IN-PLANT MEASUREMENTS

Overall sound pressure level for similar operating conditions of in-lab and in-plant measurements are shown in Figure 4-8. In cases of both the in-lab and in-plant measurements, it is clear that increasing the plenum pressure increases the overall sound pressure level of the noise generated by gas wiping in both cases. This trend agrees with the measurements of Dubois (2001a, 2001b) and Park (2001).

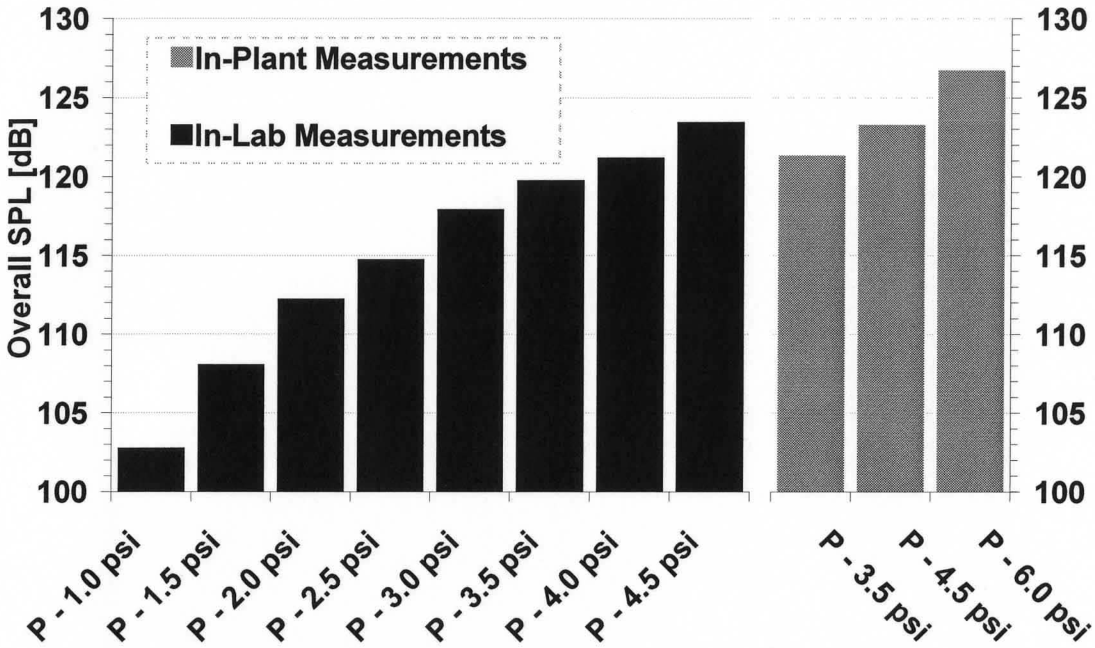

Figure 4-8: Comparison of overall SPLs of in-plant and in-lab measurements. In-plant conditions: $z/h_e = 4.95$, $\alpha = 3°$. In-lab conditions: $z/h = 5$, $\alpha = 3°$.

Previous investigators such as Dubois (2001a, 2001b) have noted the significant impact of jet alignment on noise generated in the gas wiping process, specifically on the generation of discrete acoustic tones. Accurate jet alignment in jet-jet impingement has been shown to generate strong acoustic tones and higher overall sound pressure levels compared to cases with misaligned jets. Figure 4-9 shows a comparison between in-plant and in-lab measurements for cases with aligned and misaligned jets. Part (a) shows measurements performed in an in-plant production setting while part (b) shows measurements resulting in a similar response for the in-lab galvanizing simulator. In both cases, it is evident that alignment of the jets produces a strong acoustic tone, at $f \approx 1900$ Hz in both cases, whereas a similar vertical jet offset of $\Delta y = 3$mm for both in-plant and in-lab cases results in the suppression of the tone. The spectra obtained for the in-plant measurements also display a very high level of low frequency noise ($f < 100$Hz) which was not present in the laboratory facility. This low frequency noise can be attributed both to the high levels of airflow due to cooling fans near the Zinc pot as well as a variety of other large mechanical equipment used in the immediate vicinity in-plant measurements. It should be noted that the conditions of the two sets of test cases for in-lab and in-plant measurements shown here are different (*In-plant conditions*: P = 6psi (0.41 Bar), z/h_e = 4.95, h_e = 2.3mm. *In-lab conditions*: P = 2.5 psi (0.175 Bar), z/h = 6, h = 1mm), the two cases have been selected to have the same dominant tone frequency. As will be shown later in Chapter 5, the frequency of the acoustic tones can predicted accurately by Equation (5-3) on page 75, an expression developed using the results of the extensive in-lab measurements. Table 3 shows the results of Equation (5-3) of predicting the acoustic tone frequencies for measurements performed in both locations. The predicted frequency of the tone is within 3.5% of its actual value, which is exceptional when considering the uncertainty of the parameters of the wiping process for the in-plant measurements.

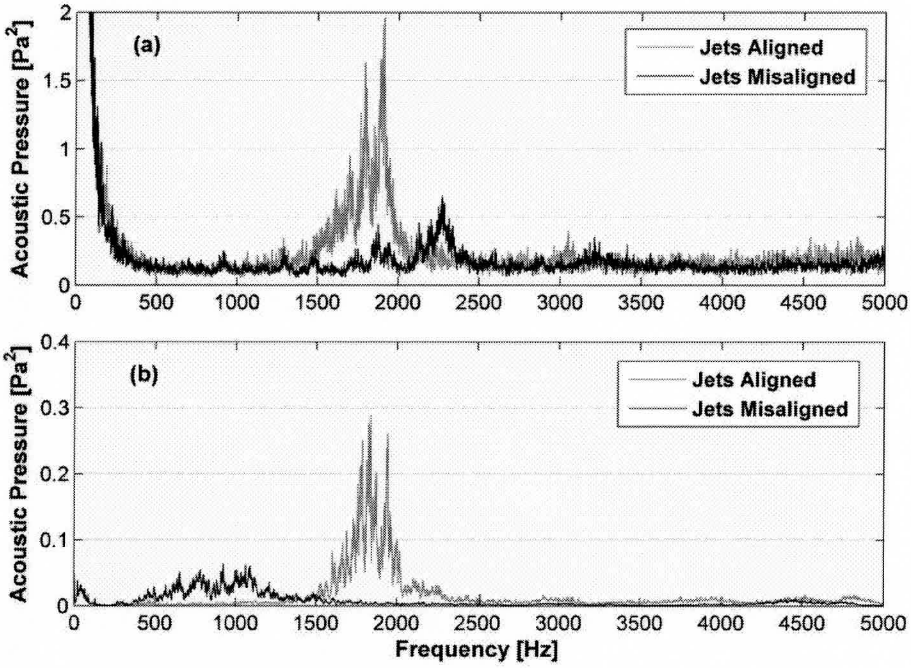

Figure 4-9: Comparison of in-lab and in-plant measurements showing acoustic spectra of aligned and misaligned jet cases. (a) In-plant: $P = 6$ psi (0.41 Bar), $z/h_e = 4.95$, $h_e = 1.8$mm, $\alpha = 3°$, $\Delta y \approx 3$mm. (b) In-lab: $P = 2.5$ psi (0.170 Bar), $z/h = 6$, $h = 1$mm, $\alpha = 3°$, $\Delta y = 3$mm.

Table 3: Predicted vs. actual tone frequencies for in-plant vs. in-lab measurements.

Measurement	P [psi]	V_l [m/s]	z [mm]	h [mm]	z/h	f_{actual} [Hz]	$f_{predicted}$ [Hz]
In-Plant	6.00	246	8.91	1.8	4.95	1911	1977
In-Lab	2.50	164	6.00	1	6.00	1836	1858

In addition, the results of the current study were compared to the results of two previous studies performed by Dubois (2001a, 2001b) which consisted of measurements performed in both laboratory and production environments. The predictions of Equation (5-2) are within 10% of the actual frequency of the tone in all but one case. Furthermore, the measurements presented here represent a very large range of parameters used in the gas wiping process (0.7mm $\leq h \leq$ 2.1mm, 1.45 psi $\leq P \leq$ 5.8 psi, 7.1 $\leq z/h \leq$ 21.4). In addition, the measurements included configurations using various jet inclination angles (α), which have been shown to affect the frequency of the acoustic tones generated.

Table 4: Predicted vs. actual tone frequencies of measurements of Dubois (2001a, 2001b) as predicted by Equation (5-3).

P [psi]	V_I [m/s]	z [mm]	h [mm]	(z/h)	f_{actual} [Hz]	$f_{predicted}$ [Hz]
1.45	127	10	1.4	7.14	870	818
2.90	176	10	1.4	7.14	1100	1138
5.80	242	10	1.4	7.14	1700	1564
1.45	127	17	1.4	12.14	450	414
2.18	154	17	1.4	12.14	550	503
2.90	176	17	1.4	12.14	580	576
5.80	242	17	1.4	12.14	850	792
1.45	127	25	1.4	17.86	280	252
2.90	176	25	1.4	17.86	375	351
5.80	242	25	1.4	17.86	566	482
1.45	127	15	0.7	21.43	360	399
1.45	127	15	1.4	10.71	470	486
1.45	127	15	2.1	7.14	500	545

In summary, the measurements performed in the in-lab facility have successfully reproduced the features of noise generated in the gas wiping process by both aligned and misaligned jet cases. These features include the overall sound pressure level, acoustic tone generation and tone frequency for aligned jet cases performed in the manufacturing environment. Furthermore, the in-lab facility has proven successful in reproducing the noise and spectral characteristics measured by other investigations, which have been performed in both laboratory and production environments.

4.2.2 - NOISE CHARACTERIZATION

4.2.2.1 - EFFECT OF SPECTRAL AVERAGING

Some analysis was performed to characterize the nature of the noise generated by gas wiping in order to determine the most accurate method of measuring and evaluating the noise generated. Figure 4-10 shows a waterfall plot of power spectra obtained of a case of jet-jet impingement every second for 50 seconds using no spectral averaging and the inset figure presents the final averaged spectrum utilizing the same data but constructed using 50 spectral averages. The gas wiping configuration used had a plenum pressure of P = 2.5 psi (0.175 Bar), z/h = 10 and an inclination angle of α = 3°. Each spectrum was obtained using a sample rate of 25 kHz, collecting 25,000 samples per spectra, resulting in the generation of one spectrum per second, with a frequency range of 0 - 12.5 kHz and a spectral resolution of 1 Hz. The main plot gives a clear indication that the overall peak amplitude and of the acoustic tone is fluctuating significantly during a relatively short period, which has important implications in the signal analysis and interpretation of the noise.

Figure 4-11 shows histograms of the same data set, graphically illustrating the variation of the acoustic tone frequency and maximum amplitude of each individual spectrum as well as the variation in overall sound pressure level. The modulation in amplitude and frequency of the acoustic tone is thought to originate due to the non-constant impingement length of each of the two jets. The frequency of the dominant acoustic tone of the impinging jets is determined by the jet impingement length z, which is determined by the position of the impingement interface of the two jets. Since this impingement interface is not tied to any physical boundary, but rather the pressure field of the impinging jets, the frequency of the acoustic tone is subject to small amounts of variation. Furthermore, the tones generated by the jet impinging on the steel sheet, which will be presented later in Chapter 6, are also subject to the same modulation behavior due to small sheet vibrations.

The amplitude and frequency of the dominant acoustic tone in each single spectrum were averaged over all the individual spectra, and compared to the frequency and amplitude of the final ensemble averaged spectrum. The average value of the peak acoustic pressure ($P_{average}$ = 1.6845 Pa_{RMS}^2) from the series of individual spectra is approximately three times higher than the resulting peak acoustic spectra of the final ensemble averaged spectra (P_{spec} = 0.6388 Pa_{RMS}^2), which is shown in the inset of Figure 4-10. The variation of the tone frequency with time tends to smear the acoustic energy of the spectral peak over a range of frequencies on the final averaged spectrum, which underestimates the actual magnitude of the acoustic tone of the final averaged spectrum. However, *the overall sound pressure level of the final spectrum is quite accurate* since the overall acoustic energy of each spectrum is approximately constant, and does not change appreciably from spectrum to spectrum.

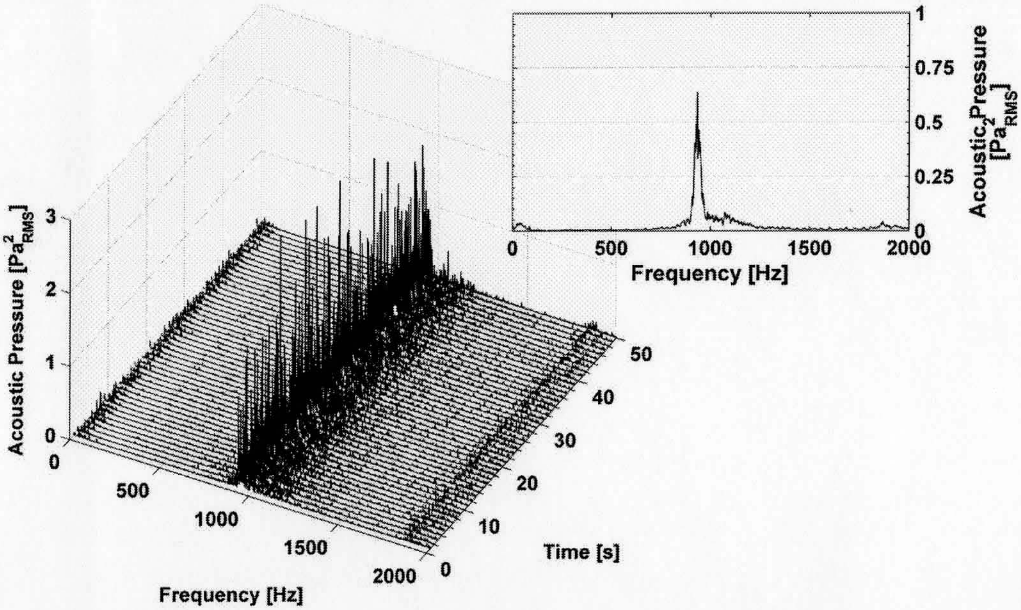

Figure 4-10: Waterfall plot of 50 seconds of noise signal and final ensemble averaged frequency spectrum (inset) captured from galvanizing simulator showing variation in amplitude and frequency of the dominant acoustic peak. (P = 2.5psi (0.175 Bar), z/h = 10, α = 3°, Averaged spectrum: 50 averages)

Table 5: Effect of spectral averaging on overall SPL, tone frequency and tone intensity.

	Average of Individual Spectra	Ensemble Averaged Spectrum
Overall SPL	114.01 dB	114.01 dB
Acoustic Pressure	1.6845 Pa_{RMS}^2	0.6388 Pa_{RMS}^2
Frequency	935.85 Hz	935 Hz

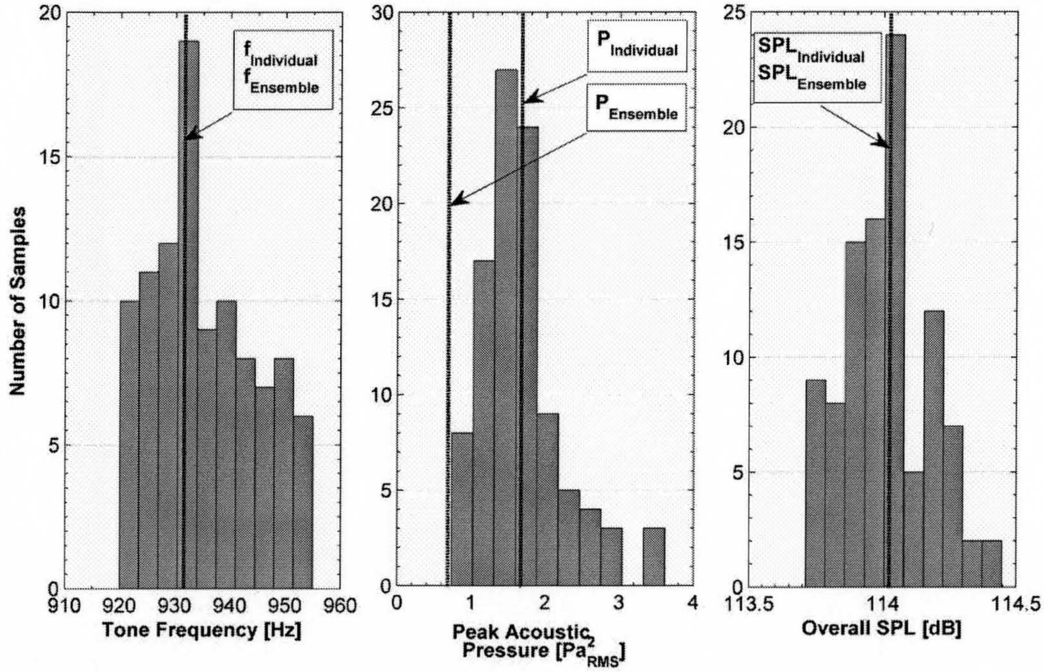

Figure 4-11: Histogram showing the variation in peak acoustic pressure, tone frequency and overall SPL, and the results of spectral averaging.

Measurements were performed in order to characterize the effect of the number of spectral averages on the peak and overall acoustic pressure of the noise due to gas wiping. The same single case of jet-jet impingement considered above was used (P = 2.5 psi (0.175 Bar), z/h = 10, α = 3°) and 50 separate spectra sampled using 5, 10, 25 50, 75 and 100 spectral averages were recorded. The mean values and standard deviation of the tone intensity and overall sound pressure were computed for the spectra taken using each number of averages in order to assess repeatability and reduction in tone intensity for each case. A single averaged spectrum using 1000 averages was also recorded to show the effects of averaging for a very long time. Figure 4-12 shows the results of the effect of the number of averages on the averaged overall and peak acoustic pressures and on sound pressure levels of the spectra. It is clear that the number of spectral averages has a pronounced effect on the peak acoustic pressures recorded in the final averaged spectra, with more averages resulting in lower spectral peaks of the acoustic tone of the averaged spectrum, but increased consistency.

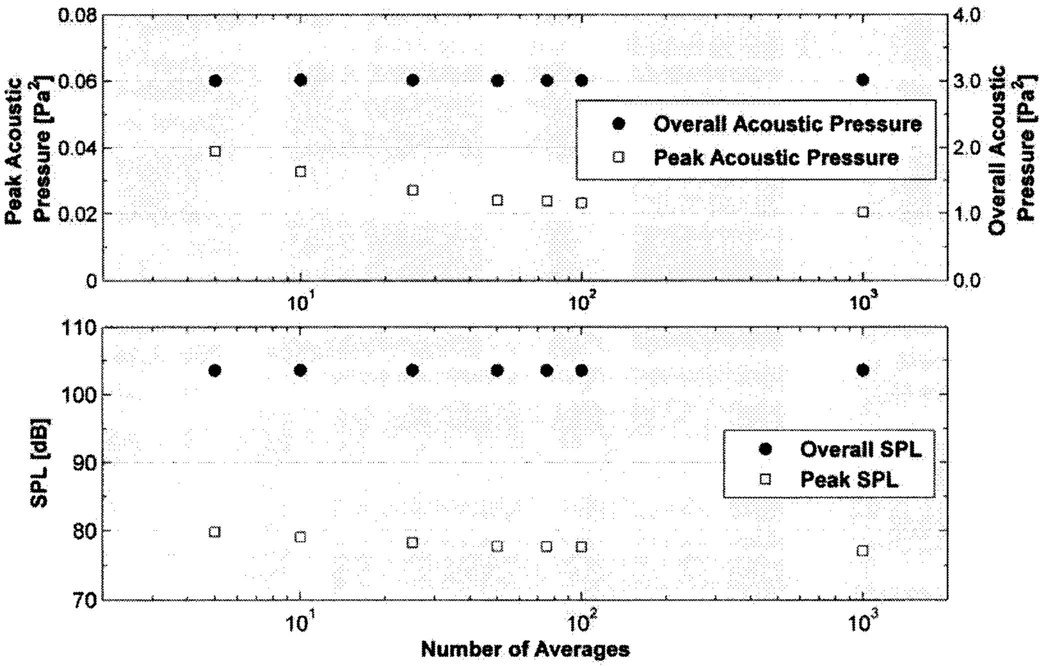

Figure 4-12: Effect of spectra averaging on acoustic pressure and SPL of dominant acoustic peak and overall acoustic pressure.

In addition, the effect of spectral averaging on the standard deviation (σ) of the peak and overall acoustic pressures and sound pressure levels was also investigated. Figure 4-13 shows that the standard deviation of both the overall averaged acoustic pressures and sound pressure levels has very little variation for all cases of spectral averaging from 5 averages to 100 averages, with the standard deviation being less than 1% of the mean value in all cases. The values of standard deviation of peak SPL and peak acoustic pressure vary much more significantly with the number of spectral averages taken. It was necessary to take 50 or more spectral averages in order to resolve the standard deviation of the peak acoustic pressure to less than 10% of the mean value. The variation of peak SPL is much lower, due to logarithmic nature of the decibel scale, with a standard deviation of less than σ = 0.5% for 50 or more spectral averages.

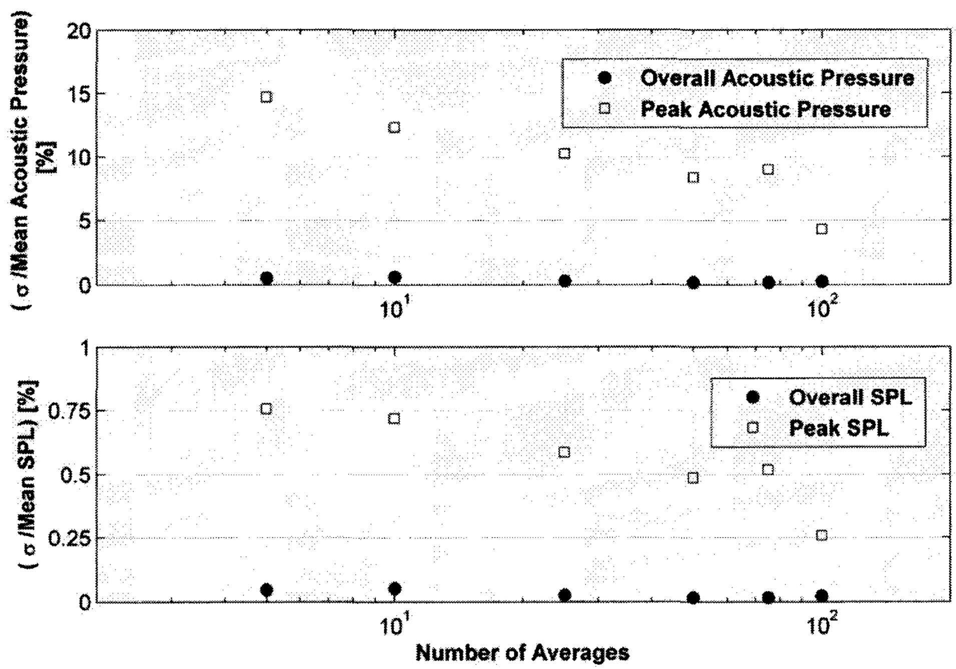

Figure 4-13: Effect of spectra averaging on standard deviation (σ) of peak & overall SPL's.

Spectral averaging of noise produced in the gas wiping process has been shown to significantly reduce the tone intensity, while accurately presenting the overall levels of noise. In order to accurately determine the value of the peak acoustic pressure to a sufficiently low uncertainty, a large number of averages were necessary. However, as it has been previously shown, increasing the number of spectral averages decreases the peak acoustic pressure of the final averaged spectra, and underestimates the instantaneous tone intensity of the actual noise. Table 5 shows results of measurements performed at z/h

= 10, 17.5 & 25 which show that the loss in tone intensity due to spectral averaging is approximately constant over the range of impingement ratios tested. The loss in tone intensity due to averaging is equivalent to a reduction of 8.5 dB in the tone intensity of the averaged spectrum, although this trend has not been confirmed for all gas wiping configurations and cases.

Table 6: Loss in tone intensity due to the effects of spectral averaging.

	$(z/h) = 10$	$(z/h) = 17.5$	$(z/h) = 25$
Average Peak Value [Pa_{RMS}^2]	1.6845	1.7231	2.0398
Averaged Spectral Peak [Pa_{RMS}^2]	0.6388	0.6332	0.7383
Tone Intensity Addition [dB]	8.4	8.7	8.8

4.2.2.2 - Effect of Measurement Position

The effect of microphone position was examined in the in-lab environment to determine the effects of reverberation and any directionality effects in the noise field resulting from jet-jet impingement, and to ensure that all acoustics measurements were performed in the near field. The effects of both microphone distance and inclination angle were investigated, with all measurements being taken at the centerline of the steel sheet. Microphone distance is measured from the jet impingement point at the center of the sheet, and microphone angle is measured in degrees from the horizontal. A simplified schematic of the side and plan views of the jet-jet impingement setup is given in Figure 4-14 which shows the position and orientation of the microphone used for acoustics measurements. Measurements of frequency spectra and overall sound pressure level were taken at a constant microphone inclination angle of $\theta = 65°$ at microphone distances ranging from D = 0.1m to 0.8m and to ensure that all measurements were performed in the near field to minimize the effects of reverberation of the room. Figure 4-15 shows the overall sound pressure level as a function of the microphone distance (D), where the microphone distance is presented in a log scale. The plot clearly shows a linear decay in overall sound pressure level with increasing microphone distance over the entire range of distances examined, indicating that all measurements within this range are within the acoustic near field (Hodgson & Warnock, 1992).

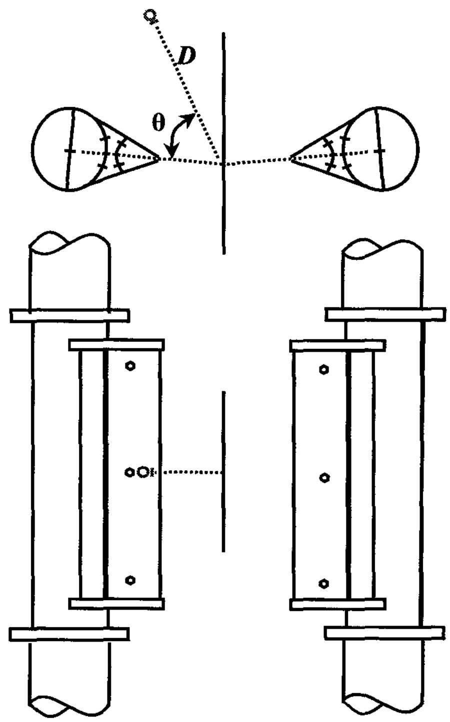

Figure 4-14: Side and plan views of jets and sheet of jet-jet impingement setup showing microphone distance (*D*) and angle (θ).

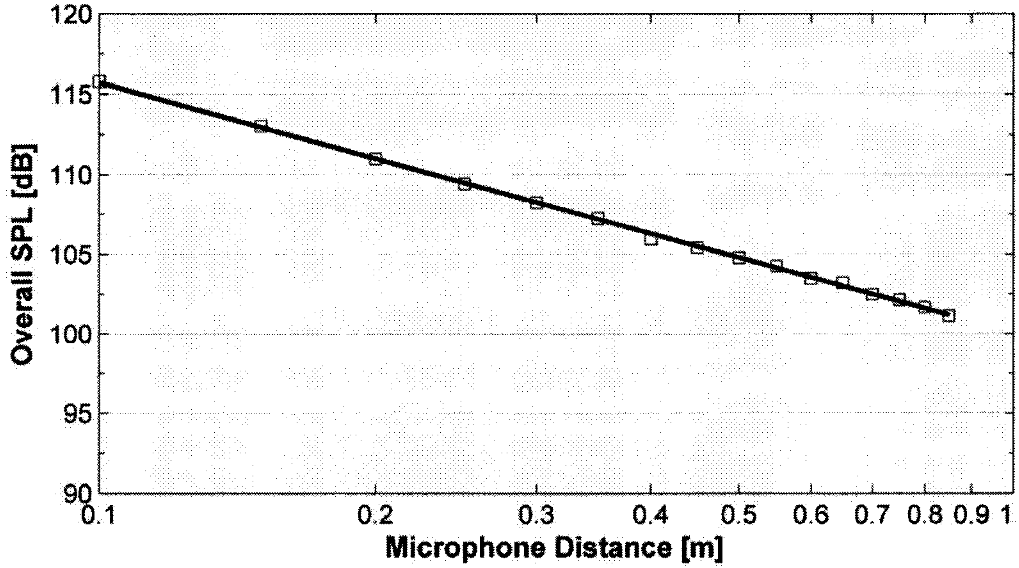

Figure 4-15: Overall SPL as a function of microphone distance (*D*) for a constant inclination angle of θ = 65°.

Measurements were also performed for a variety of microphone inclination angles (θ) to assess any potential effects of directionality within the noise field. All measurements investigating the effect of microphone inclination angle were made at a constant microphone distance of D = 0.5m as shown in Figure 4-14, while microphone distance was varied from θ = 35° to θ = 75°. A waterfall plot showing acoustic spectra as a function of the microphone inclination angle is shown in Figure 4-16, while the overall sound pressure level as a function of inclination angle is shown in Figure 4-17. Figure 4-17 shows a slight dependence of the overall SPL on the angle of inclination, varying just under 2 dB from θ = 35° to θ = 75°. This could be due in part to reflection of noise generated by the jet impingement off of the steel sheet, since the microphone is closer to the sheet in cases of greater impingement ratio. Figure 4-16, shows no significant difference in the spectral content as a function of inclination angle, except a low frequency component in the case of microphone inclination angle exceeding $\theta = 65°$. This increase in low frequency noise at higher inclination angle is due to microphone being subjected to significant airflow, due to the impingement of the jets and the microphone's proximity to the steel sheet.

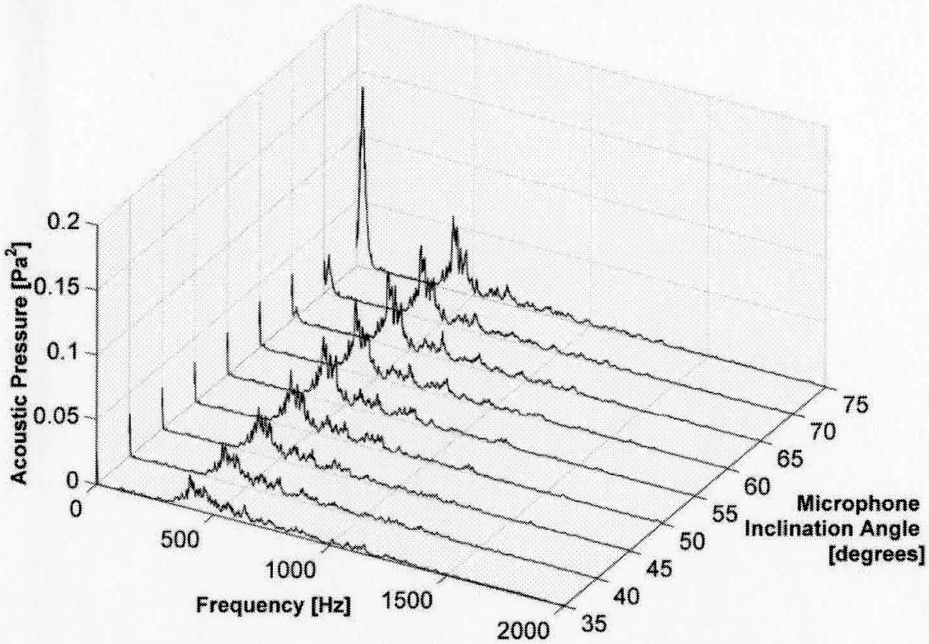

Figure 4-16: Waterfall plot of acoustic spectra of galvanizing noise while varying the microphone inclination angle (*D*). *P* = 2.0 psi (0.136 Bar), *z/h* = 17.5, *D* = 50cm.

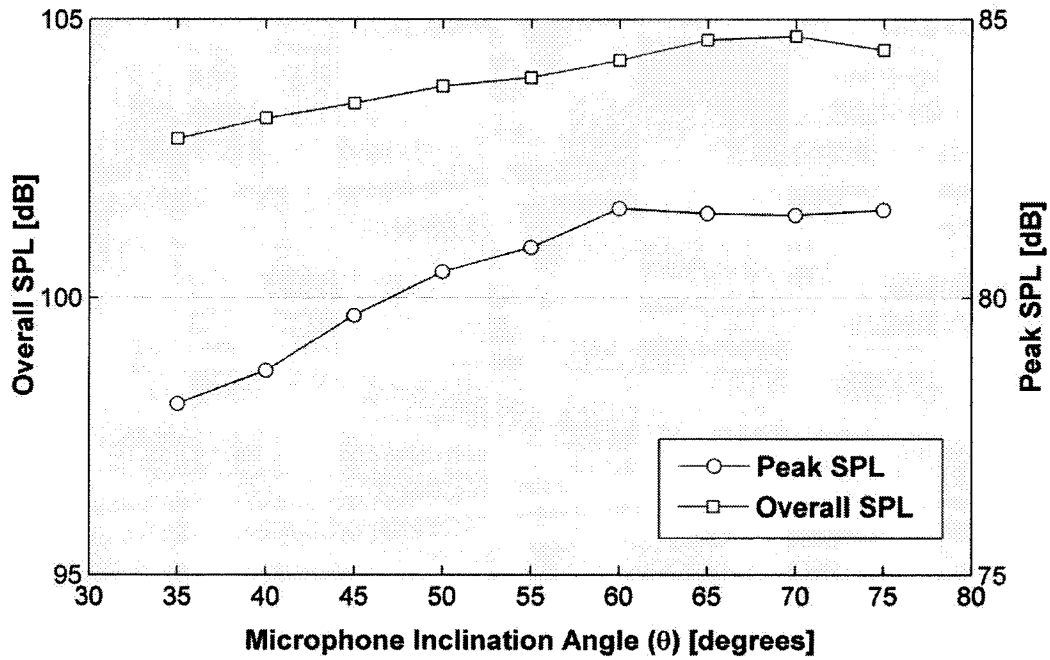

Figure 4-17: Overall SPL as a function of microphone inclination angle (θ).

A final microphone position of D = 0.3m and θ = 65° was chosen to ensure that all measurements were performed in the near field and that the microphone was positioned in the direction of maximum acoustic directivity without being subjected to any significant mean airflows due to impingement.

4.2.2.3 - Effect of Blower Noise

Due to the range of pressures and flow rates examined during in-lab testing, it was necessary to pressurize the jets using only one blower for low pressure configurations ($P < 2.5$ psi) and two blowers for higher pressure configurations ($P \geq 3.0$ psi). It was necessary to mount the blowers used to pressurize the air jets in close proximity to the measurement position, in order to maximize the range of pressures which could be supplied to the jets, by minimizing pressure drop due to flow through the supply piping.

A series of acoustic baffles were constructed using plywood and insulated with ROXUL® Enerwrap 80 mineral fiber insulation, in order to acoustically insulate the blowers and prevent direct acoustic radiation from the blower mounting location to the jet-jet impingement point and the measurement position.

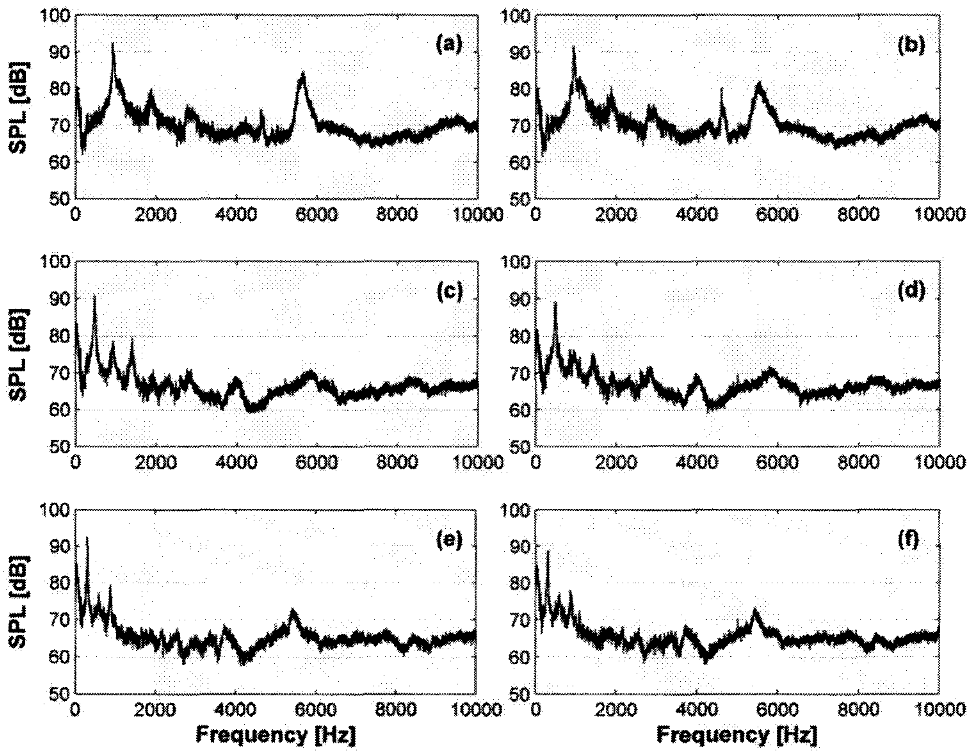

Figure 4-18: Effect of blower noise on acoustic spectra of galvanizing simulator. P = 2.5 psi (0.175 Bar) One Blower: z/h = 10 (a), 17.5 (c) & 25 (e). Two Blowers: z/h = 10 (b), 17.5 (d) & 25 (f).

The effects of the noise generated by the two centrifugal blowers were measured to ensure that noise generated by the blowers did not significantly impact the acoustic measurements of the jet-jet impingement. Three cases of basic jet-jet impingement were measured while being pressurized with one and two blower to determine the difference in the acoustic spectra, if any, due to blower noise. Figure 4-18 shows six acoustic spectra measured for jet-jet impingement cases of z/h = 10, 17.5 & 25, using one blower and two blowers, to generate a constant plenum pressure of P = 2.5 psi (0.170 Bar). There is no significant difference between the frequency content or amplitude of any portion of the two sets of the three impingement cases. It was concluded from these results that acoustic signature of the blower makes no appreciable contribution to the measurements of jet-jet impingement.

4.2.2.4 - Effect of the Steel Sheet as a Noise Source

Due to the long span between the upper and lower rollers that direct the sheet in both the in-plant and in-lab facilities, the steel sheet is susceptible to relatively small, low frequency vibrations due to turbulent buffeting of the impinging jets. These small vibrations were observed in both the in-plant and in-lab measurements. Because of these vibrations, the large surface area of the steel sheet and the proximity of the sheet to the measurement location, additional measurements were performed in order to investigate whether significant noise is radiated from the steel sheet. A single case of jet-jet impingement was considered, and measurements were performed with the bare steel sheet in place and with the sheet covered in a high damping, fibrous material. The material added to the mass of the sheet significantly, lowering its natural frequency and eliminating any detectable vibration of the sheet. One third octave spectra for both cases are shown in Figure 4-19. They show a 5 dB increase in acoustic band power level for the 1/3 octave band centered at 63Hz, near the natural frequencies of the various modes of the sheet for the case with the bare sheet. The band power levels for center frequencies exceeding 400 Hz show a slight reduction in band power level in the case of the covered sheet, which can be explained by the effect of the covering material which absorbs sound at higher frequencies. In general however, it does not appear that the sheet is responsible for any significant acoustic radiation, except in the case of the 63Hz octave, which is significantly removed from the frequency range of typical jet-jet impingement noise (300Hz $\leq f \leq$ 4500Hz). The bare steel sheet was found to be the source of some low frequency noise, due to sheet vibration, however this noise is far removed from the frequency range of interest. Further testing was carried out with a bare sheet

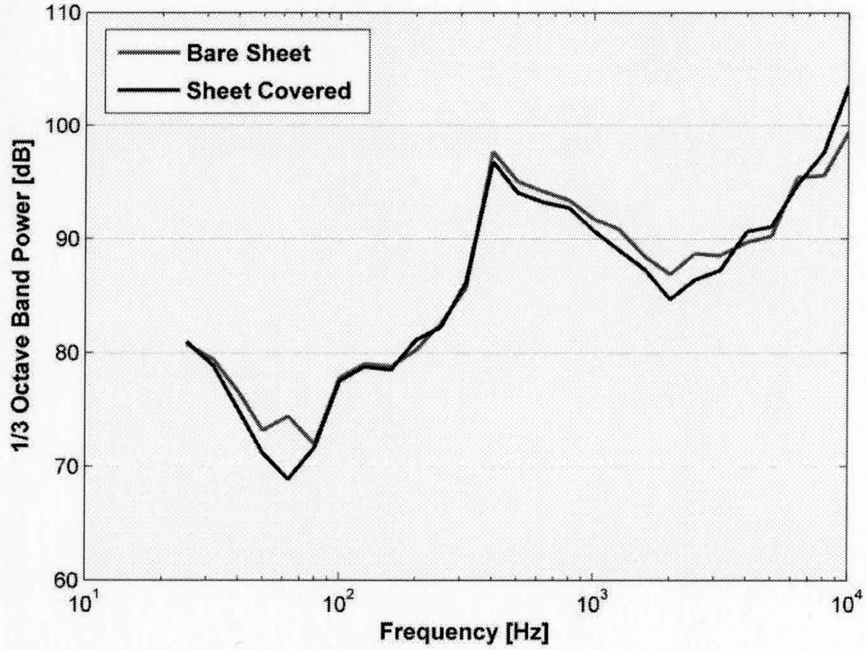

Figure 4-19: 1/3 octave spectra of cases with bare sheet vs. covered sheet.

4.2.3 - Jet Slot Profile Characterization

Measurements were performed to characterize the dimensions of the jet slot width along the length of the jet at various plenum pressures, to investigate the effect of plenum pressure and potential flex of the jet structure. Both jets were set to a nominal jet slot width of h = 1mm at a plenum pressure of P = 1.0 psi (0.068 Bar). Measurements of the jet slot width across the jet span made in increments of 50mm starting at the jet centerline (y = 0mm) were made using a Mitutoyo® digital caliper accurate to +/-0.01mm. The plenum pressure supplied to the jets was then increased to 2.0, 3.0 and 4.0 psi while not making any adjustments to the jet, with jet slot measurements being performed at the same locations for all pressures. Because the air knives were constructed largely of clear Acrylic, whose Young's modulus changes significantly with temperature, all measurements were performed after allowing the temperature of the airstream and jet surfaces to reach steady state.

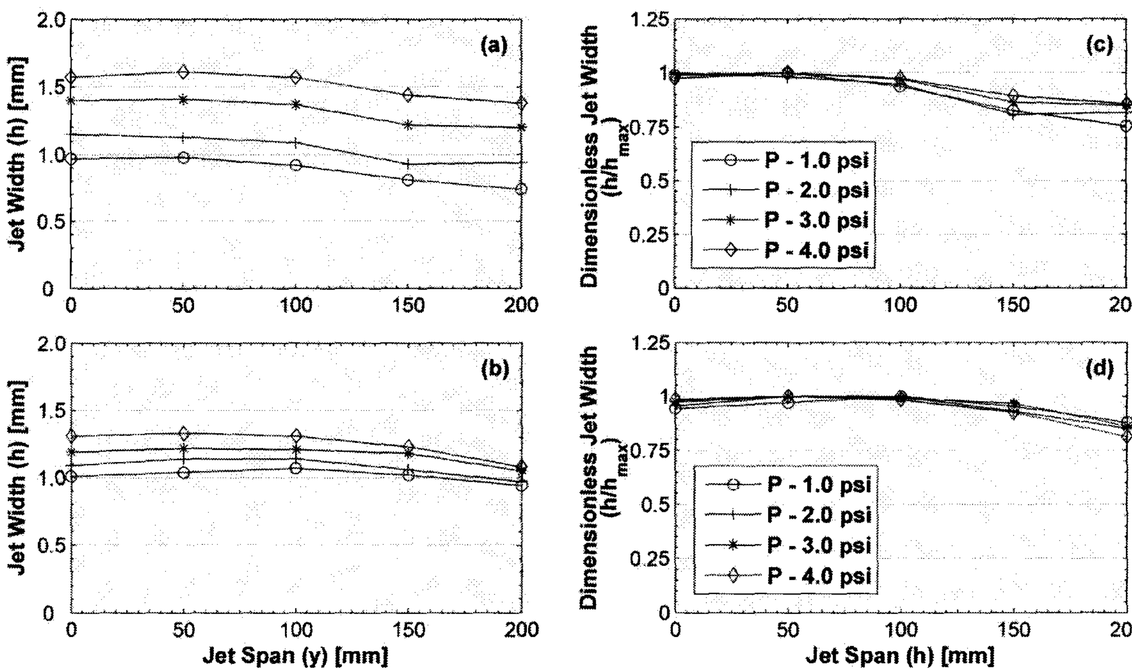

Figure 4-20: Actual and dimensionless jet slot width profiles for Jet #1 (a) & (c) and Jet #2 (b) & (d) for varying plenum pressures (*P*).

Figure 4-20 (a) & (b) and Figure 4-21 shows that both jets flex significantly under increasing plenum pressure, with Jet #2 being approximately three times stiffer than Jet#1, due to differences in construction. The dimensionless profiles of the two jets as shown in part (c) & (d) of Figure 4-20, shows that while the two jets are very susceptible to changes in pressure affecting the jet slot width, the pressure does not significantly affect the dimensionless profile across the span of the jet, meaning that if the jet slot width is set at a given value for each separate plenum pressure used, the jet slot profile will not change appreciably for different plenum pressures.

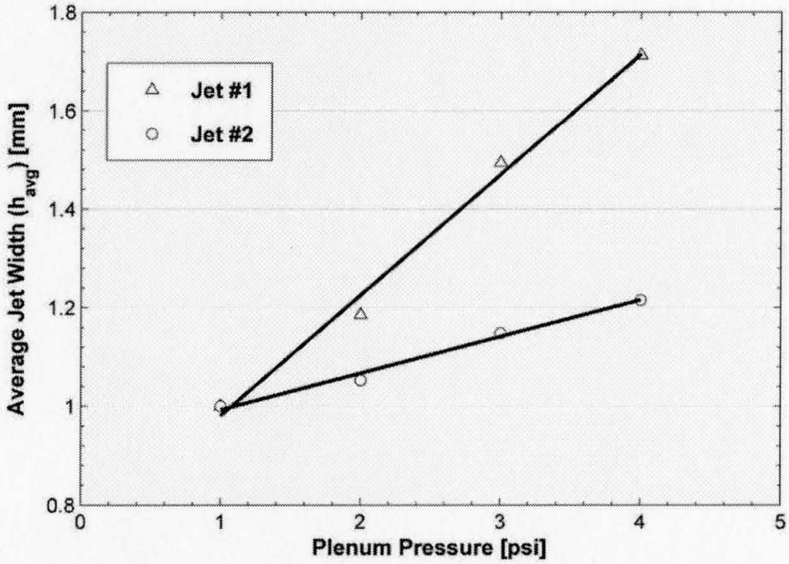

Figure 4-21: Average jet slot width as a function of plenum pressure (*P*), showing the different mechanical stiffness of Jet #1 & Jet #2.

The actual magnitude of the jet slot width is a crucial parameter for this study which needed to be controlled accurately. For all testing performed in the course of this study, plenum pressures were held constant during experimental runs, and the jet slot width was set using feeler gauges and checked using a digital caliper. Any adjustments of plenum pressure during testing were also accompanied by an adjustment in jet slot width to return it to its nominal value. Furthermore, all testing was performed after allowing the air supply from the blowers and jets to reach a steady, constant temperature.

Chapter 5 - BASELINE JET-JET CONFIGURATION

5.1 – DEFINING A BASELINE CONFIGURATION

Various steel manufacturers participating in this experimental study were informally polled in order to determine a commonly used baseline gas wiping configuration which would be used as a basis for studying the effect of various system parameters on the resultant noise production. Using this baseline configuration, noise maps of the process were constructed as functions of the plenum pressure P, and impingement ratio z/h, the two major parameters manipulated during the wiping process. The noise maps will give manufacturers and process engineers a quantitative measure of the relative noise level of any process configuration contained in the baseline. In addition, these maps, when used in conjunction with various coating weight models, will provide a means to optimize the wiping process to minimize the noise produced for a particular coating weight and line speed. Other gas wiping parameters such as jet inclination angle, the effect of baffle plates and various forms of jet incidence asymmetry were examined using the baseline configuration as a common starting point. The gas wiping process as it is currently used in steel galvanization is subject to a very wide range of process parameters. The current study aims to cover as much of that range as possible, however, using a commonly agreed to and commonly used baseline configuration ensures that the results obtained here will have maximum applicability and benefit to manufacturers.

The baseline configuration selected for this investigation was an aligned jet case (Δy = 0 mm) with equal jet inclination angles of α = 3°. Measurements used to construct the noise maps were made between impingement ratios of z/h = 5 to 30 and plenum pressures from P = 1.0 psi to 4.5 psi (0.068 Bar to 0.306 Bar) in increments of 0.5 psi (0.035 Bar). It should be noted that in some industrial cases the plenum pressures used exceed the range tested here, however, pressures exceeding P = 4.5 psi could not be tested due to pressure restrictions of the centrifugal blowers and of the air jets. Figure 5-1 shows the measurement grid utilized for performing all acoustics measurements of the baseline configuration and to create the noise maps shown later in this section. Acoustics measurements were made at each point shown on the measurement grid, and power spectrum, amplitude spectrum and power spectral density were obtained. In addition, averaged overall SPL and peak SPL using a peak and hold sound pressure level meter were recorded as well as the tone intensity, a measure of the acoustic tone strength, was determined for each measurement point. Measurements were made in series of runs made at a constant plenum pressure while varying the impingement ratio throughout its range from z/h = 5 to 30. Jet slot width (h) was adjusted after each pressure adjustment, prior to commencing the measurement run, and re-checked at z/h = 17 and 30 to ensure that no changes had taken place during a given run.

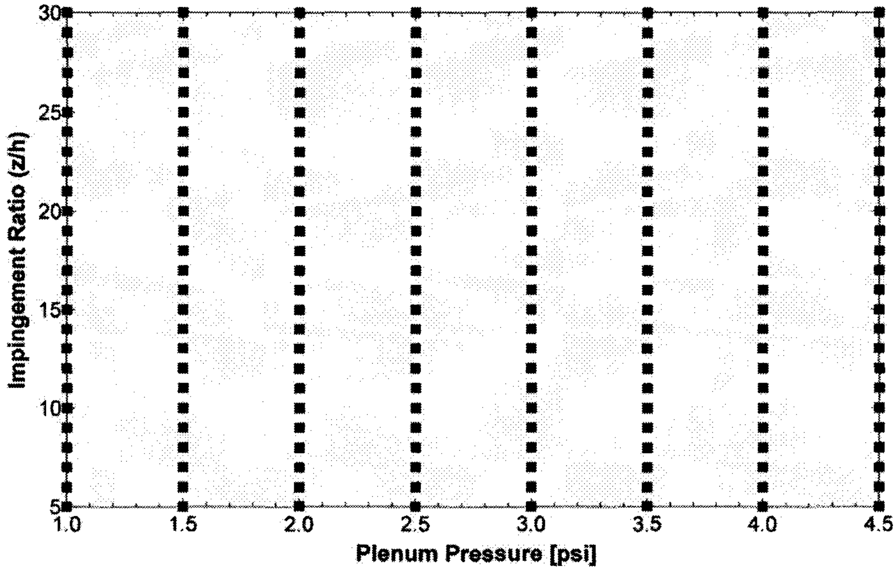

Figure 5-1: Measurement grid used for baseline jet-jet impingement configuration.

5.2 – ACOUSTIC RESPONSE

One case of a single measurement run made at a plenum pressure of P = 4.0 psi (0.272 Bar) for the baseline jet-jet impingement case will be presented in order to characterize some re-occurring features of the acoustic response. Figure 5-2 shows a waterfall plot of acoustic spectra for this case, with the amplitude shown in sound pressure level [dB], with a reference pressure of P_{ref} = 20 μPa. A number of strong acoustic tones in the spectra are evident, often occurring simultaneously for the same wiping configurations, with the frequency of each tone showing an approximately hyperbolic behavior, being inversely proportional to the impingement ratio, z/h. In order to more clearly illustrate some of the spectral behavior of the jet-jet impingement response, a contour plot of the same data is given in Figure 5-3. In this contour plot, the amplitude of a given spectra at each frequency is represented by the color of the plot, as shown by the color scale at the right of the figure. In addition, some of the key elements of the acoustic response have been labeled.

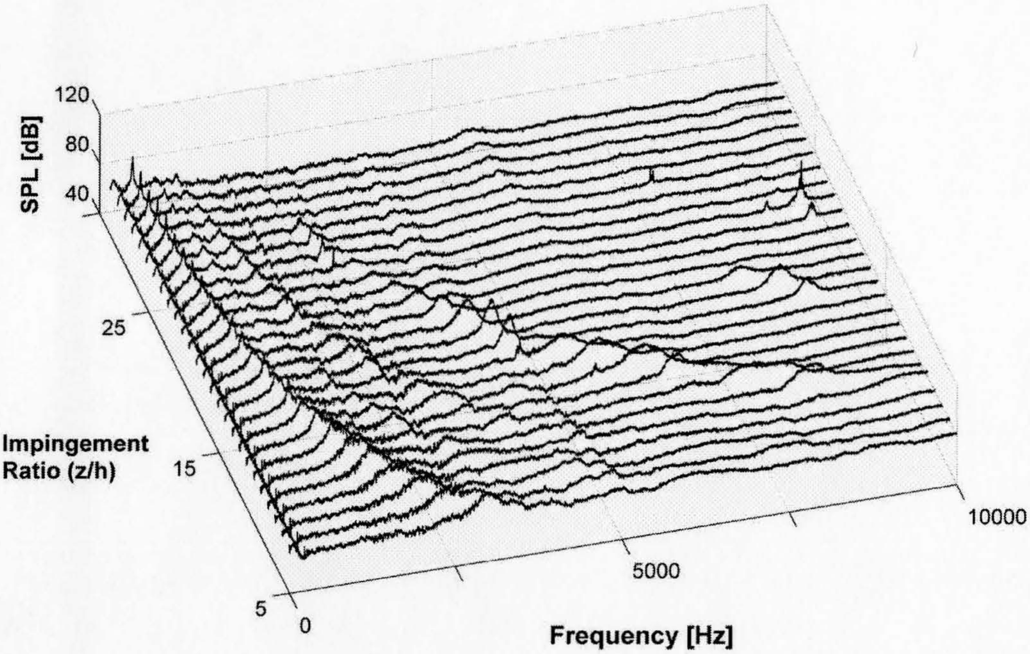

Figure 5-2: Waterfall plot of baseline jet-jet configuration for a plenum pressure of P = 4.0 psi (0.272 Bar).

Referring to the contour plot, the frequency response of the various acoustic tones generated in gas wiping are more evident. The primary jet-jet tone (f_j), as shown in Figure 5-3, is present throughout the entire range of impingement ratio tested ($5 \leq z/h \leq 30$) and the frequency of the mode is approximately inversely proportional to the impingement ratio. Additionally, the mode was present for all other plenum pressure cases tested from P = 1.0 psi to 4.5 psi. For a plenum pressure of 4.0 psi, the frequency of the primary jet-jet mode varies between $f_j \approx 3000$ Hz and $f_j \approx 350$ Hz between impingement ratios of z/h = 5 to 30 respectively. It will be demonstrated later in Section 5.3 of this thesis that the frequency of this mode and others encountered in gas wiping for all tested pressures is proportional to the flow velocity of the impinging jets, and approximately inversely proportional to the impingement ratio and the jet slot width (h). Also present throughout the entire range of impingement ratios for this case, are the secondary jet stage tones, f_{j2} & f_{j3}. These secondary jet-jet stage tones have frequencies of two and three times the primary jet-jet mode respectively. The amplitude of these tones is considerably lower than that of the primary tone for almost all jet-jet impingement configurations, and they do not present a significant impact to the overall noise level of any specific configuration. Both the primary and secondary jet-jet tones have been found to originate from the region of jet-jet impingement, near the two edges of steel strip. Evidence supporting this conclusion will be presented in later results of this thesis.

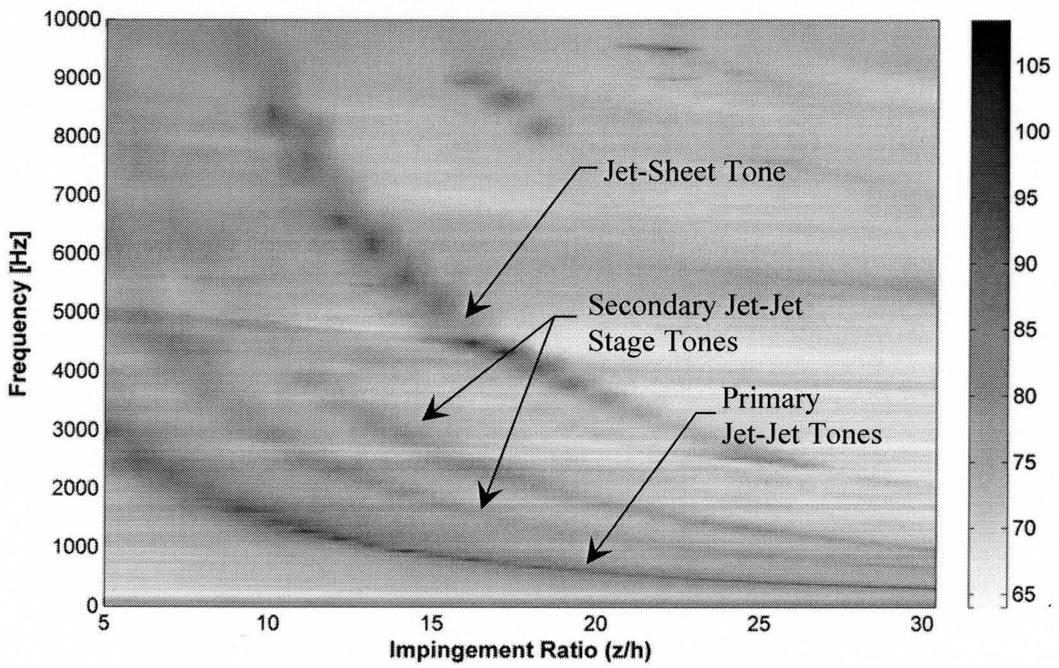

Figure 5-3: Contour plot of baseline jet-jet configuration for a plenum pressure of $P = 4.0$ psi (0.272 Bar).

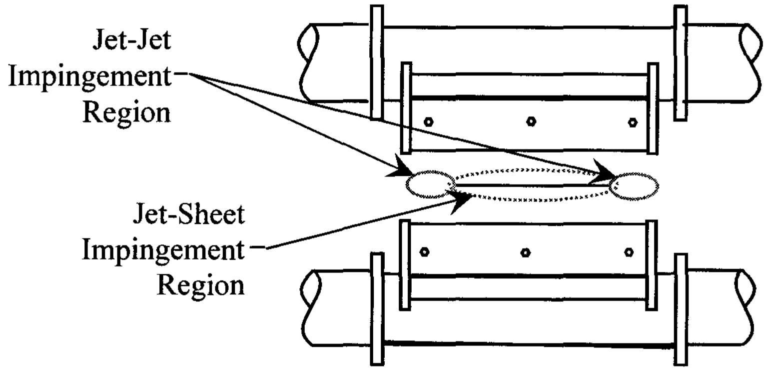

Figure 5-4: Simplified schematic of basis jet-jet impingement and the resulting impingement regions.

A higher frequency jet-sheet mode is also present for a limited range of impingement ratio for the baseline configuration. The range of test conditions at which the jet-sheet tones are generated varies with the velocity of the incident jet; higher flow velocities result in larger lock-in ranges, however in general this mode was observed between impingement ratio of z/h = 6 to 25. The jet-sheet tones were found to originate in the jet-sheet impingement region due to the impingement of the jets on the steel sheet. Evidence to support this finding, along with a more thorough investigation of this mode will be presented in Chapter 6 of this thesis. These jet-sheet tones are only present for the higher plenum pressure cases, typically exceeding P = 2.0 psi (0.136 Bar), and their acoustic pressure can be very significant. In some cases of the baseline configuration, they can be the dominant acoustic tone in the spectrum. As with the previously mentioned jet-jet modes, the frequency of the jet-sheet mode is also approximately inversely proportional to the impingement ratio, but is approximately four times higher than the primary jet-jet mode. A full analysis of the jet sheet modes will be discussed in Chapter 6 of this thesis.

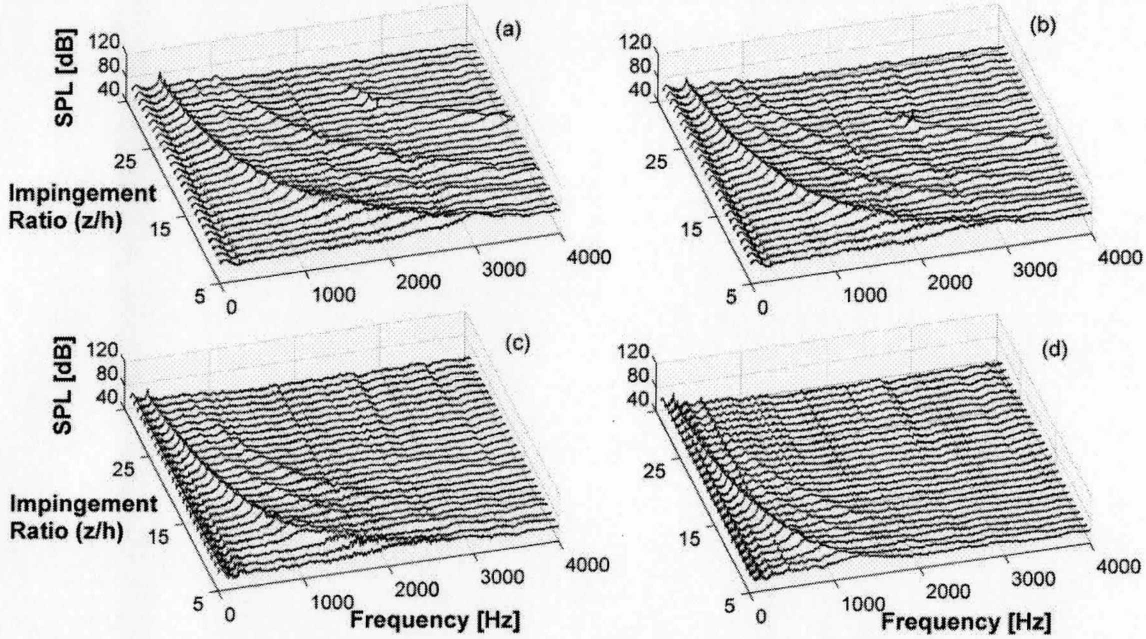

Figure 5-5: Waterfall plot of acoustic response of baseline configuration for *P* = 4.0 psi (a), 3.0 psi (b), 2.0 psi (c) and 1.0 psi (d).

Figure 5-5 and Figure 5-6 show waterfall plots of the acoustic spectra for individual four plenum pressures of P = 1.0, 2.0, 3.0 & 4.0 psi (P = 0.068, 0.136, 0.204 & 0.272 Bar) for frequency ranges to 4 kHz and 10 kHz, respectively. In all cases, the primary and secondary jet-jet modes are clearly excited throughout the entire tested range of impingement ratio. For the higher pressure cases, $P \geq 2.0$ psi shown in parts (a), (b) & (c) of the figure, the jet-sheet tones are visible for successively larger ranges of impingement ratio. The amplitude and frequency of both the primary jet-jet and jet-sheet tones increase with plenum pressure. A thorough analysis of the frequency of the primary jet-jet tones will be presented in the following section.

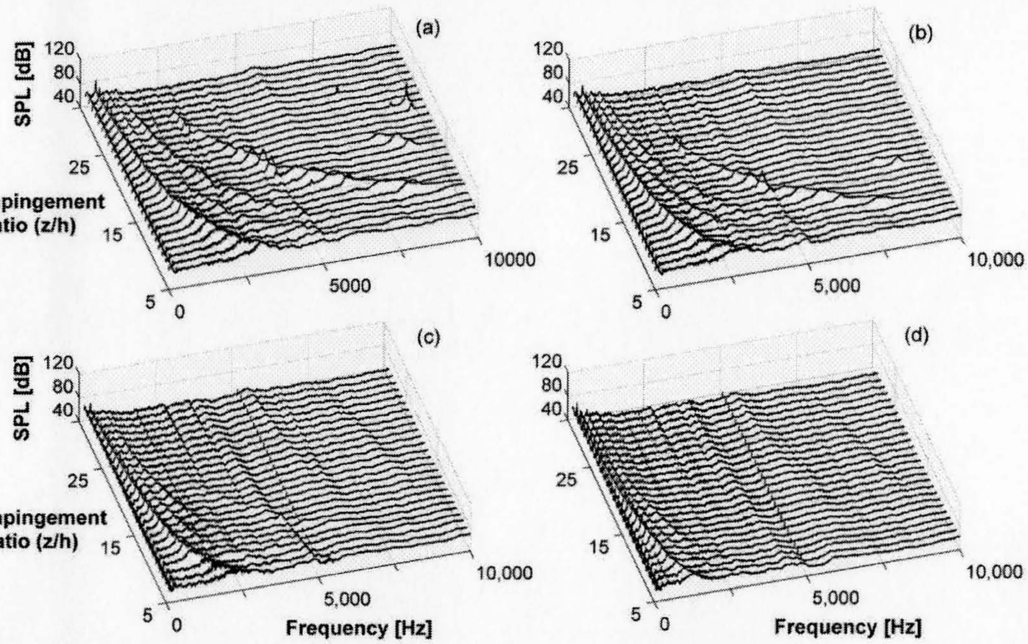

Figure 5-6: Waterfall plot of acoustic response of baseline configuration for P = 4.0 psi (a), 3.0 psi (b), 2.0 psi (c) and 1.0 psi (d).

5.3 – Baseline Configuration: Frequency Analysis

Figure 5-7 shows the frequency of the primary jet-jet and jet-sheet tones as a function impingement ratio for plenum pressure of P = 1.0, 2.0, 3.0 & 4.0 psi. The frequency of these tones scales approximately inversely with the impingement ratio, and is proportional to the isentropic jet velocity V_i. The isentropic jet velocity is simply the velocity of the jet resulting from the applied plenum pressure P in the case of an isentropic nozzle. The isentropic jet velocity was calculated using Equation (5-1), which is derived from the equation for a standard compressible flow, isentropic nozzle. No direct flow velocity measurements of the jet were performed during the course of this study. Figure 5-8 shows the frequency of the primary jet-jet mode divided by the isentropic jet velocity V_i, showing the collapse of the data along a single curve, which has been fitted by a power curve fit given by Equation (5-3). The constant and power coefficients of this expression were determined to three decimal places using a least squares regression, and fitted to the data using a power curve fit. This confirms that frequency of this jet-jet mode scales with the jet velocity, and allows the frequency of the entire data set to be calculated with a single expression as a function of the impingement ratio *z/h*, and the isentropic jet velocity, V_j. This expression was developed using a Strouhal number analysis shown in Equations (5-2) and (5-3) below.

$$V_i = c\sqrt{\frac{2\left[\left(\frac{P_o}{P_o+P}\right)^{-\left(\frac{\gamma-1}{\gamma}\right)}-1\right]}{\gamma-1}} \tag{5-1}$$

$$St_h = \left(\frac{f\cdot h}{V_i}\right) = C\left(\frac{z}{h}\right)^{-k} \tag{5-2}$$

$$f = 0.117\left(\frac{z}{h}\right)^{-1.273}\left(\frac{V_i}{h}\right) \tag{5-3}$$

Table 7: List of plenum pressures tested and resulting isentropic flow velocities and Reynolds numbers.

P [psi]	*P* [Bar]	V_i [m/s]	Re_h
1.0	0.068	105.7	7207
1.5	0.102	128.7	8777
2.0	0.136	147.8	10079
2.5	0.170	164.3	11207
3.0	0.204	179.0	12212
3.5	0.238	192.4	13122
4.0	0.272	204.6	13957
4.5	0.306	216.0	14731

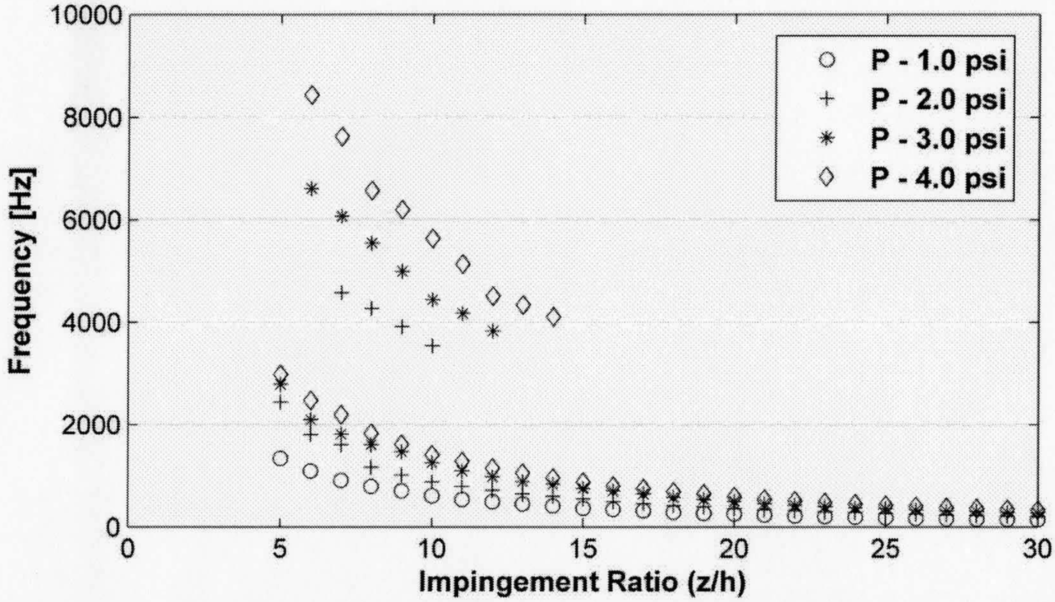

Figure 5-7: Frequency of primary jet-jet and jet-sheet acoustic tones as a function of impingement ratio, for varying plenum pressures.

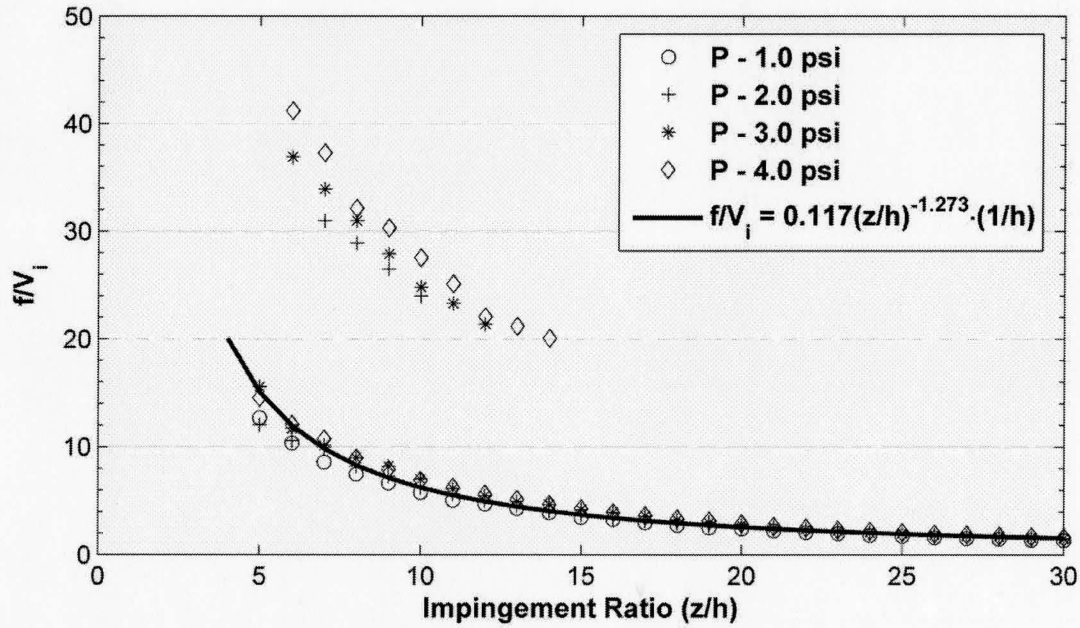

Figure 5-8: Frequency of the dominant acoustic mode divided by the isentropic jet velocity as a function of plenum pressure (*P*) and impingement ratio (*z*/*h*).

As a comparison, and to validate this expression to predict frequency of results from other data sets, results of the measurement of similar jet-jet configurations of Dubois (2001a, 2001b) and Park (2001) have been plotted with the power fit expression in Figure 5-9. The measurements performed by Dubois, which are shown here, are obtained from both in-plant and in-lab facilities, and the measurements of Park were performed exclusively in a manufacturing environment. The figure shows that in general, the expression is a reasonably good fit for these measurements, which are comprised of configurations with varying jet slot widths, impingement ratios, and plenum pressures.

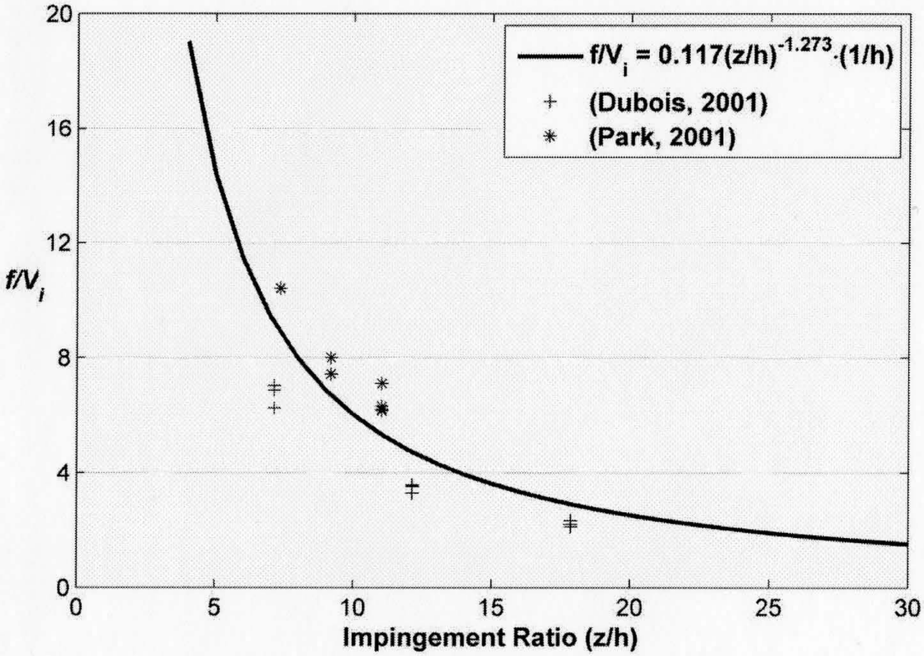

Figure 5-9: Measurements of Dubois (2001a, 2001b) and Park (2001) compared to power fit of measurements of the current study.

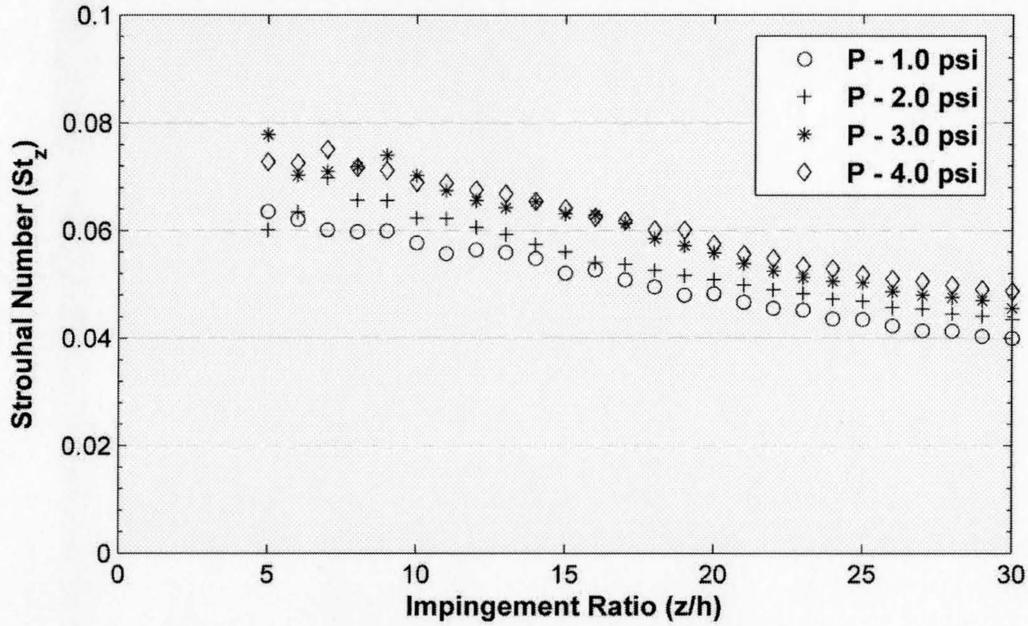

Figure 5-10: Strouhal number (St_z) of the dominant acoustic mode for jet-jet impingement as a function of plenum pressure (*P*), and impingement ratio (*z/h*).

The primary and secondary jet-jet modes are thought to originate from a flapping instability of the planar jet, although no direct evidence exists in the literature that confirms this hypothesis. A study by Goldschmidt & Bradshaw (1973) found that the flapping mode of a free turbulent planar jet with $Re_h = 2.6\times10^4$ and an aspect ratio of $L_j/h \approx 50$ occurred at a Strouhal number of approximately $St_h = 5.5\times10^{-3}$, which is in the middle of the range of Strouhal numbers found for jet-jet impingement. Varieras et al. (2007) performed flow visualizations of an impinging confined laminar plane jet on a flat plate and observed that the jet oscillated in a flapping column mode. The flapping or "preferred" mode as it is sometimes called in the literature, occur at a Strouhal number approximately two orders of magnitude less than traditional unstable frequencies predicted by linear stability theory for vortex shedding and other typical shear layer instabilities.

5.4 – Baseline Configuration: Noise Maps

In order to give manufacturers broad overview of noise in the gas wiping process, noise maps were generated using measurements performed at each gas wiping configuration. Maps showing overall sound pressure level in dB (P_{ref} = 20 μPa) and tone intensity were produced a function of the plenum pressure supplied to the jets and the impingement ratio. These maps will allow manufacturers to see the trends in the overall levels of noise as well as the spectral behavior, and when used in conjunction with expressions developed to predict frequency of the acoustic tones, gives manufacturers a complete picture of noise in the gas wiping process within the range of parameters tested.

The overall sound pressure level and tone intensity were obtained for the measurements taken at each position and a series of noise maps were constructed to illustrate the overall behavior of the gas wiping process in the baseline configuration. Figure 5-11 shows the noise map of the baseline wiping configuration for averaged overall sound pressure level as a function of plenum pressure P, and impingement ratio z/h. This figure clearly shows that the noise generated by the wiping process increases with increasing plenum pressure supplied to the jets, and thus the incident jet velocity. The noise level decreases with increasing jet-to-strip distance z, and impingement ratio z/h. These noise maps will give manufacturers insight and a broad overview into noise generation in the gas wiping process that was not previously available, and give operators and process engineers the ability to quantitatively assess a myriad of possible gas wiping configurations, and allow for reductions in overall sound pressure levels. The figure however, only displays the overall sound pressure levels at each point and does not give any indication of the spectral content such as to the presence or magnitude of discrete acoustic tones within the spectra, which may result in annoyance factors being added to the overall level in an industrial setting.

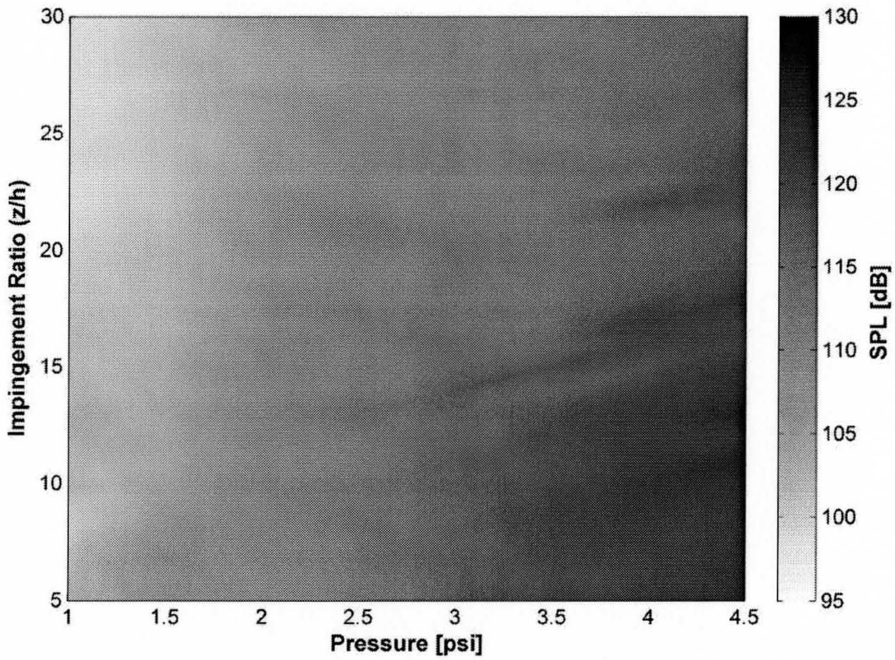

Figure 5-11: Average overall SPL for baseline jet-jet configuration as a function of plenum pressure (*P*) and impingement ratio (*z*/*h*).

In order to characterize and quantify the strong acoustic tones generated for the configurations tested, a similar map of tone intensity is shown in Figure 5-13. For the purposes of this investigation, tone intensity will be defined as the difference in decibels between the average sound pressure level of the acoustic spectrum between 0 Hz and 10 kHz, and the peak sound pressure level of the acoustic tone of the same spectrum. Figure 5-12 shows an example of an acoustic spectrum from the baseline configuration with a dominant jet-sheet mode. The average sound pressure level and sound pressure level of the dominant peak are shown, along with the resulting tone intensity shown in decibels. Figure 5-13 shows that the tone intensity of a given configuration is largely a function of the impingement ratio, with stronger acoustic tones being generated for configurations with larger jet-to-strip distances. The tone intensity appears to be nearly independent of the plenum pressure and the resultant isentropic jet velocity, although in general lower tone intensities are observed for higher jet velocities.

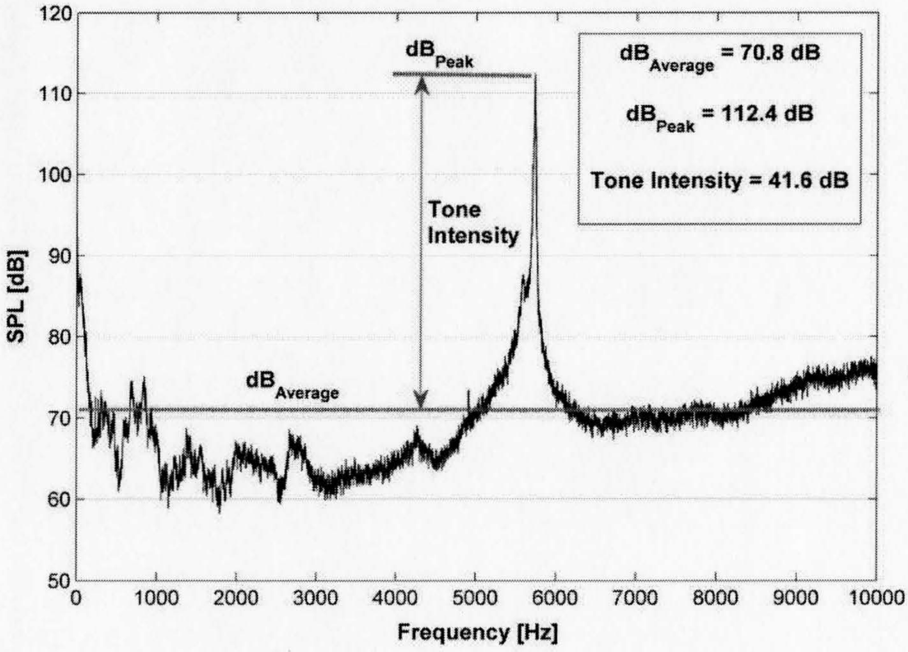

Figure 5-12: Acoustic spectra of jet-plate acoustic tone and resulting tone intensity.

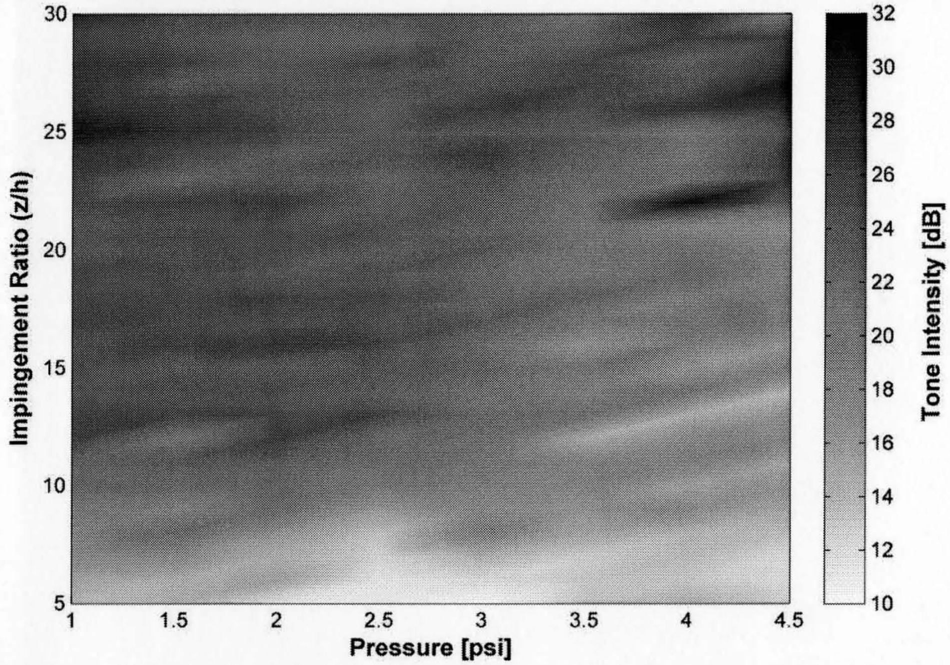

Figure 5-13: Tone intensity of the dominant acoustic mode as a function of plenum pressure (*P*) and impingement ratio (*z/h*) for baseline configuration.

In a practical industrial environment, the effect of the overall sound pressure and the tone intensity at any particular configuration will have to be evaluated together, to obtain a final overall perceived sound pressure level. Standards of evaluating noise vary greatly between different areas, with a multitude of different criteria and evaluation techniques being employed to deal with industrial noise with strong acoustic tones. Typically, some spectral weighting is applied to the acoustic spectrum, where A, C and Z-weighting are the most common, and depending on the strength and frequency of the acoustic tone, some annoyance factor will be added to the weighted overall sound pressure level. The two noise maps will have to be evaluated together to determine the overall perceived noise level map based on local standards and practices. Once the overall perceived noise level map has been constructed, the process may be optimized to minimize the perceived noise level for targeted coating weight and line speed. Further details on process optimization will be outlined in Chapter 8 of this thesis.

Chapter 6 - JET-PLATE IMPINGEMENT

In previous investigations by Dubois (2001a, 2001b) and Park (2001), consisting of both in-lab and in-plant measurements of similar configurations, the presence of high frequency jet-sheet tones has not been observed. This discrepancy may be explained by the use of bowtie air knives in some of the previous studies. The non-constant jet slot width of a bowtie air knife has the effect of continuously changing the impingement ratio over the span of the jet, L_j. This configuration is physically analogous to inclining the sheet along the span for a nozzle with a flat profile, so that one edge of the sheet is closer to the nozzle than the other. By varying the impingement ratio over the jet span, the frequency of the acoustic tone also continuously varies, and the jet is unable to lock-in at a distinct frequency over the entire jet span. In Section 6.5 of this thesis, the effect of span-wise inclination of the plate on jet-plate tones is investigated, and the lock-in of such tones is found to be very sensitive to span-wise inclination, completely suppressing the jet-plate mode for an inclination of only 1.25°. Bowtie air knives, with their continuously varying impingement ratio, may have a similar effect explaining their absence of these modes in industrial cases utilizing these gap profiles.

Significant jet-sheet tones were found to arise in the tested baseline configuration for plenum pressures exceeding P = 2.0 psi (0.136 Bar) over a limited range of impingement ratios, typically from z/h = 7 to 17. As mentioned earlier, the two distinct tones observed in the baseline configuration are thought to be originating from the two separate jet impingement regions: the jet-jet impingement region for the primary and secondary jet-jet tones, and the jet-sheet impingement region for the higher frequency jet-sheet tones. In order to further investigate the jet-sheet modes arising in the baseline configuration, and to separate any effects due to sheet motion and strip vibration arising from turbulent buffeting, experiments were performed of a single plane jet impinging at an angle of $\alpha = 0°$ on an "infinite" flat plate. A simplified schematic of the test configuration is shown in Figure 6-1. The plate has been rigidly mounted to avoid any motion or vibration and to provide a stationary impingement interface. The plate used for impingement measured 200mm x 490mm and was constructed of $^3/_8$" plate aluminum and was mounted on a manual three axis traverse capable of movement in the *x-y-z* direction to within ±0.02 mm. Inclination of the jet-plate impingement was made possible by means of a pivot allowing span-wise inclination and by inclining the jet about it axis relative to the plate to allow for stream-wise inclination. Impingement of the jet took place entirely within the confines of the flat plate, with no portion of the jet not impinging on the plate. The same ½" GRAS pressure microphone and data acquisition system was used for all measurements. Details of the experimental apparatus used are outlined in full in Chapter 3 of this report.

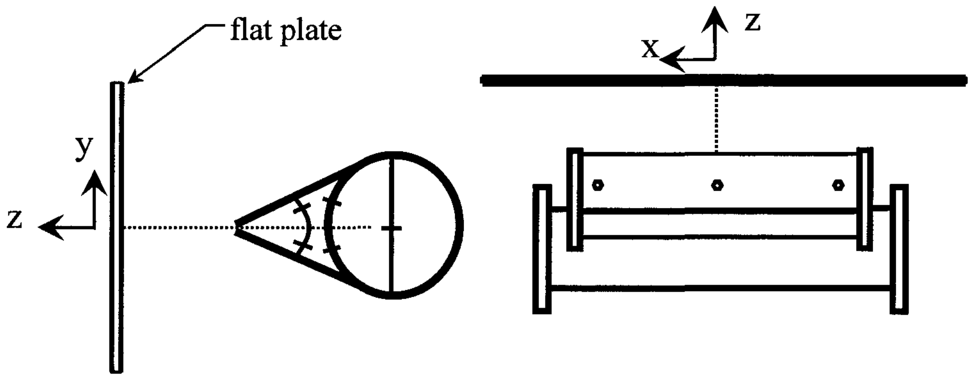

Figure 6-1: Simplified schematic of jet-plate impingement setup.

6.1 – Effect of Microphone Proximity

The effect of microphone proximity D and microphone inclination angle θ was investigated in order to assess any directionality effects on the amplitude and spectral content of the noise, as well as to ensure that all noise measurements were performed in the near field. Figure 6-2 shows the effect of microphone distance on the overall sound pressure level of jet-plate impingement. The sound pressure shows an exponential decay for the entire range of microphone distance D tested ($0.05\text{m} \leq D \leq 0.6\text{m}$), indicating that all measurements within this range are within the near field. Figure 6-3 shows the peak and overall sound pressure level the noise as a function of the microphone inclination angle, θ. It is clear that there is some directionality of the magnitude of the peak and overall SPL, with the peak level reaching a maximum at a microphone inclination angle of $\theta = 65°$, and the overall sound pressure level increasing steadily for increasing microphone inclination up to 70°. For microphone inclination angles exceeding 70°, the microphone is exposed to significant mean airflow, caused by the re-directed airflow from the jet-plate impingement, which artificially increases the overall sound pressure level due to increased low frequency noise. With the exception of this low frequency noise increase at large inclination angles, the spectral content of the jet-plate impingement noise is relatively constant over the range of microphone inclination angle tested. Figure 6-4 shows a waterfall plot of jet-plate impingement spectra for varying microphone inclination angle for $\theta = 35°$ to $\theta = 80°$.

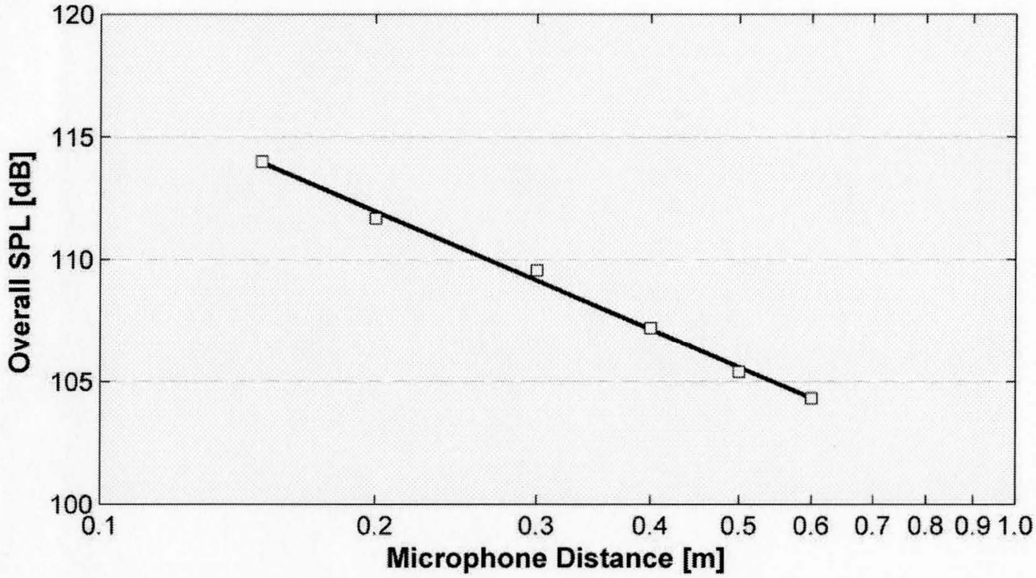

Figure 6-2: Effect of microphone distance *D* on the overall SPL for jet-plate impingement. θ = 65°.

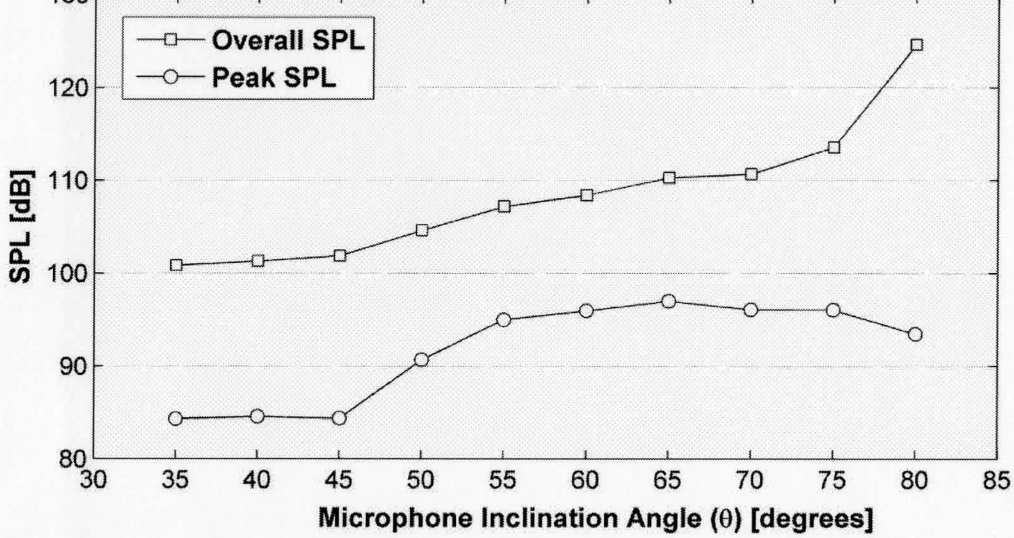

Figure 6-3: Effect of microphone angle θ on the overall SPL and the peak SPL of the acoustic tone for jet-plate impingement. D = 0.3 m. [lines shown for visual aid only]

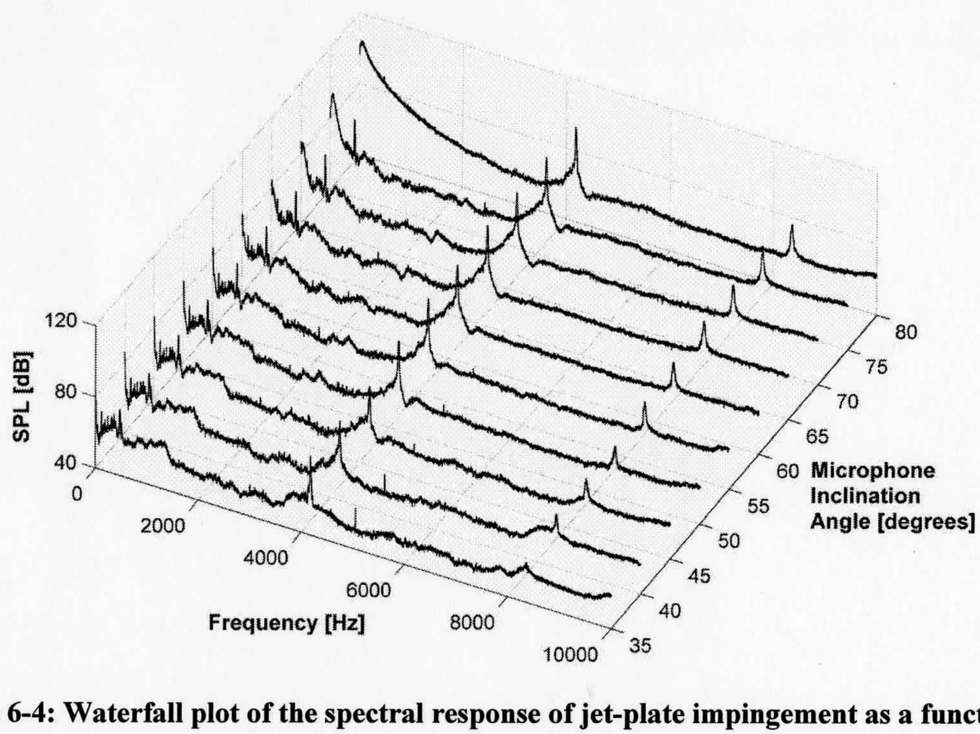

Figure 6-4: Waterfall plot of the spectral response of jet-plate impingement as a function of microphone inclination angle θ. D = 0.3m.

6.2 – Jet-Plate Acoustic Response

Measurements of the jet-plate acoustic response were taken in a series of eight experimental runs at pressures from P = 1.0 psi to 4.5 psi in increments of 0.5 psi for impingement ratios from z/h = 1 to 30. Results of pressure runs of P = 1.0, 2.0, 3.0 and 4.0 psi will be shown here, although all experimental runs showed similar trends in frequency and amplitude. Figure 6-5 shows a series of waterfall plots for the different plenum pressure cases showing the development of the jet-plate modes. The behavior of this tone is very similar to that observed for the baseline configuration, however the tone amplitude is stronger for the case of jet-plate impingement, and the frequency of the tone occurs over a narrower band of frequency, which is a consequence of the lack of sheet movement in the case of jet-plate impingement. The frequency of the tones for the two cases of jet-sheet and jet-plate impingement occurs at the same frequencies for similar configurations of plenum pressure and impingement ratio. This similar behavior confirms that the jet-sheet/jet-plate tone is originating from the jet impinging on a flat surface, and the lack of any jet-jet modes confirms that the jet-jet mode arises from instability in the jet-jet impingement region at the edge of the sheet.

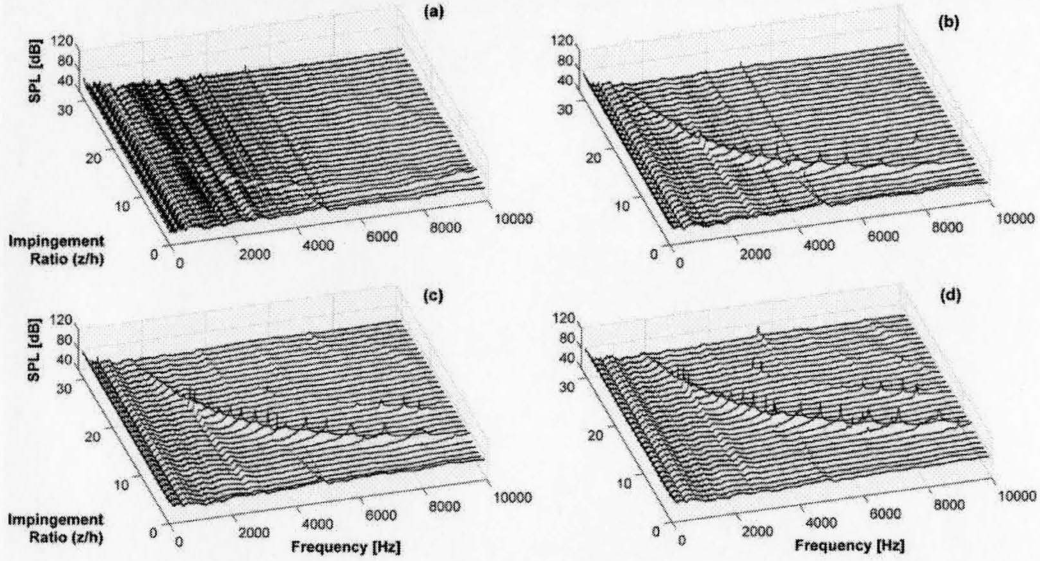

Figure 6-5: Waterfall plot of acoustic response of jet-plate impingement for plenum pressures of $P = 1.0$ psi (a), 2.0 psi (b), 3.0 psi (c) & 4.0 psi (d).

Figure 6-6 shows two spectra taken from two similar configurations of jet-sheet and jet-plate impingement, which shows the effect of strip vibration and motion on the strength and spectral content of the acoustic tones. Both cases shown are for a system configuration of $P = 4.0$ psi (0.272 Bar) and $z/h = 15$ with the jet-sheet spectra taken from the baseline configuration results and the jet-plate spectra from the current set of jet-plate impingement results. It is clear that the peak of the jet-plate case is much stronger, with a peak sound pressure level nearly 10 dB higher than the case of jet-sheet impingement, and the frequency of the acoustic tone is concentrated in a much narrower band of frequency. This is due to the stationary impingement interface and constant impingement ratio in the case of the jet-plate case. It is also interesting to note that the total acoustic energy of the jet-plate tone is more than twice as large as the tone of the jet sheet case when integrating the acoustic spectra over the same frequency range, indicating that strip vibration is interfering with the formation of the jet-sheet mode.

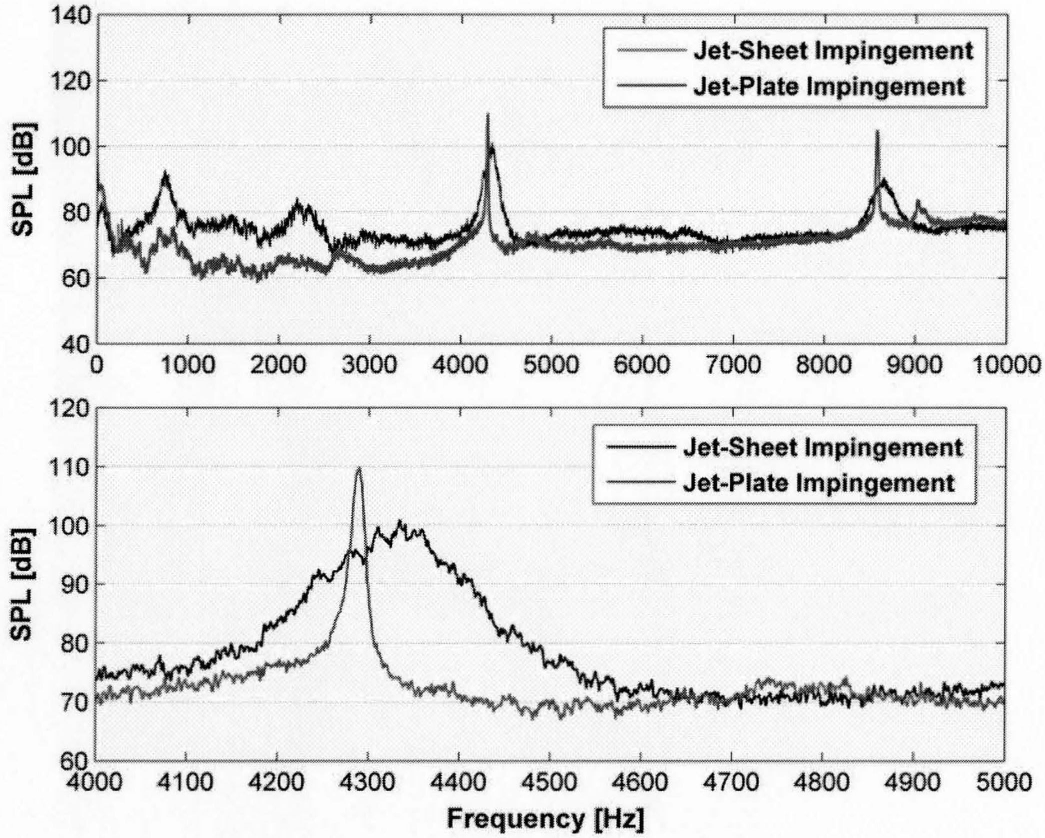

Figure 6-6: Spectra of jet-sheet and jet-plate impingement for P = 4.0 psi (0.272 Bar), z/h = 15 showing the effect of sheet vibration on acoustic tone strength.

6.3 – FREQUENCY ANALYSIS

The frequency response of the jet-plate mode, as it has been mentioned in the previous section, is approximately inversely proportional to the impingement ratio and proportional to the isentropic jet velocity V_i. Figure 6-7 shows the frequency of the dominant acoustic tone for jet-plate impingement as a function of varying impingement ratios. For the pressure runs of 1.0 psi and 1.5 psi (0.068 Bar & 0.105 Bar), there was no significant excitation of jet-plate modes. Jet-plate tones were excited beginning at pressures of 2.0 psi, with excitation beginning at z/h = 6 for all cases and extending to successively larger ranges of impingement ratio for progressively higher plenum pressures. Figure 6-8 shows the acoustic tone frequency divided by the isentropic jet velocity as a function of varying impingement ratios. The data collapses along a single curve which has been fitted with a power curve given by Equation (6-1). The constant and power coefficients of this expression were determined to three decimal places using a least squares regression, and fitted to the data using a power curve fit. The frequency of this mode both in the jet-sheet and jet-plate cases can be predicted to within ~8% of the actual frequency by this equation.

$$f = 0.462\left(\frac{z}{h}\right)^{-1.146}\left(\frac{V_i}{h}\right) \tag{6-1}$$

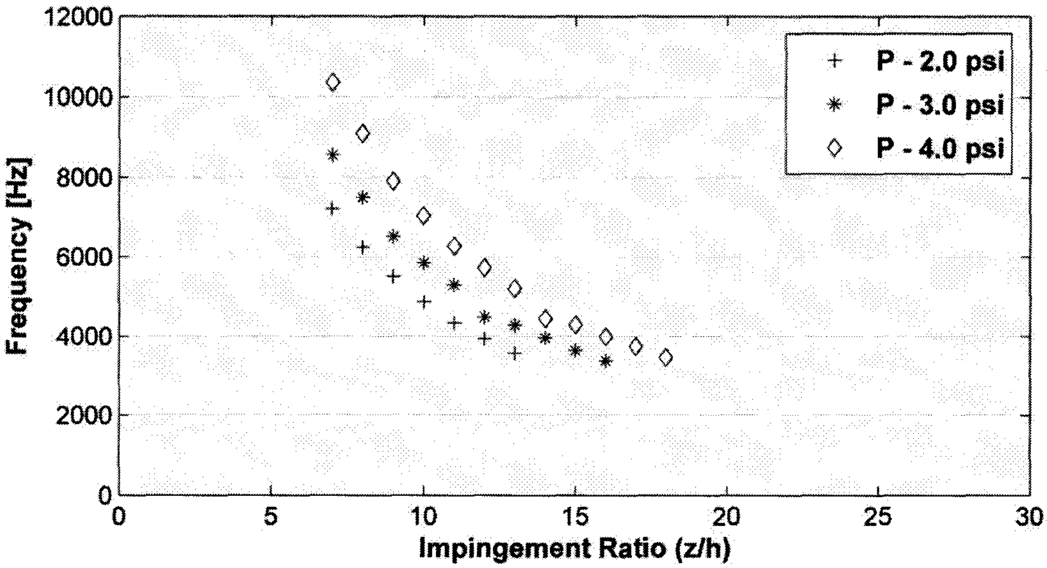

Figure 6-7: Frequency of the dominant acoustic tone for jet-plate impingement.

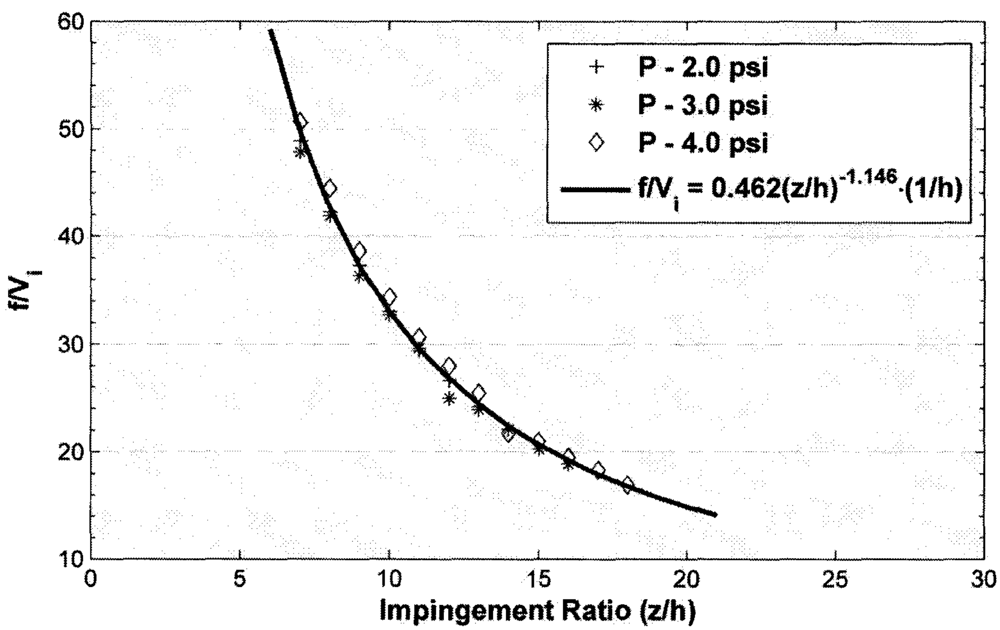

Figure 6-8: Frequency of the dominant acoustic tone divided by isentropic jet velocity (V_i) for jet-plate impingement as a function of plenum pressure (P) and impingement ratio (z/h).

As shown in Figure 6-9, the Strouhal number (St_z) based upon the impingement distance z for the jet-plate tones is approximately constant for all the pressure cases, with a weak dependence on the impingement ratio. The Strouhal number for this mode averages $St_z = 0.309$ for all the configurations tested.

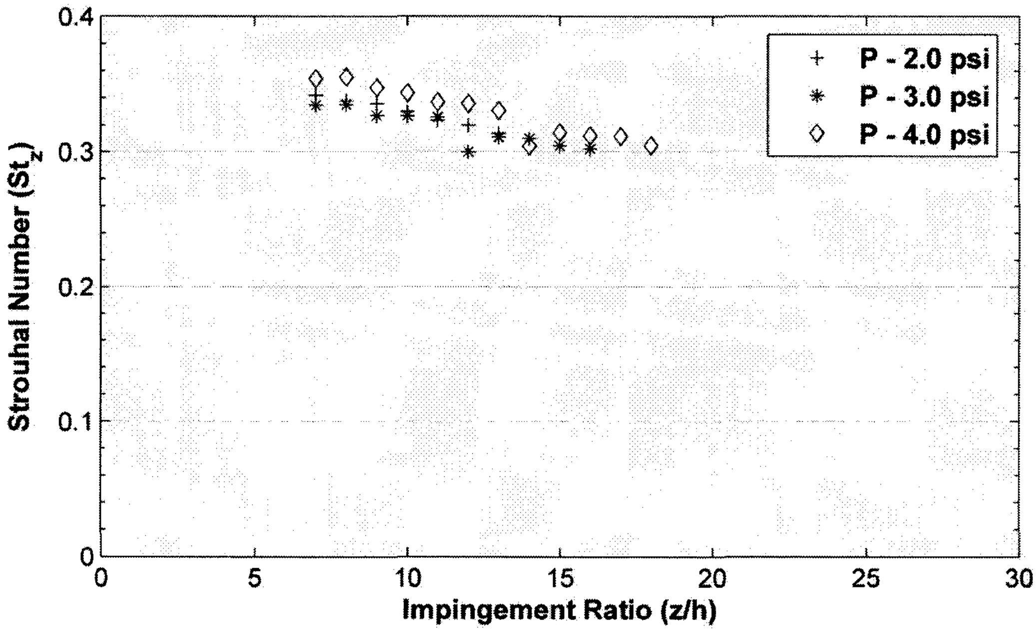

Figure 6-9: Strouhal number (St_z) of the dominant acoustic mode for jet-plate impingement as a function of plenum pressure (*P*) and impingement ratio (*z/h*).

6.4 – JET-PLATE IMPINGEMENT: NOISE MAPS

Noise maps showing averaged overall sound pressure level and tone intensity were constructed to give an overview of the noise generated as a result of jet-plate impingement. Figure 6-10 shows the tone intensity, as defined in Figure 5-12, for all tested configurations of jet-plate impingement. From this figure, it is clear that there are no significant tones generated for the pressure runs of 1.0 and 1.5 psi. Significant acoustic tones are present for plenum pressures of P = 2.0 psi and greater starting at an impingement ratio of z/h = 6. The generation of this tone occurs for successively larger ranges of impingement ratio for increasing pressures, and seems to occur over two distinct regions. The reason for tone production over two ranges of z/h is not currently known.

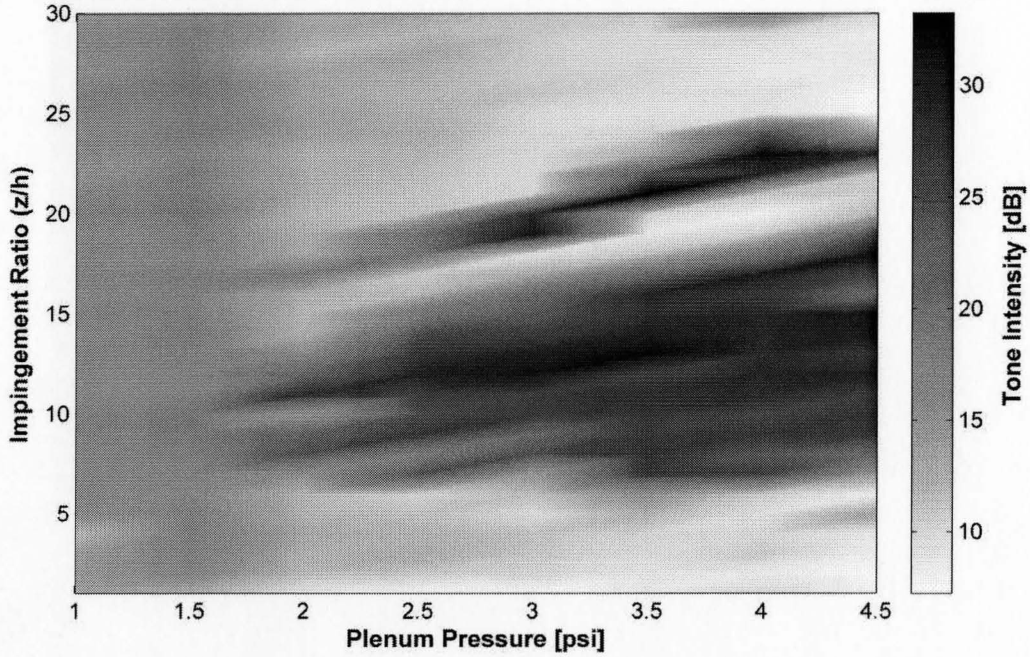

Figure 6-10: Tone intensity as a function of plenum pressure (*P*) and impingement ratio (*z/h*) for jet-plate impingement.

Figure 6-11 shows the noise map of the averaged overall sound pressure level of jet-plate impingement. It is clear from comparison of Figure 6-10 and Figure 6-11 that the overall sound pressure level of jet-plate impingement is strongly dependant on the acoustic tone intensity. The acoustic response of jet-plate impingement has much lower levels of broadband noise and much larger acoustic tones compared to jet-jet impingement. The overall sound pressure levels encountered in jet-plate impingement are as high or higher for like configuration of jet-jet impingement, despite the fact that these jet-plate measurements were performed using only one jet, as opposed to two for jet-jet impingement.

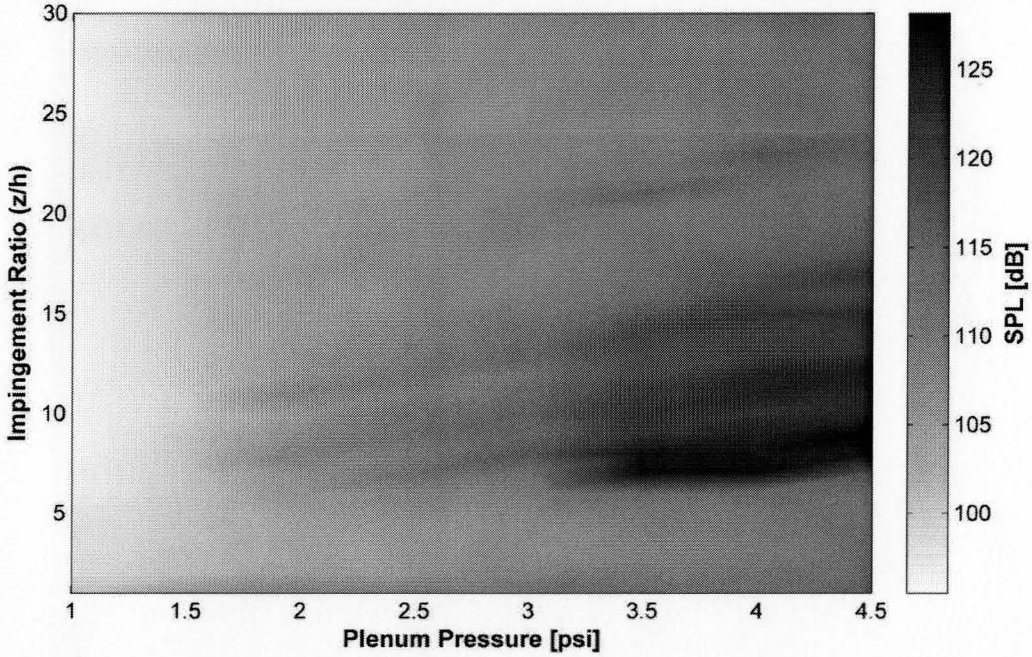

Figure 6-11: Averaged overall SPL as a function of plenum pressure (*P*) and impingement ratio (*z/h*) for jet-plate impingement.

6.5 – Effect of Plate Inclination

One configuration which is a particular risk for the production of large jet-plate tones in the gas wiping process, are cases with edge baffles. Edge baffles typically consist of flat plates which are inserted into the jet-jet impingement region, in order to prevent the collision of the opposing jets, and eliminate the generation of jet-jet tones. The jet impinging on the rigid baffle plate however, presents a significant risk for the promotion of jet-plate tones. In this section, the jet-plate acoustic tones and their sensitivity to plate inclination, both in the span-wise and stream-wise directions are investigated. The results of this investigation may be used to improve the design of baffle plates, and make them less susceptible to strong jet-plate tones.

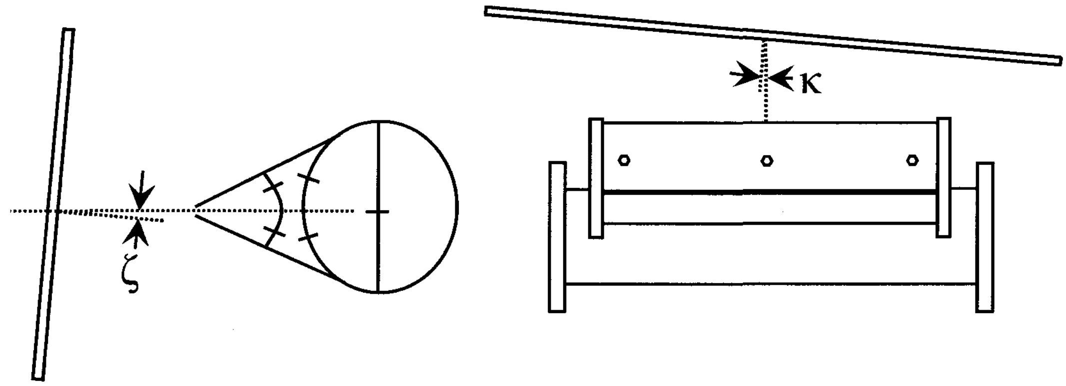

Figure 6-12: Basic schematic showing stream-wise (ζ) and span-wise (κ) plate inclination angles.

Figure 6-12 shows simplified schematic of stream-wise (ζ) and span-wise (κ) plate inclination. The purpose of these measurements is to investigate possible methods to suppress or reduce the formation of jet-plate modes. It has been shown that these jet-plate tones can have significant amplitudes, and in some cases, they can be the dominant acoustic mode for specific configurations. Span-wise inclination angles of κ = 1.25°, 2.5° and 5.0° and stream-wise inclination angles of ζ = 5°, 10° and 15° were studied for varying impingement ratios, at a constant plenum pressure of P = 3.0 psi (0.204 Bar) . The results are presented in the two sections below.

6.5.1 – Effect of Stream-wise Inclination

The effect of stream-wise inclination, which is physically analogous to the jet inclination angle in the gas wiping process, is investigated in order to determine its effect on the gas wiping process. Inclination angles of ζ = 0°, 5°, 10° and 15° for impingement ratios from z/h = 1 to 20 and a plenum pressure of P = 3.0 psi (0.204 Bar) are shown in Figure 6-13 below. The figure shows a series of water fall plots with the acoustic response of the jet-plate impingement as a function of impingement ratio for varying stream-wise inclination angles. The figure clearly shows that increasing the stream-wise inclination angle from 0° to 15° completely suppresses the formation of the jet-plate mode, and that significant reductions in tone amplitude are achieved for each inclination angle tested. This is more clearly shown in Figure 6-15, which shows the peak sound pressure level of the jet-plate tone as a function of impingement ratio for the different stream-wise inclination angles. This result may be useful in cases of gas wiping with strong jet-plate/jet-sheet modes, where simply by increasing the jet inclination angles, the formation of such tones may be reduced or eliminated. In addition, design of baffle plates may be modified in order to increase the effective stream-wise inclination angle.

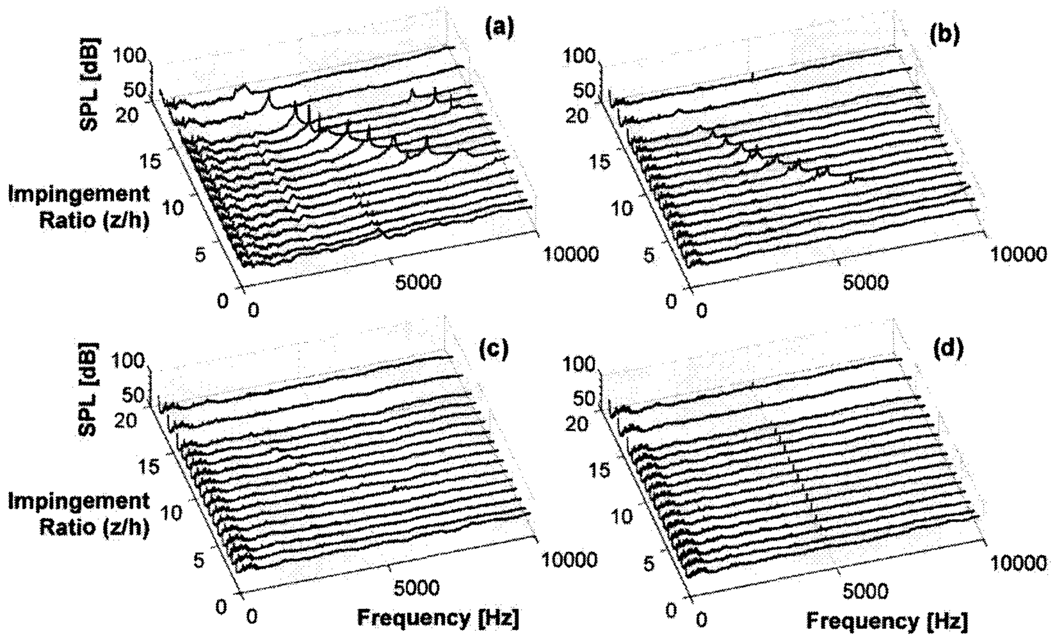

Figure 6-13: Waterfall plot showing the effect of stream-wise inclination (ζ) on jet-plate acoustic response for ζ = 0° (a), 5° (b), 10° (c) and 15° (d).

6.5.2 – Effect of Span-wise Inclination

The effect of span-wise inclination angle on the generation of jet-plate tones was also investigated. Because the impingement ratio is varying along the span of the jet, the impingement ratio given represents the ratio at the center of the jet span. Span-wise inclination angles of $\kappa = 0°$, 1.25°, 2.5° and 5° were tested, however only the results of the 1.25° inclination will be presented here, as it was found that the jet-plate tones are much more sensitive to span-wise inclination than stream-wise inclination. An inclination angle of only 1.25° results in a complete suppression of the mode. Figure 6-14 shows the results of span-wise plate inclination angles of $\kappa = 0°$ and 1.25°. Figure 6-15 shows the peak sound pressure level of the jet-plate acoustic tone as a function of span-wise inclination angle.

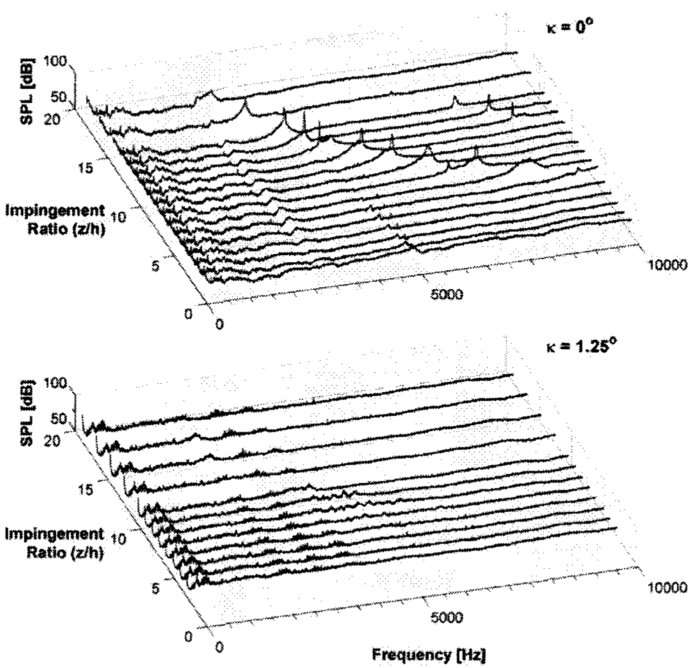

Figure 6-14: Waterfall plot showing the effect of span-wise inclination (κ) on jet-plate acoustic response.

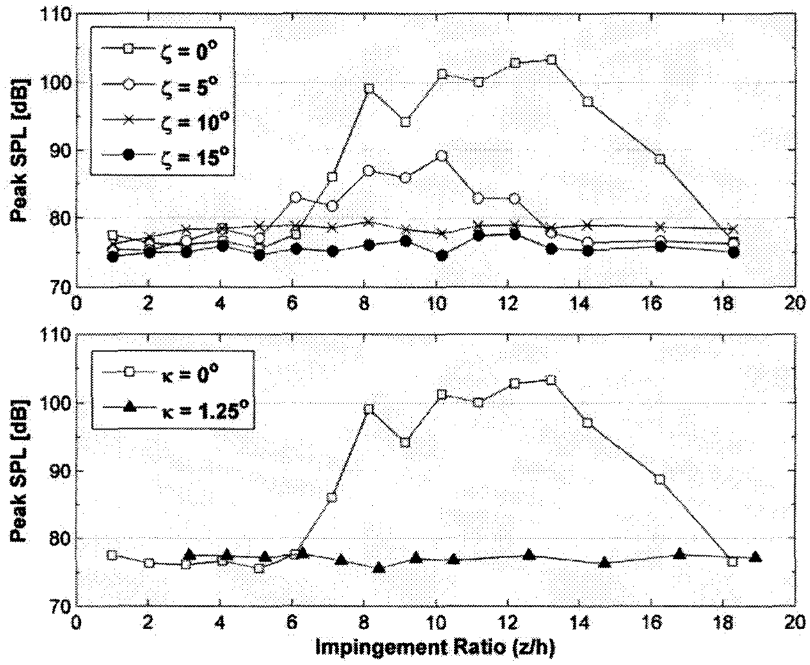

Figure 6-15: Acoustic response of jet-plate impingement for span-wise and stream-wise inclination of the plate.

Chapter 7 – JET INCIDENCE EFFECTS

7.1- EFFECT OF EDGE BAFFLES

A common countermeasure to suppress noise generation and the formation of strong acoustic tones in the gas wiping process is the use edge baffles. Edge baffles vary in design at various manufacturing facilities, and they have not been universally adopted throughout the galvanization industry. Most edge baffles simply consist of a flat plate, typically ¼" thick, made of steel or aluminum which is inserted between the two opposing wiping jets, in-line with the steel strip. Many different systems have been implemented for holding the plates in position, such as gravity slider system detailed in Park (2001), which automatically compensates for sheet wander on the mill rollers to keep the baffles a constant distance from the sheet edge. Other systems utilizing pneumatic cylinders allow the baffle plates to be inserted and retracted quickly so that the sheet or baffles are not damaged as a sheet weld passes through the wiping process.

The edge baffle to strip distance (D_{EB}) used by various manufacturers varies greatly, and the quantitative effect of edge baffles on noise in the gas wiping process is not well understood. Originally designed to help eliminate edge overcoating of the steel strip, where coating thicknesses are greater near the edge of the strip causing coiling and annealing problems, edge baffles have also proven useful in reducing sound pressure levels in areas surrounding the Zinc pot by reducing or eliminating the jet-jet impingement region and resulting jet-jet acoustic tones. Figure 7-1 shows a simplified schematic of the gas wiping setup with edge baffles in place, at a edge baffle distance of D_{EB}.

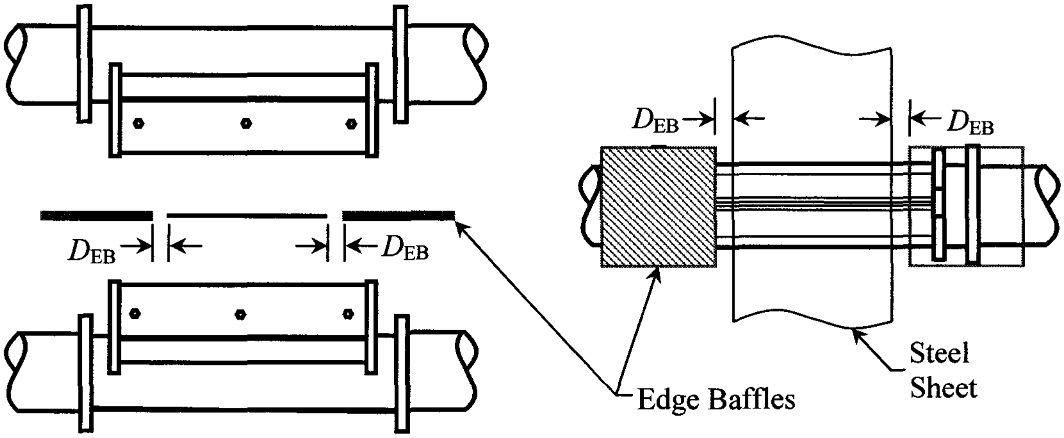

Figure 7-1: Simplified schematic showing the plan view of the gas wiping process with edge baffles in place at a distance of D_{EB}.

A series of experiments have been carried out to characterize the behavior of noise generation in the gas wiping process with the addition of baffle plates. The effect of edge baffle distance (D_{EB}) as a function of plenum pressure and impingement ratio has been investigated. A pair of baffle plates has been constructed of $^1/_8$" sheet aluminum and mounted on a pair of fabricated aluminum slides, allowing the edge baffle distance to be adjusted to within ±0.02mm. The overall jet-jet impingement region length D_j at each end of the jets is 48 mm long, and the edge baffle distance is varied from D_{EB} = 48 mm to D_{EB} = 0 mm. The edge baffles were sufficiently rigid to prevent any vibrations or movement due to the impingement of the jets.

7.1.1 – EDGE BAFFLE EFFECTIVENESS

The first test carried out to investigate the effect of edge baffle distance (D_{EB}) was performed at a fixed pressure of P = 2.5 psi (0.175 Bar) and a fixed impingement ratio. Measurements were recorded for a series of tests with varying edge baffle distances from $D_{EB} = \infty$ to D_{EB} = 0 mm. The impingement ratio was then fixed at a new value and the test of edge baffle distance was repeated. Edge baffle distances of $D_{EB} = \infty$, 44, 40, 36, 32, 28, 24, 20, 16, 12, 10, 8, 6, 4, 2 & 0mm were tested for z/h values from 5 to 30 in increments of z/h = 2.5.

The results of a single test run at z/h = 15 and varying edge baffle distances are shown in a contour plot in Figure 7-2 and in the acoustic response plot of Figure 7-3. The primary and secondary jet-jet modes are clearly evident on the plot for large impingement ratios. The plot shows that as edge baffle distance is reduced gradually from D_{EB} = 48mm to D_{EB} = 15mm, there is little effect. The frequency of the acoustic tone remains unchanged, and the overall sound pressure level is relatively constant, but the tone amplitude reduces slightly for D_{EB} values less than 24mm. For edge baffle distances of less than 14 mm, there is a slight shift in the frequency of the acoustic tone and the amplitude of the tone continues to decrease gradually. For edge baffle distances of less than D_{EB} = 9mm, the frequency shift becomes more pronounced. At an edge baffle distance of D_{EB} = 3mm, the jet-jet mode abruptly ceases, and the overall sound pressure level drops accordingly. The frequency response of other impingement ratios is very similar.

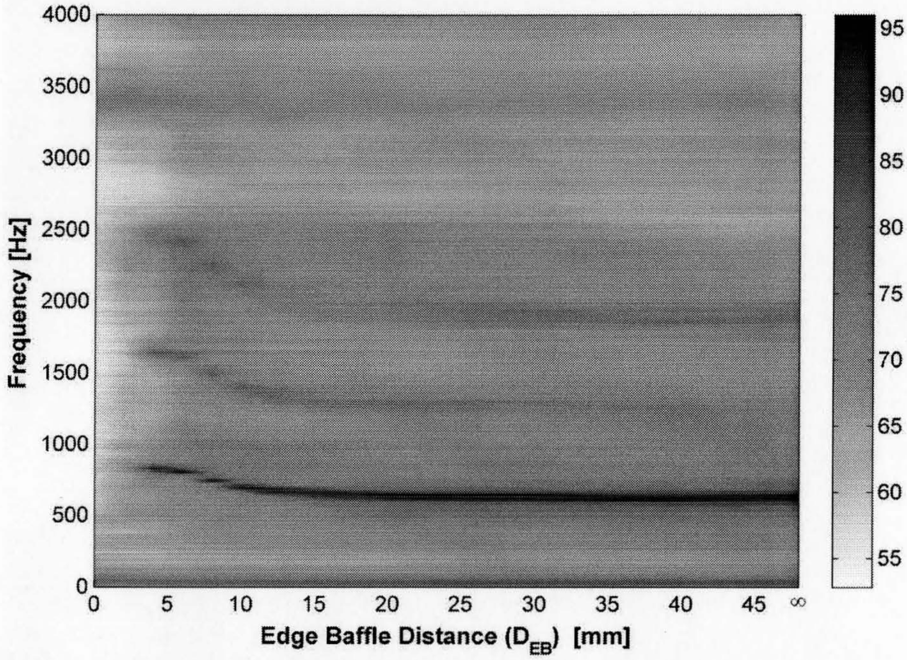

Figure 7-2: Contour plot of the frequency response of jet-jet impingement with baffle plates. P = 2.5 psi (0.170 Bar), z/h = 15, α = 3°.

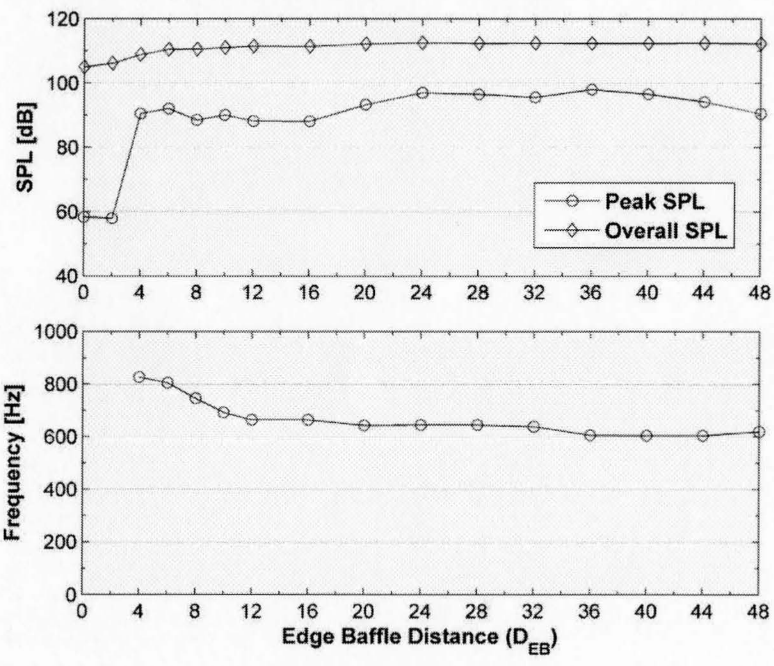

Figure 7-3: Acoustic response of peak and overall SPL and tone frequency of jet-jet impingement with varying edge baffle distance for P = 2.5 psi (0.170 Bar), z/h = 15.

A waterfall plot of the acoustic response of the system with baffle plates is shown in Figure 7-4 for a constant plenum pressure of P = 2.5 psi and four separate edge baffle distances of D_{EB} = 0, 2, 4 & 6 mm. For an edge baffle spacing of D_{EB} = 0mm, a strong, high frequency jet-sheet mode is excited. As the edge baffle distance is increased to 2, 4 & 6mm, the jet-sheet mode is slowly suppressed and the jet-jet mode begins to dominate the spectrum. These results seem to indicate that while the edge baffles are very effective at suppressing the primary jet-jet modes for small edge baffle spacing, the same configurations seem to promote higher frequency jet-sheet modes, which may generate significant tones, and offset any reduction in the jet-jet modes.

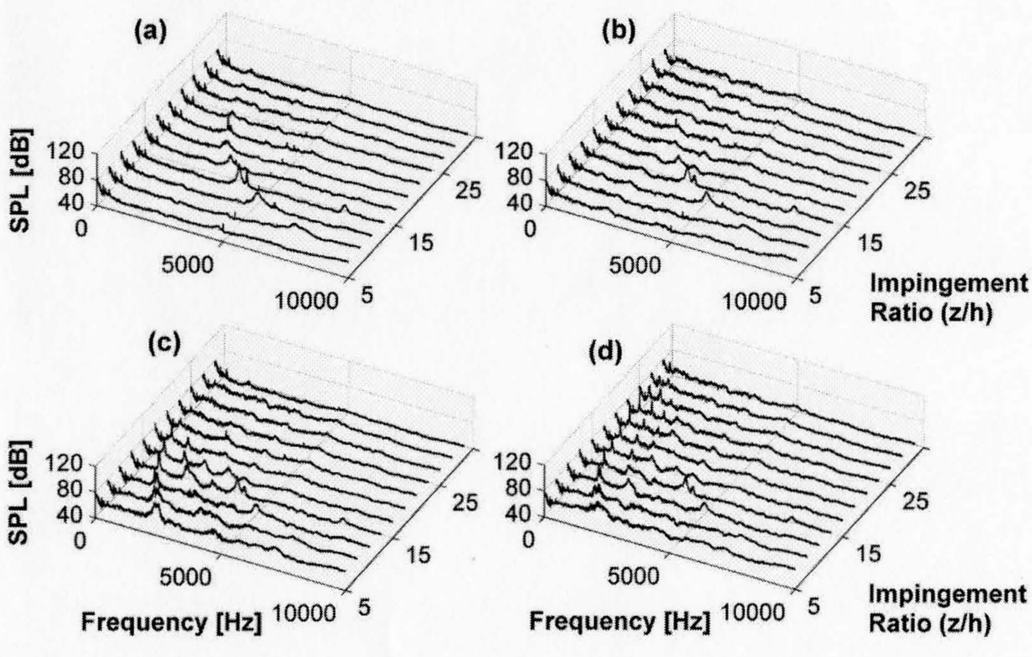

Figure 7-4: Acoustic response of the system for edge baffle spacing of D_{EB} = 0mm (a), 2mm (b), 4mm (c), 6mm (d).

A noise map of the averaged overall sound pressure level for each measurement point is shown in Figure 7-5. The figure shows that for the entire range of impingement ratios tested, the overall sound pressure level is reduced very little as the edge baffle distance decreases up to $D_{EB}/D_j \approx 90\%$, after which the reduction in overall SPL occurs very rapidly. Dubois (2001a, 2001b) reported relatively little reduction in overall sound pressure level for edge baffle distances of greater than 2mm, which is consistent with the observations of the current study.

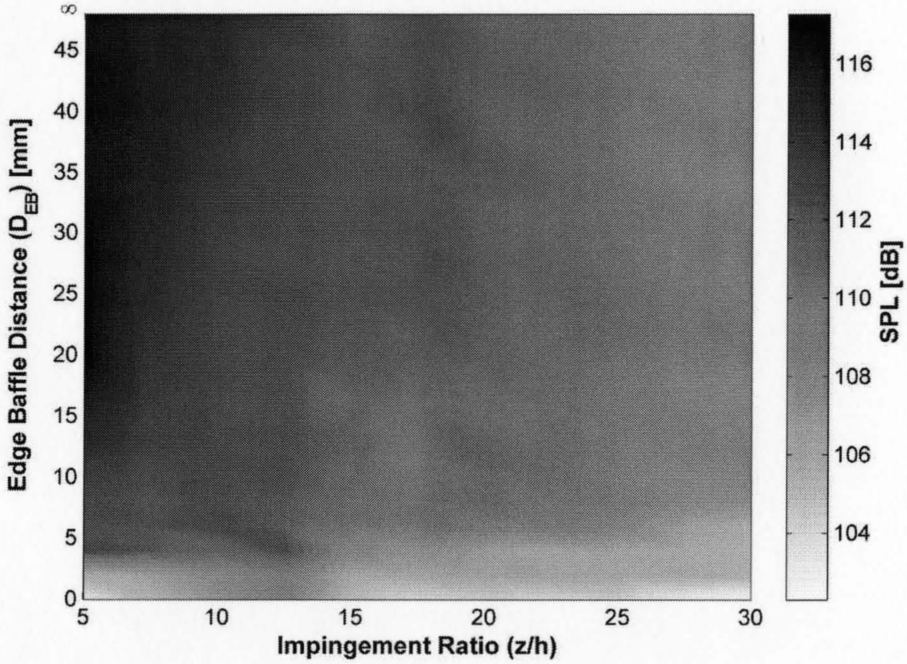

Figure 7-5: Averaged SPL as a function of impingement ratio (*z*/*h*) and edge baffle distance (D_{EB}) for P = 2.5 psi (0.170 Bar).

7.1.2 – EDGE BAFFLES: NOISE MAPS

The previous set of experiments quantified the effectiveness of the edge baffles at a single plenum pressure as a function of the edge baffle distance (D_{EB}) and the dimensionless impingement ratio, z/h. Some of the previous results however suggested that while presence of baffle plates can be effective at suppressing jet-jet modes for relatively small edge baffle distances, in some cases the baffles can enhance the generation of jet-sheet tones, which can even stronger than jet-jet tones for certain configurations, particularly higher plenum pressures and intermediate impingement ratios. In order to assess the effectiveness of edge baffles over the complete range of operating parameters for the process, noise maps similar to those presented for the original baseline configuration have been constructed for a single edge baffle distance. An edge baffle spacing of D_{EB} = 2 mm was chosen, as it was expected that this would be practical for manufacturers. Tests were performed with a constant edge baffle distance of D_{EB} = 2mm for a series of pressures from P = 1.0 to P = 4.5 psi in 0.5 psi increments. To reduced the amount of data to manageable level, only the results of P = 1.0, 2.0, 3.0 and 4.0 psi are shown here as measurements for all other plenum pressures showed similar trends.

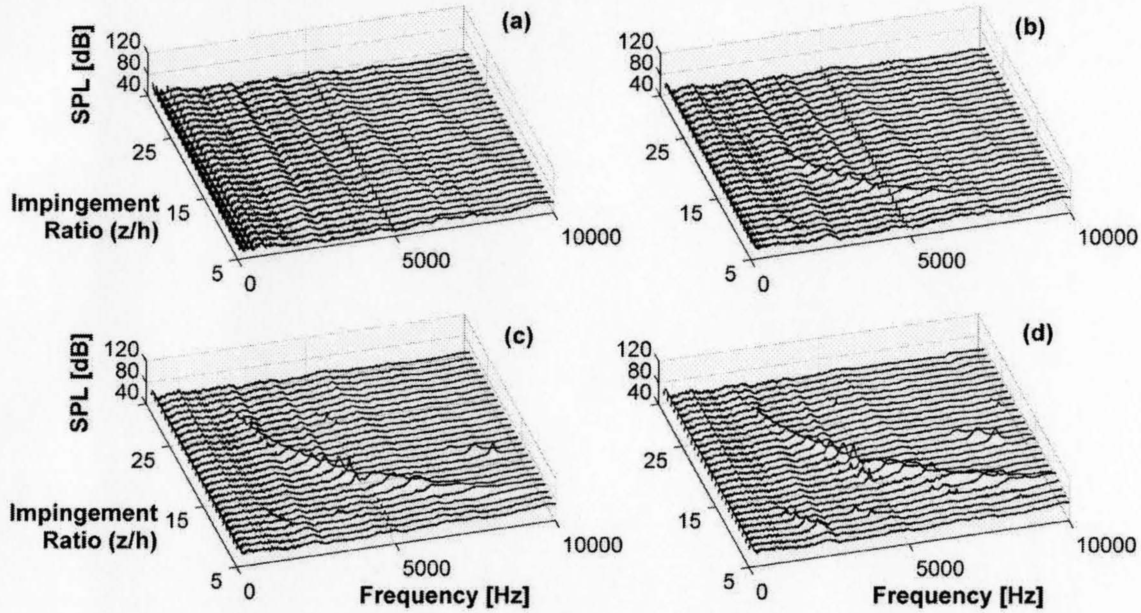

Figure 7-6: Acoustic response of jet-jet impingement case with edge baffles at a distance of D_{EB} = 2mm for P = 1.0 psi (a), 2.0 psi (b), 3.0 psi (c) and 4.0 psi (d).

Figure 7-6 shows a series of waterfall plots for constant pressure runs of P = 1.0, 2.0, 3.0 & 4.0 psi which illustrates the acoustic response of jet-jet impingement with edge baffles. The results of this figure are very similar to the results of Figure 6-5 of the jet-plate impingement section, indicating that the impingement of the jets on the baffle plates does promote the generation of jet-sheet tones as expected. In general, the amplitude of the acoustic tones generated in the jet-jet impingement with edge baffles are not as strong or narrow as in the case of jet-plate impingement, due to the non-fixed impingement distance associated with sheet motion and vibration. The acoustic tones and overall sound pressure levels generated by the jet-sheet tones with the edge baffle present were significant however, when compared to the response of the original baseline configuration. There is some excitation of the lower frequency jet-jet modes for smaller jet-jet impingement ratios and higher plenum pressures, however the amplitude of these modes is much smaller than the jet-sheet modes present in the same spectra, and they do not contribute significantly to the overall sound pressure levels.

Figure 7-7 and Figure 7-8 show noise maps of overall sound pressure level and tone intensity constructed from the measurements taken at each plenum pressure and impingement ratio. From inspection of these two figures, it is clear that they are qualitatively similar to the noise maps generated for jet-plate impingement shown in Figure 6-10 and Figure 6-11 due to the strong presence of jet-sheet modes in both test setups. From Figure 7-7, we can see that for higher plenum pressures and intermediate dimensionless impingement ratios, the amplitude of averaged overall sound pressure level can be as high, or in some cases higher than the sound pressure levels of the baseline configuration. The acoustic tone generation, shown in the tone intensity map of Figure 7-8, shows that the edge baffle configurations with small edge baffle distances generate tones in a very similar fashion to jet-plate impingement, with strong excitation of jet sheet modes once again occurring over two distinct ranges.

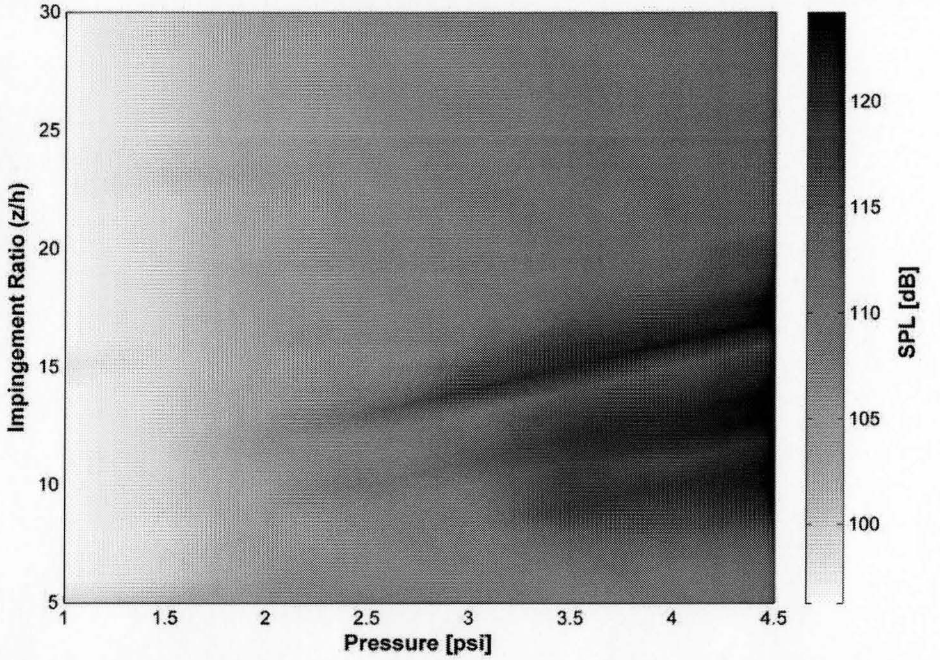

Figure 7-7: Averaged overall SPL as a function of plenum pressure (*P*) and impingement ratio (*z/h*) of jet-jet impingement with edge baffles at a distance of D_{EB} = 2mm.

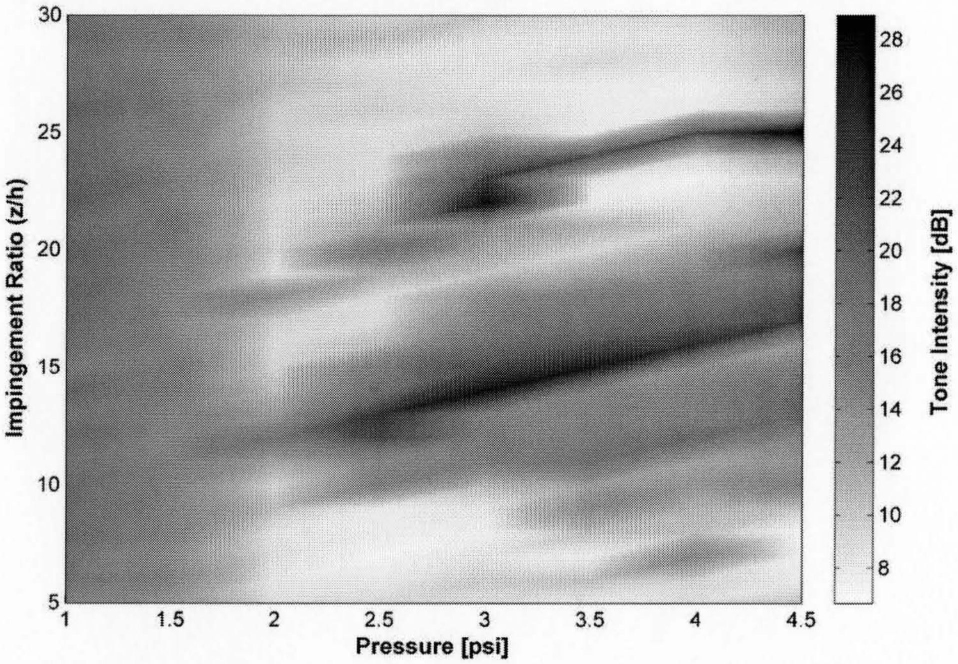

Figure 7-8: Tone intensity as a function of plenum pressure (*P*) and impingement ratio (*z/h*) of jet-jet impingement with edge baffles at a distance of D_{EB} = 2mm.

In order to compare the edge baffle case with the original baseline configuration, a plot of overall sound pressure level reduction as a function of plenum pressure and impingement ratio is shown in Figure 7-9. The averaged overall SPL of the baffle plate case for each configuration was subtracted from the SPL of the same configuration of the baseline case, yielding the reduction in SPL possible by using baffle plates at a distance of 2 mm. The figure shows that substantial reductions are possible, as much as 11 dB, for certain configurations. However, for other configurations, the baffle plates resulted in an increase in overall sound pressure level due to the enhancement of jet-sheet modes.

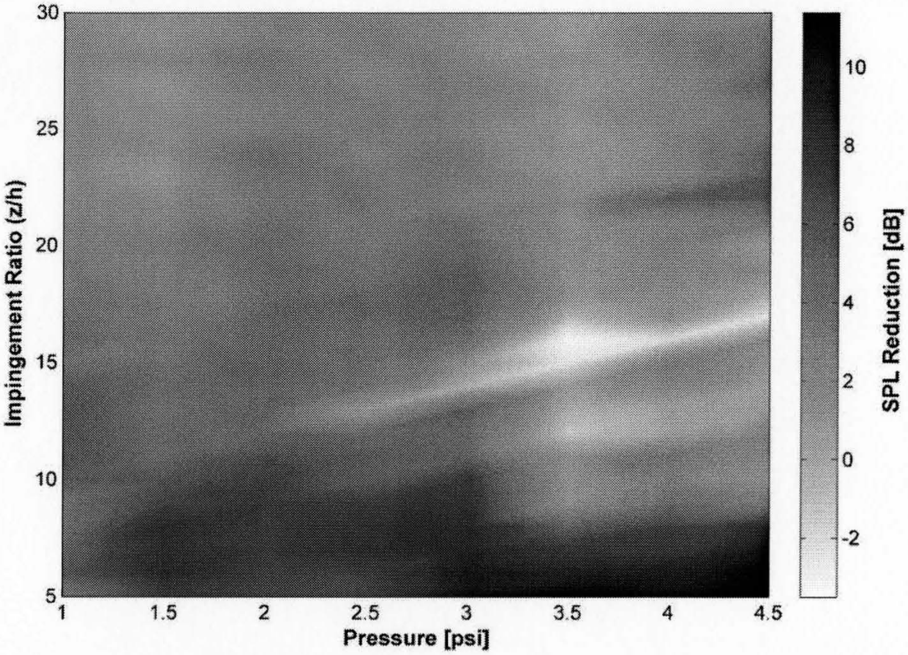

Figure 7-9: SPL reduction for case of jet-jet impingement with edge baffles at a distance of D_{EB} = 2mm vs. the baseline jet-jet impingement as a function of plenum pressure (*P*) and impingement ratio (*z*/*h*).

7.2- Effect of Jet Inclination Angle

The inclination angle of the jets, as shown in Figure 7-10, is an important parameter in the gas wiping process, and it has important effects on the coating quality for a wide range of hot-dipped galvanized steel products. In the gas wiping process, the jets are often inclined downwards from the horizontal in the direction of the oncoming steel sheet. Inclination angles in the range of α = 0° to α = 12° are most common, however inclination angles of up to α = 30° have been reported and studied in a number of investigations such as Dubois et al. (1995) and Dubois et al. (2004). Numerous studies have examined the beneficial effect of increasing jet inclination angles delaying the onset of coating splashing, where droplets of molten Zinc are sheared from the surface of the oncoming sheet, resulting in a drastic decrease in wiping efficiency and inconsistent coating quality.

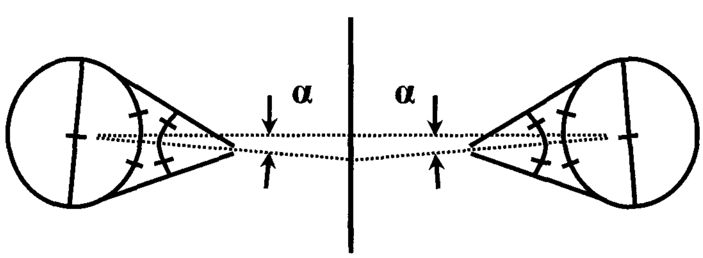

Figure 7-10: Simplified schematic of gas wiping layout showing jet inclination angle (α).

7.2.1 – Acoustic Response

A series of experiments have been performed in order to investigate the effect of jet inclination angle on the acoustic response of the gas wiping process. All measurements were performed at a constant plenum pressure of P = 2.5 psi (0.170 Bar), and the jet inclination angle was varied between α = 0° and α = 12° in increments of α =

3°. An inclination angle of the jets was set and the jet impingement ratio was varied between z/h = 5 to 30. The process was repeated for all the jet inclination angles tested.

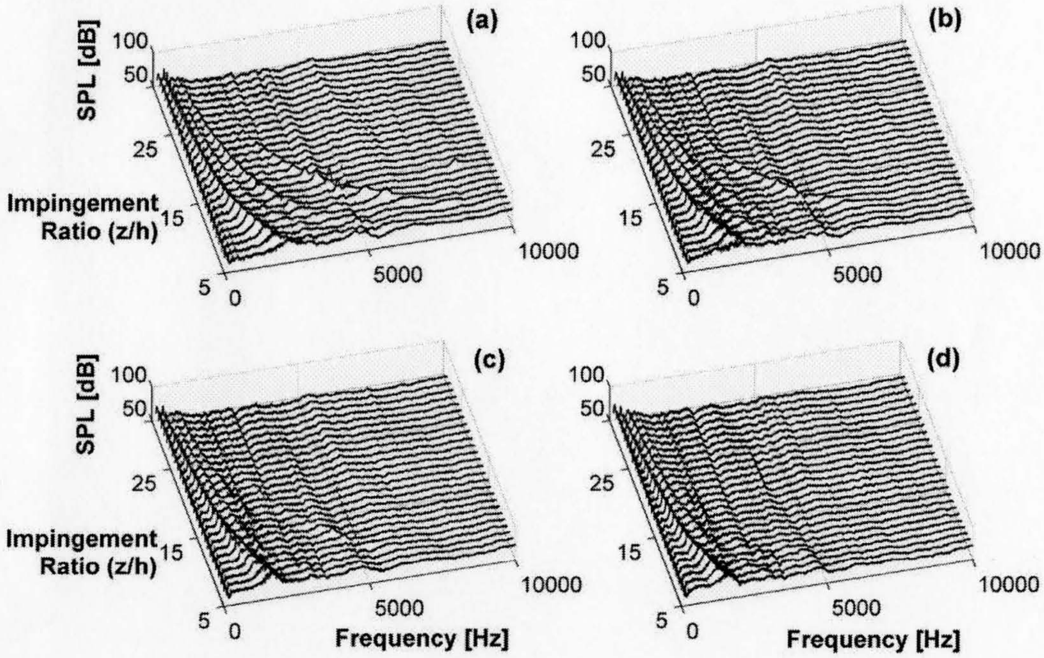

Figure 7-11: Waterfall plot showing effect of jet inclination angle (α) on acoustic response of jet-jet impingement for inclination angles of α = 3° (a), 6° (b), 9° (c) & 12° (d).

Figure 7-11 shows a series of waterfall plots of the acoustic response of gas wiping for varying jet inclination angles as a function of the impingement ratio. Plot (a) of the figure shows the acoustic response of the gas wiping process taken from the baseline configuration (P = 2.5 psi, α = 3°). The excitation of both the primary and secondary jet-jet modes is evident in the spectra, as well as the excitation of the higher frequency jet-sheet modes. As the jet inclination angle increases to 6°, 9° & 12°, the amplitude of the jet-jet modes is reduced slightly, however increasing the jet inclination angle from 3° to 12° has the effect of completely suppressing the higher frequency jet-sheet mode. This result confirms the observation made in the section investigating the effect of inclination on jet-plate tones made in the jet-plate impingement section. This effect may be useful for suppressing these tones in industrial configurations encountering jet-sheet modes. Figure 7-12 shows the frequency response of the primary jet-jet mode as a function of impingement ratios for various jet inclination angles. As the inclination angle of the two jets is increased from $\alpha = 0°$ to 12°, the frequency of the primary jet-jet mode is also decreased by approximately 20%. This decrease in frequency is more pronounced for smaller impingement ratios of less than $z/h = 15$.

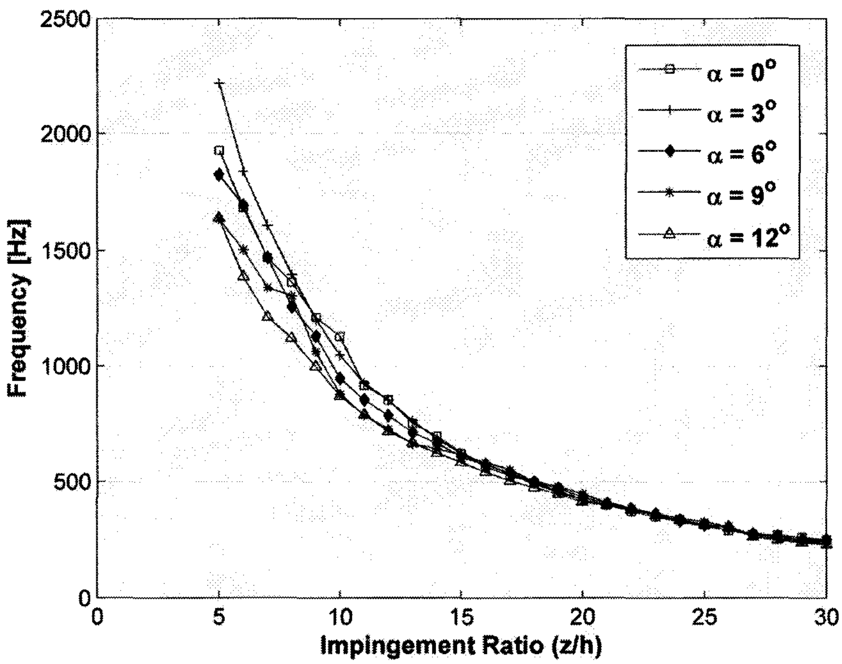

Figure 7-12: Frequency of the primary jet-jet mode for varying jet inclination angles as a function of the impingement ratio (*z*/*h*).

7.2.2 – NOISE MAPS

Figure 7-13 and Figure 7-14 show maps of the overall sound pressure level and the tone intensity of the gas wiping process with varying jet inclination angles for a constant plenum pressure of $P = 2.5$ psi (0.170 Bar). The overall sound pressure level of the process decreases slightly with increasing impingement angles, with reductions between 1 dB and 4 dB depending on the impingement ratio, and an average reduction of 2.4 dB when increasing jet inclination angle from 0° to 12°. The highest reductions in overall sound pressure level occurred for intermediate impingement ratios of between z/h = 10 and 20 where reductions of between 3 and 4 dB were achieved for inclinations of α = 6°, 9° and 12°.

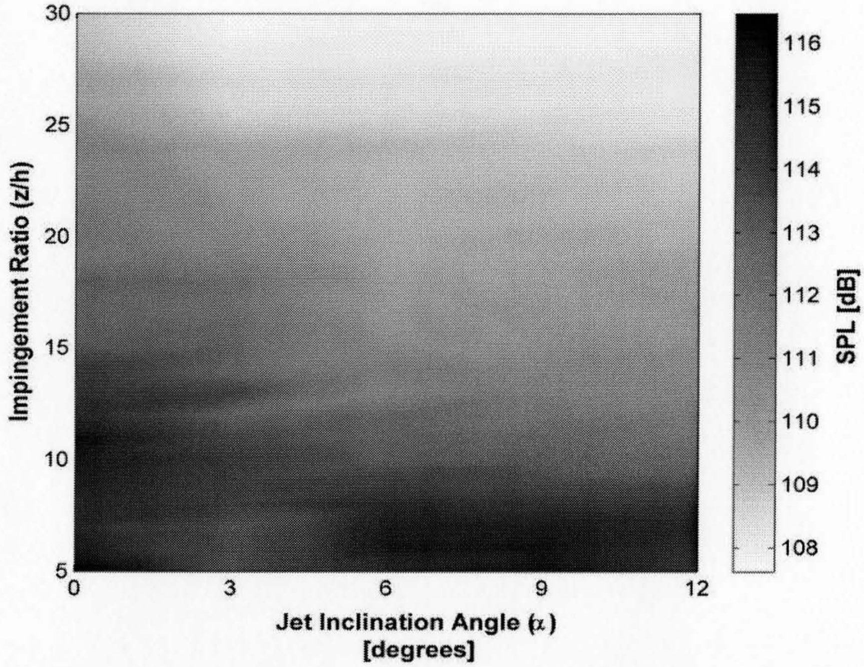

Figure 7-13: Averaged overall sound pressure level as a function of impingement ratio (z/h) and the jet inclination angle α for a constant plenum pressure of P = 2.5 psi (0.175 Bar).

Figure 7-14 shows the tone intensity of gas wiping for various jet inclination angles as a function of the impingement ratio. There are significant reductions in the tone intensity of between 4 and 7 dB for intermediate and larger impingement ratios (z/h > 15) as the jet inclination angle increases. An average reduction of 3.6 dB was achieved for inclination angles of α = 6° and higher for impingement ratios of z/h > 15.

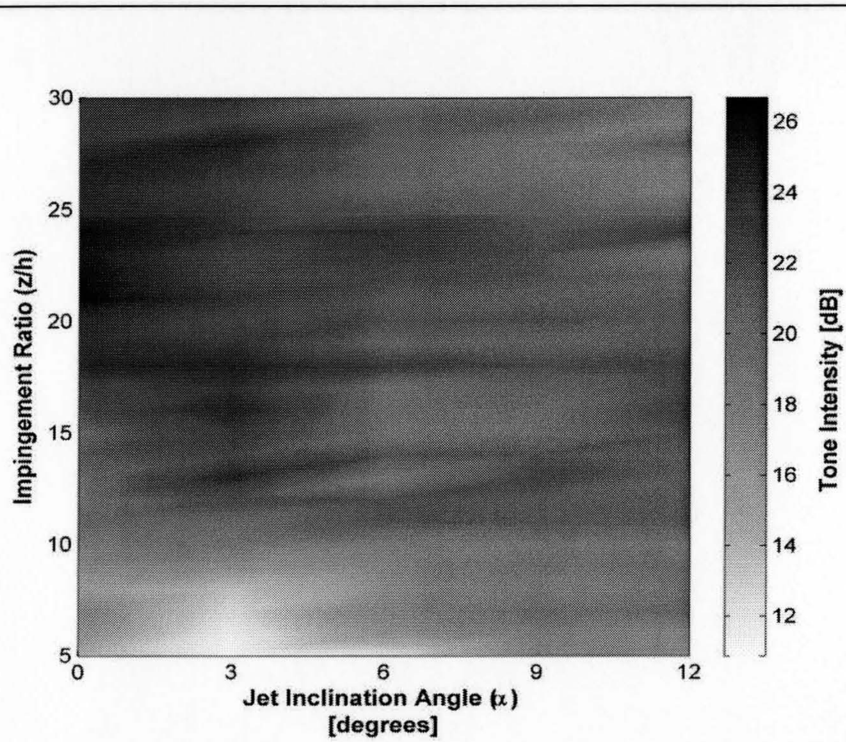

Figure 7-14: Tone intensity as a function of impingement ratio (z/h) and the jet inclination angle α for a constant plenum pressure of $P = 2.5$ psi (0.170 Bar).

The combined effect of reduced sound pressure levels and tone intensities for configurations with increased jet inclination angles may prove useful for reducing the impact of noise generated in this process, especially when combined with other noise reducing techniques such as edge baffles and jet incidence asymmetry.

7.3 - Effect of Jet Incidence Asymmetry

In many industrial cases, jet incidence asymmetry may be employed in order to help alleviate the formation of strong acoustic tones and high sound pressure levels generated during gas wiping. Simply staggering the jets vertically or slightly modifying the jet incidence angle α of one of the jets to introduce asymmetry in the jet impingement may be sufficient to suppress an acoustic tone from being generated. It is currently not well understood on a quantitative level how asymmetry in the gas wiping process affects noise and tone generation, although qualitatively it is accepted to be effective. In some cases, particularly for industrial cases utilizing higher plenum pressure, such configurations are avoided, as they have the potential to introduce problems in the quality of the finished Zinc coating. However, if the degree of asymmetry necessary to reduce noise is small, then this may prove a useful strategy for industrial applications. In this section, experiments have been carried out to assess the sensitivity of the generation of acoustic tones and overall sound pressure levels to jet incidence asymmetry in the gas wiping process. The effect of vertical jet offset and changing of jet incidence angles or "jet-shifting" will be investigated.

7.3.1 - Vertical Jet Offset

The first type in jet incidence asymmetry to be investigated is the effect of vertical jet offset shown in Figure 7-15. Vertical jet offset configurations maintain the same jet inclination angles between the two jets, but offsets one of the jets vertically with respect to the other. This vertical offset of the jets results in different impingement lengths for each of the two jets for the jet-jet impingement region and as a result, the jets should not lock-in or produce strong acoustic jet-jet tones. The jet-sheet and jet-plate regions will be unaffected by this countermeasure, as thus no reduction should be expected for the tones generated in these regions. A series of experiments have been performed to investigate the effect of vertical jet offset on the acoustic response of jet-jet impingement. The experiments have been performed at a constant plenum pressure of P = 2.5 psi (0.170 Bar) at a jet inclination angle of $\alpha = 3°$, while varying the amount of jet offset from Δy =

0 mm to Δy = 5 mm in 1mm increments, as well as the dimensionless impingement ratio from z/h = 5 to 30.

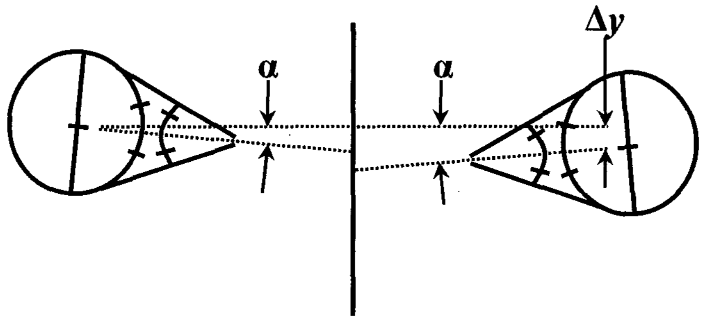

Figure 7-15: Simplified schematic of vertical jet offset (Δy) and jet inclination angle (α).

7.3.1.1 – Acoustic Response for Vertical Jet Offset

Figure 7-16 shows a series of waterfall plots illustrating the acoustic response of jet-jet impingement with varying amounts of vertical jet offset. Part (a) of the figure shows the aligned jet case (Δy = 0 mm) from the baseline configuration (α = 3°), with no vertical jet offset. The presence of the primary and secondary jet-jet modes are present throughout the entire tested range of impingement ratio, and for intermediate impingement ratios, jet-sheet tones are also present. As small amounts of vertical jet offset are added, the formation of the jet-jet modes is weakened or interrupted for the shortest impingement ratios, but the tones resume as the impingement ratio is increased. As progressively more vertical jet offset is added, the jet-jet modes are interrupted for increasingly larger impingement ratios. While vertical jet offset is effective in suppressing jet-jet acoustic tones for short and intermediate impingement ratios, it does not have a significant effect on higher frequency jet-plate acoustic tones as the asymmetry has no effect on the jet-sheet impingement geometry.

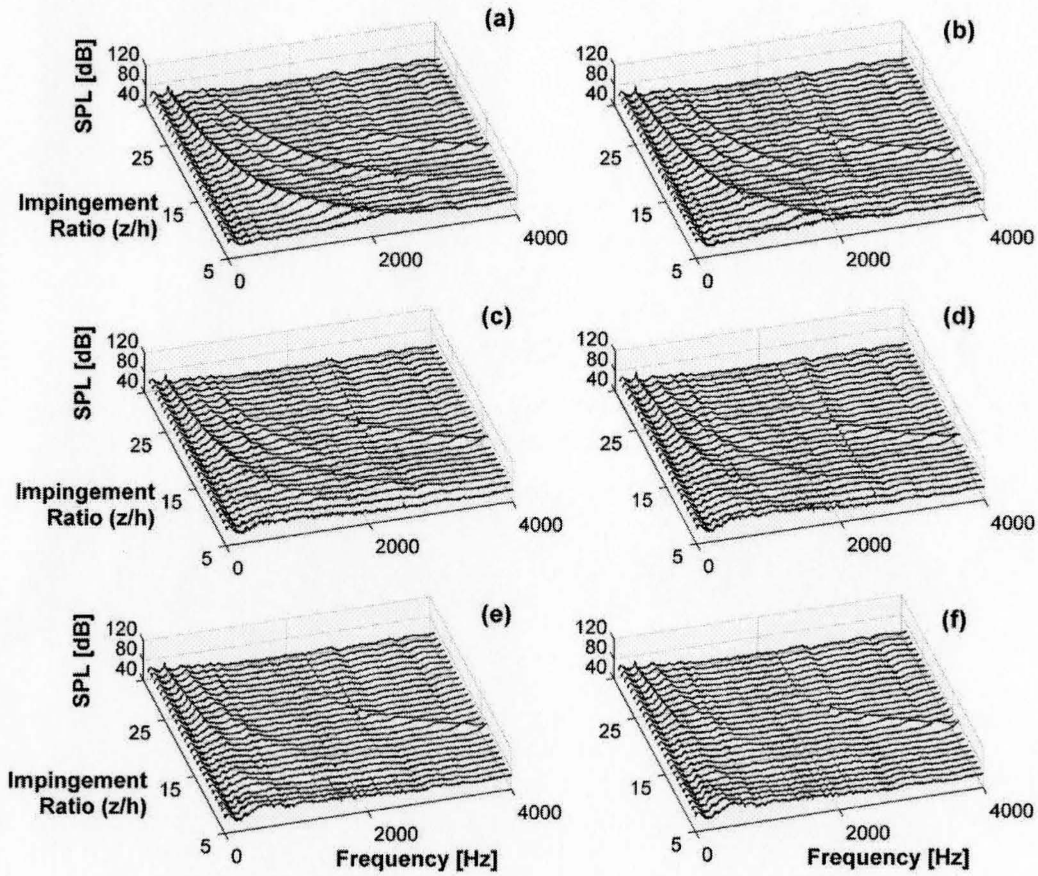

Figure 7-16: Effect of vertical jet offset on the aeroacoustic response of jet-jet impingement. Δy = 0mm (a), 1mm (b), 2mm (c), 3mm (d), 4mm (e) & 5mm (f).

The effect of jet offset on the acoustic tone frequency is clearly shown in Figure 7-17 which shows that the case of no vertical jet offset (Δy = 0mm), the frequency of the jet-jet mode is accurately predicted by Equation (5-3) on page 75. As vertical jet offset is added, the frequency of the jet-jet tone begins to deviate from the predicted frequency for relatively short impingement ratios, but as the impingement ratio is increased for a constant jet offset, the dominant acoustic tone regains its hyperbolic behavior. Larger jet offsets result in greater impingement ratios required for the jet-jet tones to resume their standard, lock-in type behavior.

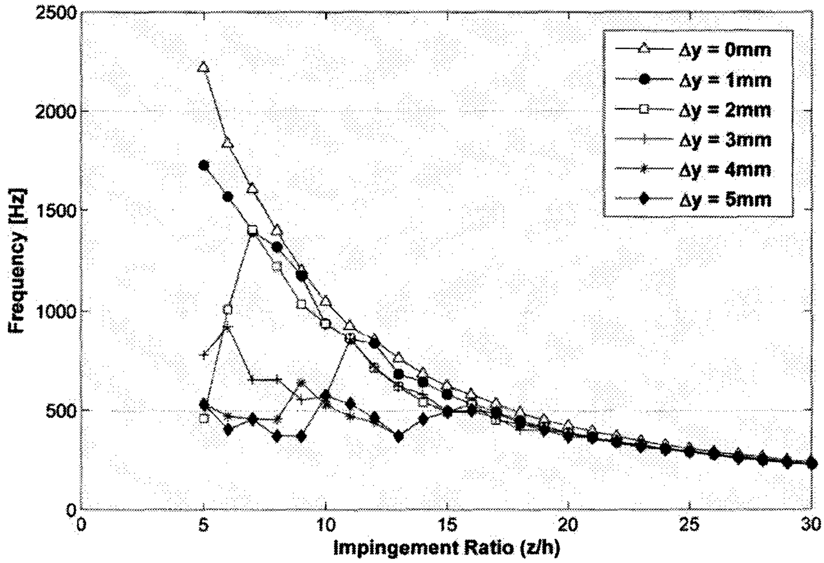

Figure 7-17: Frequency and SPL of the dominant acoustic mode for jet-jet impingement as a function of impingement ratio (*z/h*) and vertical jet offset (Δ*y*). [lines shown for visual aid only]

This result can be expressed in terms of an offset ratio $\Delta y/z$, which is simply the vertical jet offset of the jets divided by the impingement length. The larger the value of this ratio, the larger the effect of vertical jet offset on tone formation in gas wiping. If we nondimensionalize the jet offset using the offset ratio $\Delta y/z$, the results become more clear. Figure 7-18 shows the tone intensity and the difference in frequency of the jet-jet acoustic tone as a function of offset ratio for vertical jet offset cases of Δy = 2mm to 5mm. The figure shows that the frequency of the jet-jet acoustic tone diverges from the aligned jet frequency behavior for all vertical jet offset cases at an offset ratio of $\Delta y/z \approx 0.27$. Furthermore, the tone intensity of the jet-jet tone decreases continuously for all vertical jet offsets tested up to an offset ratio of approximately $\Delta y/z \approx 0.45$, with tone intensity reductions for the jet-jet tone of nearly 15 dB for some jet offset cases.

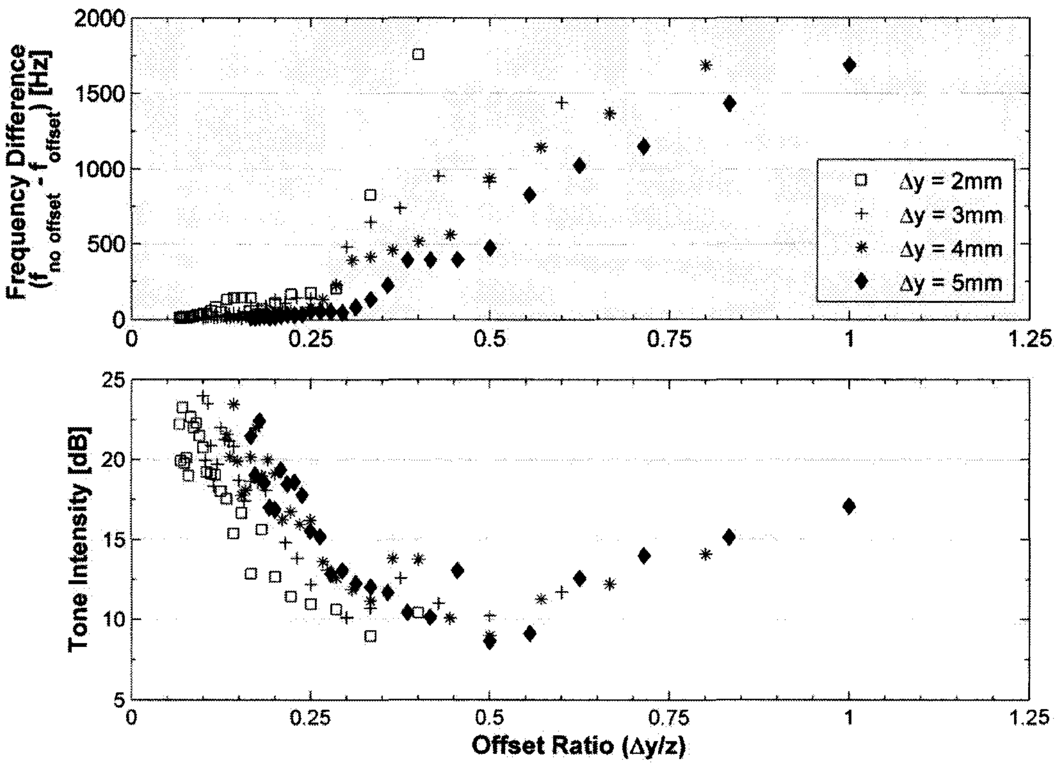

Figure 7-18: Tone intensity and difference in acoustic tone frequency as a function of offset ratio for vertical jet offset of Δy = 2mm to 5mm.

7.3.1.2 – Vertical Jet Offset: Noise Maps

Using the measurements outlined above a set of noise maps showing the overall sound pressure level as a function of impingement ratio and vertical jet offset. The overall sound pressure level for a plenum pressure of P = 2.5 psi (0.170 Bar) shown in Figure 7-19 shows relatively little reduction in overall sound pressure level at any impingement ratio for increasing vertical jet offset. The explanation for this behavior is that although offsetting the jet and introducing asymmetry in the jet impingement does effectively suppress strong tones from being generated, especially for small impingement ratios, the noise spectrum in these regions is dominated by relatively high level of broadband noise. The total acoustic energy seems to be relatively constant regardless of the amount of jet offset used, although the reduction or elimination of discrete tones will allow for the reduction of perceived overall sound pressure levels, due to less annoyance. The tone intensity map, shown in Figure 7-20, shows that a significant reduction in discrete acoustic tones can be achieved by utilizing vertical jet offset to introduce asymmetry into the jet impingement. In some cases of small impingement ratios, a reduction in tone intensity of over 16 dB can be achieved for relatively small amounts of jet offset (Δy = 2mm). This technique appears promising for use in the reduction of strong acoustic tones which are often generated during gas wiping, although they should be applied with some caution due to potential problems associated with coating quality.

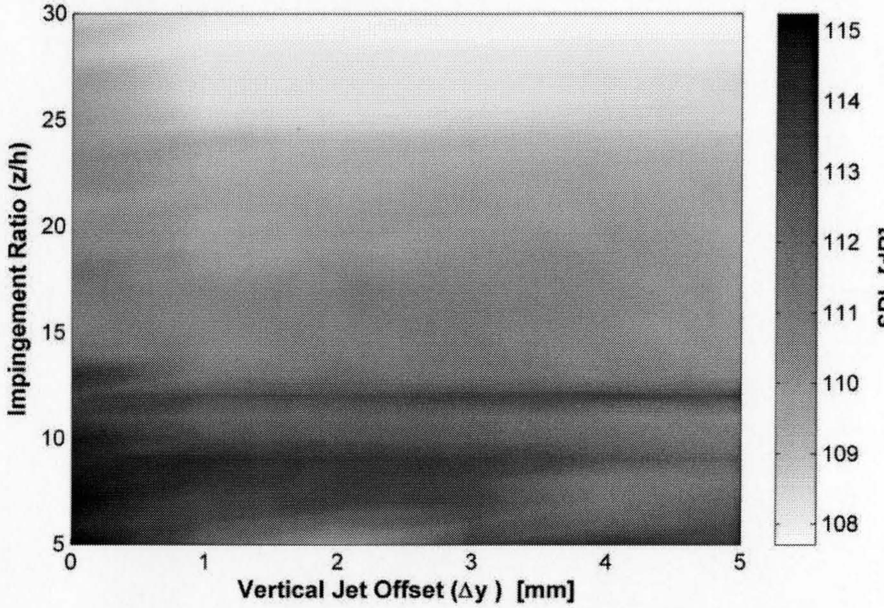

Figure 7-19: Averaged overall SPL as a function of impingement ratio (*z*/*h*) and vertical jet offset Δ*y* for a plenum pressure of *P* = 2.5 psi (0.170 Bar).

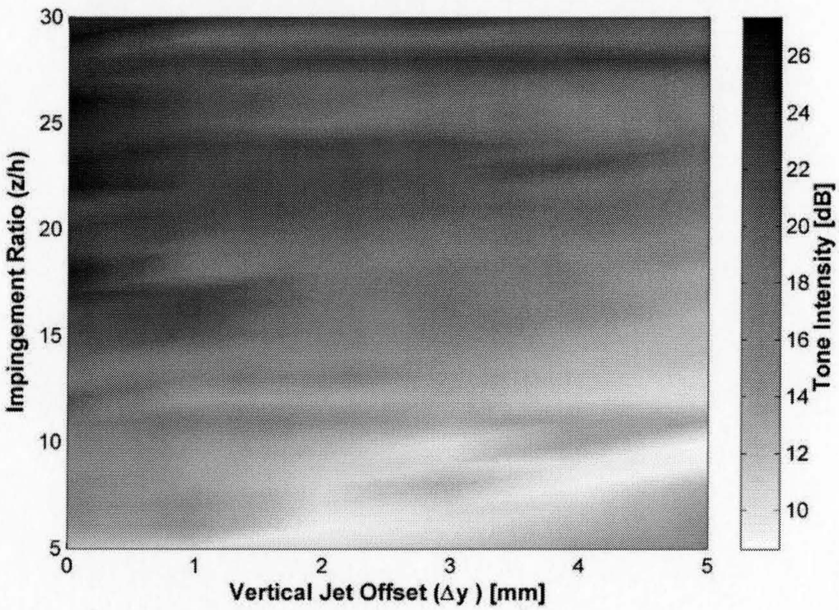

Figure 7-20: Tone Intensity of jet-jet impingement as a function of impingement ratio (*z*/*h*) and vertical jet offset Δ*y* for a plenum pressure of *P* = 2.5 psi (0.170 Bar).

7.3.2 - EFFECT OF JET SHIFTING

Jet-shifting has been used at the industrial level, although less commonly than vertical jet offset, to attempt to reduce noise and the formation of discrete acoustic tones. The principle of jet-shifting is essentially the same as vertical jet offset: introducing a given amount of jet incidence asymmetry in order to interrupt jet instability modes and generation of discrete acoustic tones. Jet-shifting involves changing the inclination angle of one jet, so that a different jet inclination angle is used for each jet. Jet-shifting is employed in production facilities where it is not possible to alter the relative jet height to introduce vertical jet offset, or simply where it is easier to change the inclination angle of the jet than the jet height. The jet-shifting angle γ, is defined simply as the difference in degrees between α, the base inclination angle, and the modified inclination angle β. The jet inclination angles and a basic schematic of a jet-shifting configuration is shown in Figure 7-21.

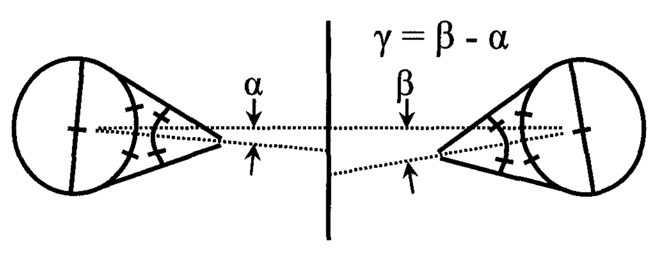

Figure 7-21: Simplified schematic gas wiping layout showing jet-shifting angle (γ).

A series of experiments were carried out in order to investigate the effect of jet-shifting on the acoustic response of gas wiping. Jet-shifting angles between γ = -4° and γ = 5° were tested at a base inclination angle of α = 3° for three different impingement ratios of z/h = 10, 17.5 and 25 and at a constant plenum pressure of P = 2.5 psi (0.170

Bar). Figure 7-22 shows the peak SPL of the primary jet-jet mode as a function of the jet-shifting angle, for the three different impingement ratios tested. As expected, the strength of the acoustic tone was strongly dependant on the degree of jet alignment, with the strongest peak level occurring at a jet-shifting angle of $\gamma = 0°$ (the symmetric case) for all three impingement ratios tested, the aligned jet case. The attenuation of discreet acoustic tones with changing jet-shifting angle is quite abrupt, with a reduction of ~20 dB in tone intensity between jet-shifting angles of $\gamma = 1°$ and $2°$ and $\gamma = -1°$ and $-2°$. This result is similar to the behavior encountered in the investigation of vertical jet offset, where strong tones were suppressed abruptly as opposed to a gradual reduction.

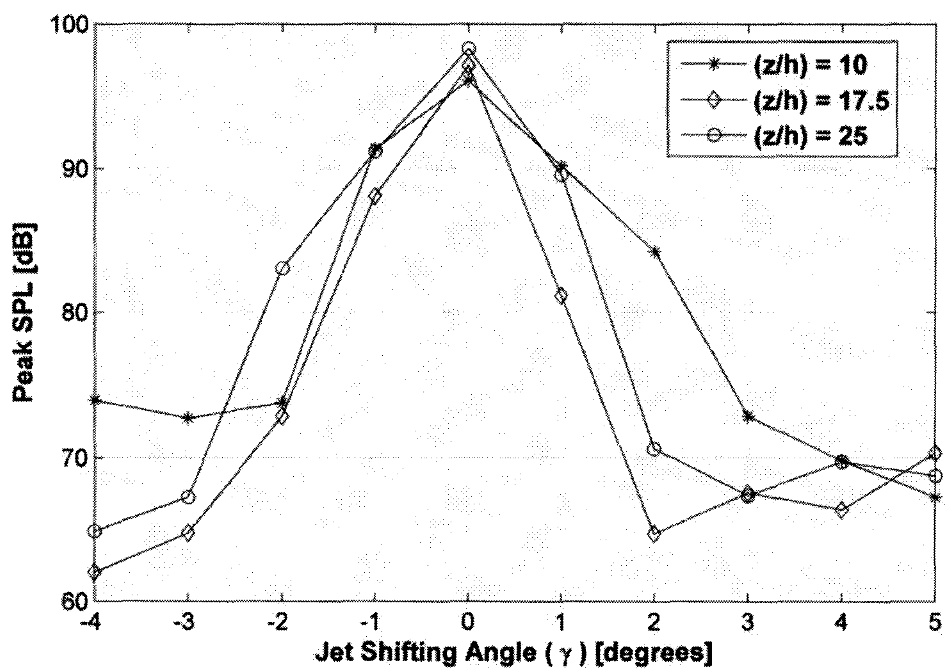

Figure 7-22: Peak SPL of dominant acoustic tone for various jet shifting angles (γ) at several impingement ratios for a plenum pressure of P = 2.5 psi (0.170 Bar). [lines shown for visual aid only]

The reduction in tone intensity for each of the three impingement ratios shows approximately the same sensitivity to increases in jet-shifting angle which is different than the results of the vertical jet offset measurements. The vertical jet offset results showed decreasing reductions in SPL with increasing impingement ratio as the jets were more liable to tone generation as the offset ratio $\Delta y/z$ decreased. In the case of jet-shifting, the asymmetry is introduced using a difference not in vertical position of the jet, but in the jet inclination angle. Planar jets in the transition and self-similar regimes have been shown to grow linearly with increasing downstream distance by several authors such as Thomas & Goldschmidt (1986) and Deo (2005). Unlike vertical jet offset, where the amount of asymmetry is fixed and does not change with impingement ratio, in the case of jet-shifting, the amount of introduced asymmetry introduced grows linearly along with the velocity profile of the jet as the impingement ratio increases. Therefore, the resulting offset ratio introduced by jet shifting remains constant and is not a function of the impingement length z.

This result may be particularly useful for gas wiping as an industrial process since a given amount of asymmetry may be introduced by jet-shifting in order to suppress the formation of tones, and this asymmetry can be maintained regardless of the impingement ratio used. Manufacturers can set a given amount of jet-shifting required to suppress the tones, and if the impingement ratio must be adjusted during manufacturing, the jet inclination angle does need to be re-adjusted in order maintain the tone suppression. In the case of vertical jet offset, if the minimum offset was being utilized to suppress the formation of acoustic tones, and the impingement ratio was increased, the tones would re-appear. The jets would then have to re-adjusted to add additional jet offset in order to suppress the tones. Noise maps of the averaged overall sound pressure level and tone intensity as a function of jet-shifting angle for the three impingement ratios tested are given in Figure B-1 and Figure B-2 in Appendix B.

Chapter 8 – PROCESS OPTIMIZATION, DISCUSSION AND CONCLUSIONS

8.1 – PROCESS OPTIMIZATION

Measurements performed in the course of this study to characterize the gas wiping process, have been performed on scale model and due to differences in scaling, the measurements cannot be directly applied to the industrial process in their current state. In order to scale the measurements so that they could be applied and the noise maps could be used directly to reduce noise in the gas wiping process, measurements would have to be performed at each manufacturing facility to obtain the noise characteristics for the baseline configuration and then extract the scaling between the in-plant and in-lab measurements. It is believed that the trends in noise behavior for the various process parameters would be similar to those encountered in the lab environment. However, the overall levels and magnitudes would change due to differences in scale. The frequency of the acoustic tones would however, be accurately predicted by the expressions developed in the course of this study. In the subsequent process optimization section, it will be assumed that such measurements have been performed, and the noise maps have been scaled to match the industrial process. If such measurements are not performed, the general trends in behavior and overall behavior of the process observed in this study will still prove very useful in process optimization.

In order optimize the gas wiping process to reduce noise for a given process output at a given facility, a myriad of factors must be considered. The first and most important factor when evaluating noise in the workplace are local regulations and codes pertaining to noise and the weighting of acoustic tones with overall SPL. General industrial noise analysis typically uses some form of spectral weighting to account for the non-linear response of the human ear, typically A-weighting for lower amplitude noise (<85dB) and C-weighting for more intense noise (>85dB). Weighting functions could easily be applied to the spectra collected in the course of this study, however at present no weighting has been applied to any of these results.

For the vast majority of configurations in gas wiping, large amplitude discrete acoustic tones are present, in addition to the already significant broadband noise. Experimental studies by Cohen & Baumann (1964) and others on hearing loss due to acoustic tones has shown that strong acoustic tones poses a greater risk for hearing loss in humans compared to broadband noise of comparable levels. The impact of these acoustic tones on workers is subject to a variety of evaluation techniques, most of which add on an annoyance factor to the overall sound pressure level. In certain jurisdictions, industrial noise with acoustic tones above a certain threshold level are subject to constant annoyance factors being added to the overall sound pressure level. For instance, an audible tone of 10 decibels above broadband noise would be subject to an annoyance factor of 5 dB added to the overall sound pressure level. If the magnitude of the tone increased to 20 dB above broadband, the annoyance factor would remain 5 dB. Areas with more stringent noise regulations compensate for the strength of the tone relative to the broadband noise by adding an annoyance factor of some fraction of the tone intensity in decibels to the overall sound pressure level. As an example, adding on 1/3 of the tone intensity for the two cases outlined above would result in annoyance factors of 3.33 dB and 6.67 dB added to the overall sound pressure levels respectively.

Optimization of the gas wiping process for noise will have to be performed using local noise guidelines and regulations for each specific area. As an example of how the optimization process would be performed for a given gas wiping configuration, the results of the baseline configuration have been analyzed using an annoyance factor of 1/3 the tone intensity added to the averaged overall sound pressure level. Figure 8-1 and Figure 8-2 show the noise maps constructed for the baseline configuration of averaged overall sound pressure level and tone intensity respectively. Adding the annoyance factor to the averaged overall sound pressure map results in the perceived overall sound pressure level map of Figure 8-3. Using this perceived overall sound pressure map in conjunction with existing coating weight models such as those shown in Figure 8-4 provides a useful tool for process optimization.

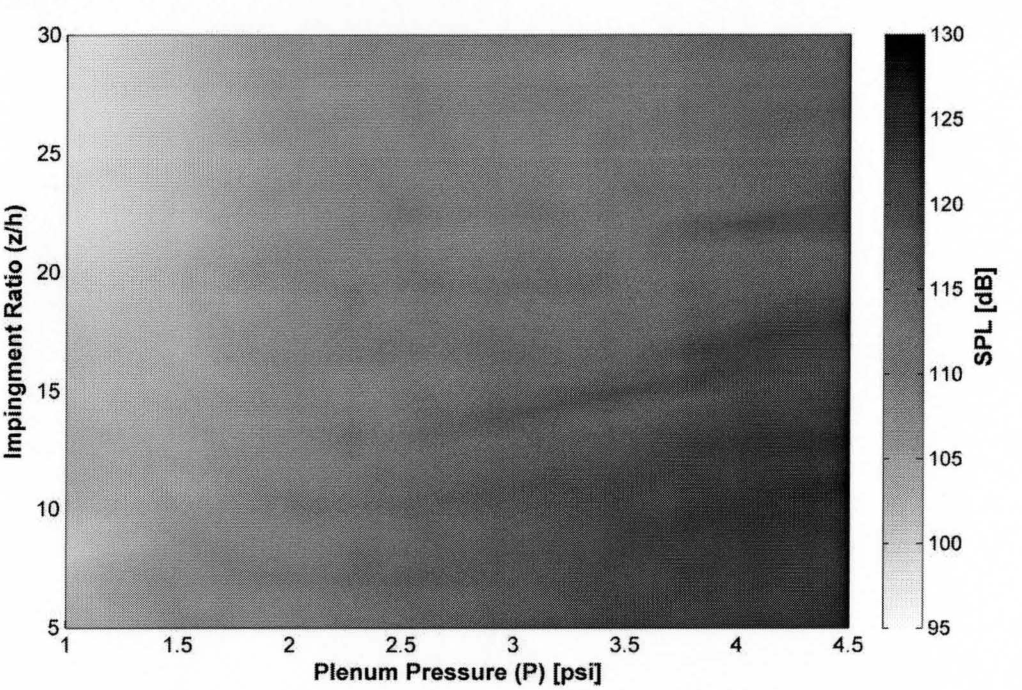

Figure 8-1: Noise map of averaged overall sound pressure level of baseline configuration.

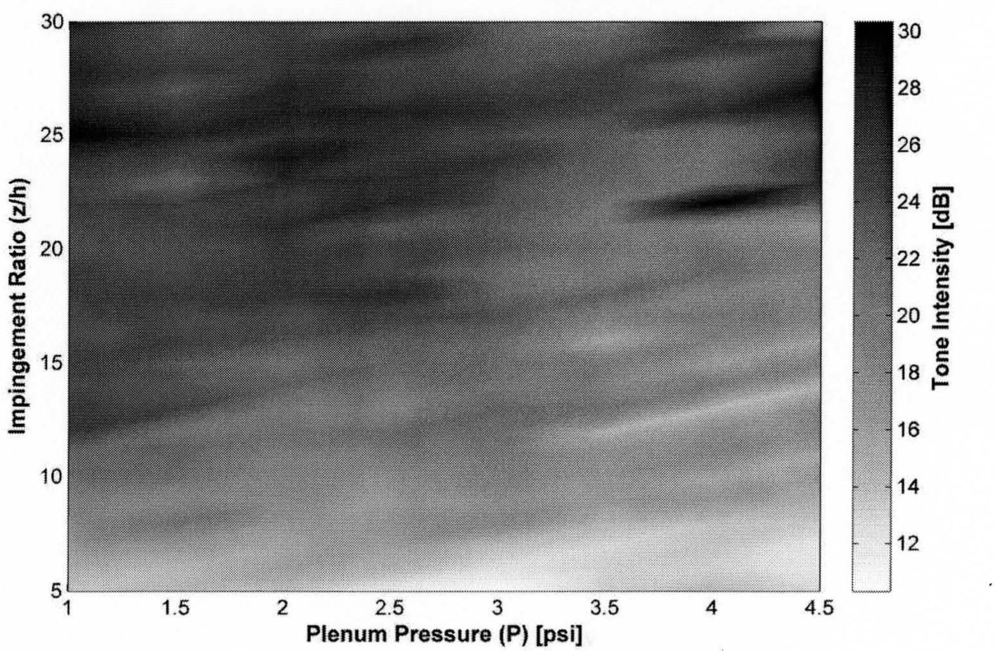

Figure 8-2: Noise map of tone intensity of baseline configuration.

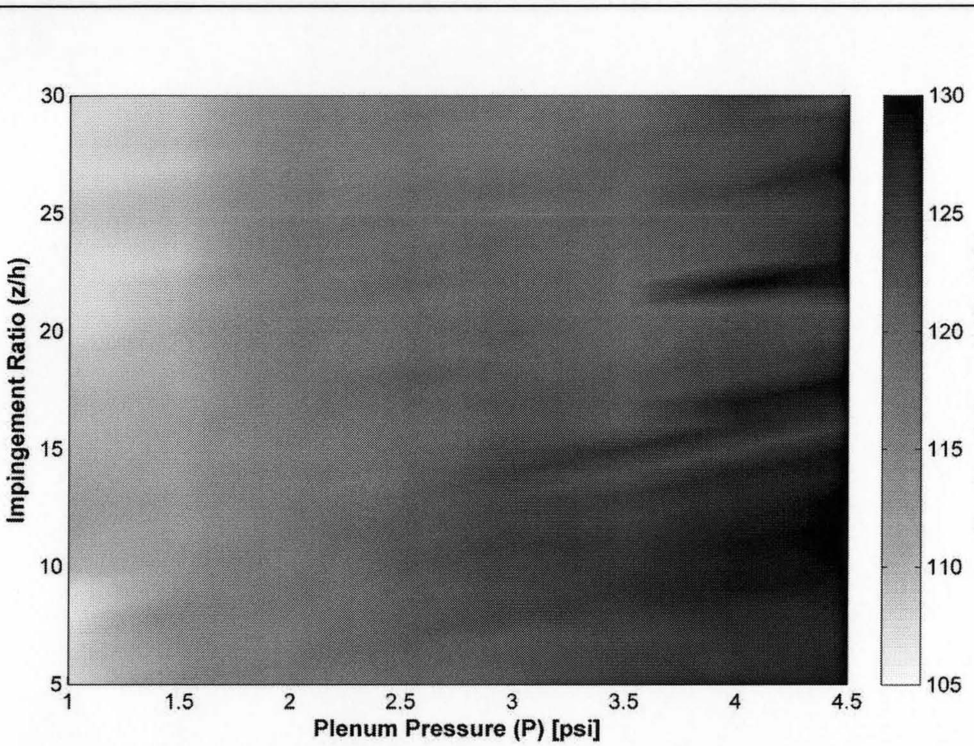

Figure 8-3: Noise map of perceived overall sound pressure level showing the combined effects of overall SPL and tone intensity (Factor of TI/3 used).

As an example, the perceived overall sound pressure level map has been overlaid with the coating weight map of Hrymak et al. (2004) in Figure 8-4 showing isocoating weight lines for a sheet speed of V_s = 2.0m/s. A simple visual inspection of this figure shows that depending on the coating weight of the desired product at a set line speed, any combination of impingement ratio and plenum pressure on the corresponding isocoating line can be utilized. Optimizing the process in this case would simply involve finding the location on the isocoating line for the particular sheet speed of interest where the perceived overall sound pressure is the lowest. In cases where the maximum line speed is restricted due to noise regulations, utilizing the perceived overall noise maps in conjunction with coating maps to optimize the process can result in increases in allowable sheet speed and overall productivity. If a maximum overall perceived SPL of

122 dB is permitted in the area of the zinc pot at a coating weight of W_c = 55 g/m^2, the perceived SPL map can be overlaid with isocoating lines for the target coating weight for varying line speeds. The configuration with the maximum line speed at the target coating weight and a perceived SPL of 122 dB can be found and this configuration can be used to maximize productivity. In cases where the gas wiping process is not the limiting factor affecting sheet speed, the noise maps can be used to achieve the lowest possible perceived sound pressure level for a given output.

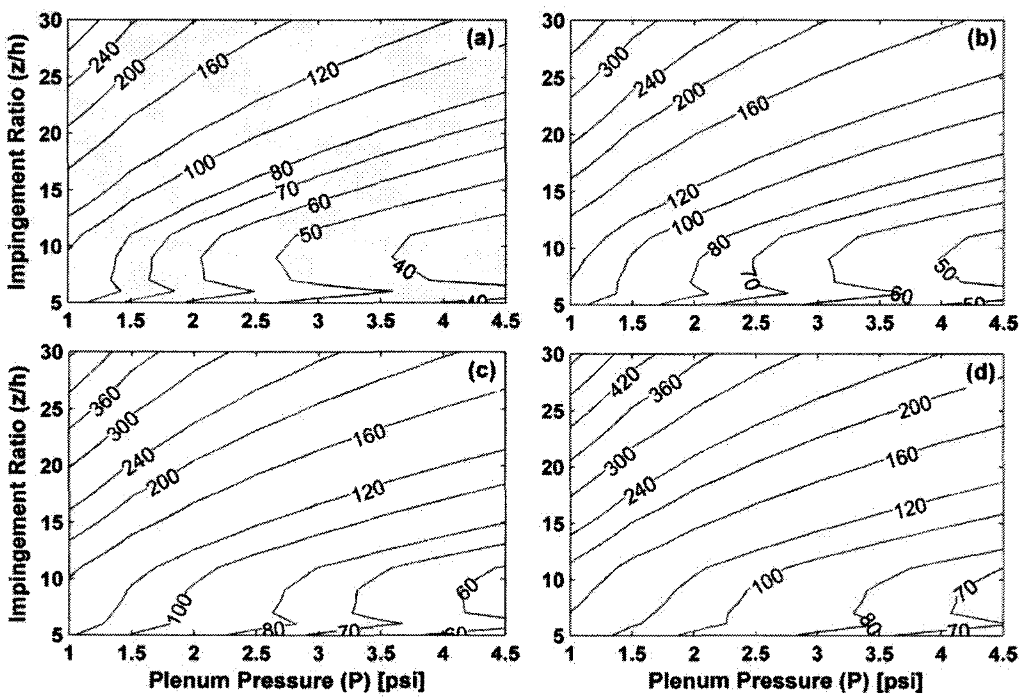

Figure 8-4: Coating weight model of Hrymak et al. (2004) showing isocoating lines for sheet speeds of V_s = 1.0 m/s (a), 1.5 m/s (b), 2.0 m/s (c) & 2.5 m/s (d).

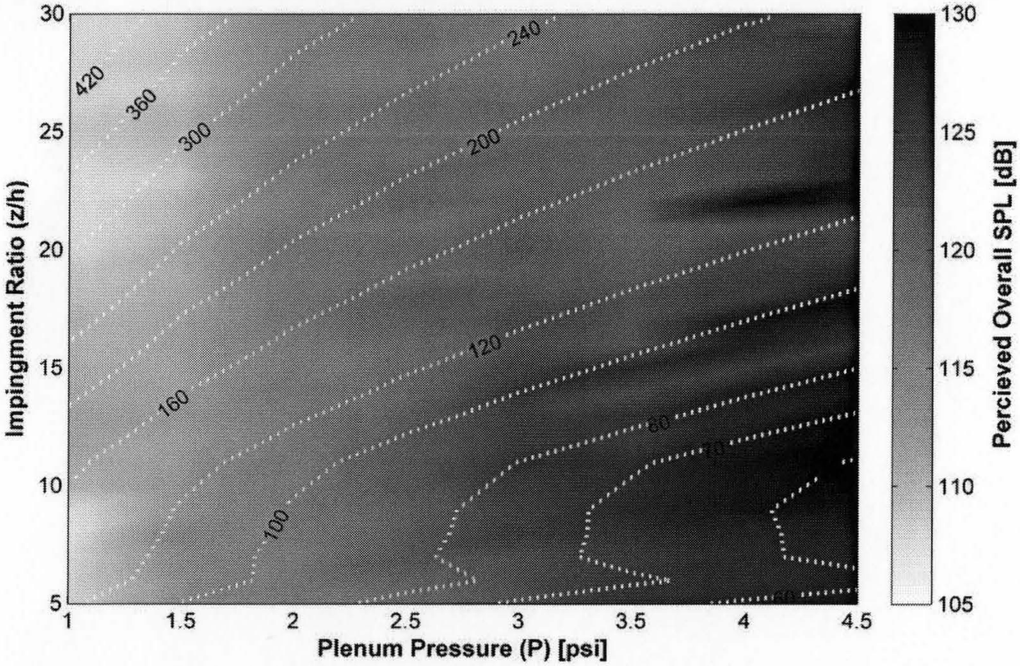

Figure 8-5: Noise map of perceived overall SPL combined with coating weight model of Hrymak et al. (2004) showing isocoating weight lines in g/m^2 for a sheet speed of V_s = 2.0 m/s.

8.2 – DISCUSSION AND CONCLUSIONS

An experimental study of noise generation in the gas wiping process has been carried out to understand the effect of the various process parameters on overall noise levels and the generation of discrete acoustic tones. A commonly used baseline gas wiping configuration was selected based on the input of industry experts and various manufacturers, to allow maximum applicability of experimental results to the industrial process. Utilizing the baseline configuration as reference point, the effect of plenum pressure and impingement ratio on the noise generated by gas wiping was investigated. Various acoustic modes of the originating from the jet-jet and jet-sheet regions were identified and semi-empirical models have been developed to accurately predict the frequency of these tones based on the process parameters used. In addition, noise maps of overall sound pressure level and tone intensity were constructed to aid manufacturers in optimizing this process to minimize noise production.

The effect of a plane jet impinging on a flat plate was also investigated in order to determine the location at which the two distinct acoustic tones (jet-sheet and jet-jet) were being generated as well as to separate any effects due to strip vibration and movement. A semi-empirical expression was developed to predict the frequency of the jet-plate tones based on the process parameters. A range of impingement ratios and jet velocities where this mode was susceptible to flow-excitation was identified. Noise maps documenting the overall sound pressure levels and tone intensities were also created to give a more complete overview of the behavior of the process.

The effect of plate inclination on the generation of this jet-plate tone was also examined. The tone was found to be more sensitive to span-wise inclination than to stream-wise inclination. Complete suppression was achieved for span-wise inclination of the plate of only $\kappa = 1.25°$, whereas a stream-wise inclination of $\zeta = 15°$ was required for complete suppression. This information will be useful in designing new baffle plate systems to combat jet-jet tone generation, while avoiding jet-plate modes resulting from the addition of edge baffles.

The sensitivity and effectiveness of more conventional edge baffle designs was also examined. Tests were performed for varying plenum pressure, impingement ratio and edge baffle distance for traditional flat edge baffle designs. It was found that in order to be effective in reducing overall sound pressure levels and suppressing jet-jet acoustic tones, the edge baffles must be placed within 3mm of the sheet edge. At higher plenum pressures, traditional edge baffle configurations were susceptible to the formation of jet-plate tones, which would negate any benefit of eliminating jet-jet tones. Noise maps of edge baffle effectiveness showing overall sound pressure levels and tone intensity were also constructed.

The effect of jet inclination in gas wiping was also investigated, with experimental tests being performed for inclination angle varying between $\alpha = 0°$ and $\alpha = 12°$ at a constant plenum pressure of $P = 2.5$ psi. Inclination angle was found to have a relatively modest effect on overall sound pressure levels and tone intensities as shown by the noise maps; however, jet inclination was demonstrated to be an effective technique for reducing or eliminating the formation of jet-plate acoustic tones. This suggests that adding inclination angle to gas wiping configurations with higher plenum pressures or the presence edge baffles may have a greater potential for reductions in noise, although more testing is required to confirm this hypothesis.

The effect of jet incidence asymmetry was also investigated in the form of vertical jet offset and jet-shifting. Both types of asymmetry were found to be relatively ineffective in reducing overall noise levels; however they had a large effect on reducing tone generation, which would lower perceived sound pressure levels. Jet-shifting was also found to be very effective in reducing tone intensities for relatively minor jet-shifting angles. It is acknowledged that these techniques cannot be used in every production case, due to potential coating quality issues however, in most cases the asymmetry required for large tone intensity reductions is quite small from a production standpoint.

Finally, process optimization was briefly discussed. Because this research was performed on behalf of an internationally based industry consortium, it does not make sense to apply noise regulations of any particular jurisdiction, but rather present the data in its raw form, so that it can be utilized wherever needed at the different manufacturing facilities.

8.3 – SUGGESTIONS FOR FUTURE WORK

Noise generation in the gas wiping process is a large and multifaceted problem with a myriad of process parameters and implications in coating performance which must be considered. This study is the first which has attempted to characterize the noise in the gas wiping process as a function of the different process parameters and give manufacturers and process engineers a broad overview of the behavior of the process. There is still considerable work which can be done before a complete understanding of the process is achieved. Investigations involving combinations of parameters, such as the effect of combining edge baffles and jet inclination used in conjunction would add understanding of the process and offer opportunities for further noise reductions and process optimization. Additionally, the range of parameters tested could be expanded, and passive countermeasures such as edge baffles could be further refined using the results of this study. An experimental study which includes the effects of process parameters both on the noise generation as well as the coating quality would be optimal; however such an experimental setup would be costly and complex.

REFERENCES

Cohen, H., & Baumann, K. C. (1964). Temporary Hearing Losses Following Exposure to Pronounced Single-Frequency Components in Broadband Noise. *The Journal of the Acoustical Society of America*, *36* (6), 1167-1175.

Deo, R. C. (2005). *Experimental Investigations of the Influence of Reynolds Number and Boundary Conditions on a Plane Air Jet.* Department of Mechanical Engineering. University of Adelaide.

Dubois, M. (2001). Characterization of noise generated by gas wiping - Part 1. *Galvanizers Meeting - 2001.* ILZRO.

Dubois, M. (2001). Characterization of noise generated by gas wiping - part 2. *Galvanizers meeting - 2001.* ILZRO.

Dubois, M., Riethmuller, M. L., Buchlin, J.-M., & Arnalsteen, M. (1995). The gas wiping jet limit: the splashing pheonomenon. *Galvatech '95 Conference Proceedings*, (pp. 667-673).

Ellen, C. H., & Tu, C. V. (1984). An analysis of jet stripping of liquid coatings. *Journal of Fluids Engineering*, *106*, 399-404.

Everitt, K. W., & Robins, A. G. (1978). The Development and Structure of Turbulent Plane Jets. *Journal of Fluid Mechanics*, *88*, 563-583.

Gaignard, S., & Dubois, M. (2004). Characterization of strip vibration at the wiping nozzles. *Proceedings of Galvatech '04.*

Goldschmidt, V. W., & Bradshaw, P. (1973). Flapping of a Plane Jet. *The Physics of Fluids*, *16* (3), 354-355.

Gutmark, E., & Wygnanski, I. (1976). The Planar Turbulent Jet. *Journal of Fluid Mechanics*, *73*, 465-495.

Ho, C., & Nosseir, N. S. (1982). Dynamics of an Impinging Jet. Part 2. The Noise Generation. *Journal of Fluid Mechanics*, *116*, 379-391.

Ho, C., & Nosseir, N. S. (1981). Dynamics of an Impinging Jet. Part1. The Feedback Phenomenon. *Journal of Fluid Mechanics*, *105*, 119-142.

Hodgson, M., & Warnock, A. (1992). Noise in Rooms. In L. L. Bernanek, & I. L. Ver (Eds.), *Noise and Vibration Control Engineering: Principles and Applications* (pp. 175-202). Jon Wiley & Sons, Ltd.

Hrymak, A. N., Elsadaawy, E. A., Hanumanth, G., McDermid, J. R., & Goodwin, F. E. (2005). Air knife coating weight models. *AISTech 2005 Conference Proceedings, II*, pp. 393-401.

Hrymak, A. N., Forbes, J. F., Elsaadawy, E., Balthazaar, A., Hu, Q., & Knight, J. (2004). *ZCO-2-3: Improving Coating Weight Consistency. Final Report.* McMaster University & University of Alberta.

Hrymak, A. N., Forbes, J. F., Knight, J., Elsadaawy, E., Balthazaar, A., & Sheng, Y. (2002). Air Knife Coating in Hot-dip Galvanizing. *44th MWSP Conference Proceedings , XL*, 853-861.

Marder, A. R. (2000). The metallurgy of zinc coated steel. *Progress in Materials Science , 45*, 191-277.

Maurel, S., & Solliec, C. (2001). A Turbulent Plane Jet Impinging Nearby and Far From a Flat Plate. *Experiments in Fluids , 31*, 687-696.

Nosseir, N. S., & Behar, S. (1986). The Flowfield of a Side-dump Combustor. *AIAA Journal , 24*, 1752-1757.

Nosseir, N. S., Peled, U., & Hildebrand, G. (1987). Pressure Field Generated by Jet-on-Jet Impingement. *AIAA Journal , 25* (10), 1312-1317.

Ontario Regulation 565/06. (2007, Decemeber 16, 2006). Retrieved August 25, 2007, from www.e-laws.gov.on.ca: http://www.e-laws.gov.on.ca/html/source/regs/english/2006/elaws_src_regs_R06565_e.htm

Park, J. L. (2001). Noise, edge over-coating and edge buildup phonomenon associated with gas wiping in continoius hot dip galvanization. *Ironmaking and Steelmaking , 28*, 53-57.

Pavageau, M., Loubiere, K., & Gupta, S. (2006). Automatic Eduction and Statistical Analysis of Coherent Structures in the Wall Region of a Confined Plane Turbulent Impinging Jet. *Experiments in Fluids , 41*, 35-55.

Petrie, A. M. (1974). An Experimental Investigation of the Noise Produced by Air Jet Impingement on Flat Plates. *Applied Acoustics , 7*, 117-126.

Powell, A. (1960). Aerodynamic Noise and the Plane Boundary. *Journal of the Acoustical Socoety of America , 32*, 982-990.

Rockwell, D., & Naudascher, E. (1979). Self-Sustained Oscillations of Impinging Free Shear Layers. *Annual Review of Fluid Mechanics , 11*, 67-94.

Sakakibara, J., Hishida, K., & Phillips, W. R. (2001). On the Vortical Structure in a Plane Impinging Jet. *Journal of Fluid Mechanics , 434*, 273-300.

Thomas, F. O., & Goldschmidt, V. W. (1986). Structural Characteristics of a Developing Turbulent Planar Jet. *Journal of Fluid Mechanics*, *163*, 227-256.

Thorton, J. A., & Graff, H. F. (1976). An analytical description of the jet finishing process on hot-dip metallic coatings on a strip. *Metalugical Transactions B*, *7B*, 607-618.

Tu, C. V. (1995). Impingement of a plane turbulent jet and application in industrial coating control. *Ph. D. Thesis*. Department of Mechanical Enginnering, University of Newcastle.

Tu, C. V., & Wood, D. H. (1996). Wall presssure and shear stress measurements beneath an impinging jet. *Experimental Thermal and Fluid Science*, *13*, 364-373.

Varieras, D., Brancher, P., & Giovannini, A. (2007). Self-Sustained Oscillations of a Confined Impinging Jet. *Flow, Turbulence and Combustion*, *78*, 1-15.

Ziada, S. (1995). Feedback Control of Globally Unstable Flows: Impinging Shear Flows. *Journal of Fluids and Structures*, *9*, 907-923.

APPENDIX A – EQUIPMENT SPECIFICATIONS

SONIC AIR SYSTEMS 700 SERIES BLOWER SPECIFICATIONS

SONIC AIR SYSTEMS

Component Specification Sheet

- Sonic 70 Blower -

Interface Dimensions

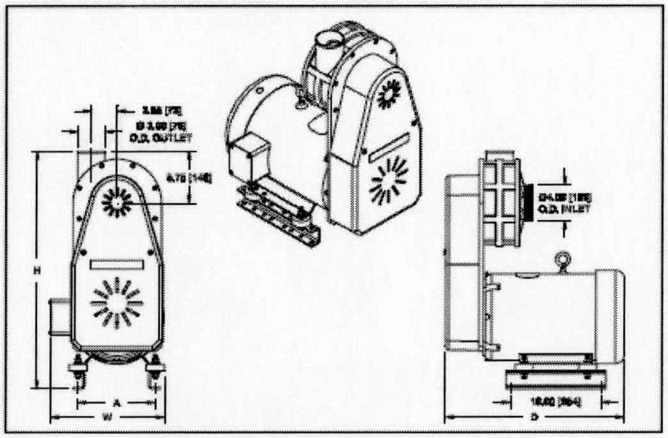

Component Specifications

Description	Blower – Sonic 70				Blower –Sonic 70 Water Cooled			
Sonic P/N	19108	19123	19135	19150	19162	19177	19189	19204
Output Flow Rate	50 cfm (24 lps) to 700 cfm (331 lps)				50 cfm (24 lps) to 700 cfm (331 lps)			
Ambient Temperature	10°F (-12°C) to 105°F (40°C)				10°F (-12°C) to 105°F (40°C)			
Air Temperature Range	< 125°F (52°C)				125°F (52°C) to 400°F (205°C)			
Motors Available	3 Hp	5 Hp	7.5 Hp	10 Hp	3 Hp	5 Hp	7.5 Hp	10 Hp
Width (W)	11.00 in (280 mm)	11.00 in (280 mm)	11.00 in (280 mm)	12.50 in (318 mm)	11.00 in (280 mm)	11.00 in (280 mm)	11.00 in (280 mm)	12.50 in (318 mm)
Depth (D)	16.56 in (421 mm)	18.0 in (458 mm)	19.63 in (499 mm)	21.00 in (534 mm)	16.56 in (421 mm)	18.0 in (458 mm)	19.63 in (499 mm)	21.00 in (534 mm)
Height (H)	25.0 in (635 mm)	25.0 in (635 mm)	25.0 in (635 mm)	25.56 in (650 mm)	25.0 in (635 mm)	25.0 in (635 mm)	25.0 in (635 mm)	25.56 in (650 mm)
Mounting Pattern (A)	7.5 in (191 mm)	7.5 in (191 mm)	7.5 in (191 mm)	8.5 in (216 mm)	7.5 in (191 mm)	7.5 in (191 mm)	7.5 in (191 mm)	8.5 in (216 mm)
Approximate Weight	103 lbs (46.8 kg)	119 lbs (54.1 kg)	133 lbs (60.5 kg)	161 lbs (73.2 kg)	103 lbs (46.8 kg)	119 lbs (54.1 kg)	133 lbs (60.5 kg)	161 lbs (73.2 kg)
Replacement Belt P/N								
Pulley 1.50 to 2.10 Diameter	12235	12235	12235	12235	12235	12235	12235	12235
Pulley 2.20 and 2.70 Only	12626	12626	12626	12626	12626	12626	12626	12626

Figure A-1: Specifications for Sonic Air Systems 700 series blowers. (http://www.sonicairsystems.com/spec-sheets/S18D%20-%20Sonic%2070.pdf)

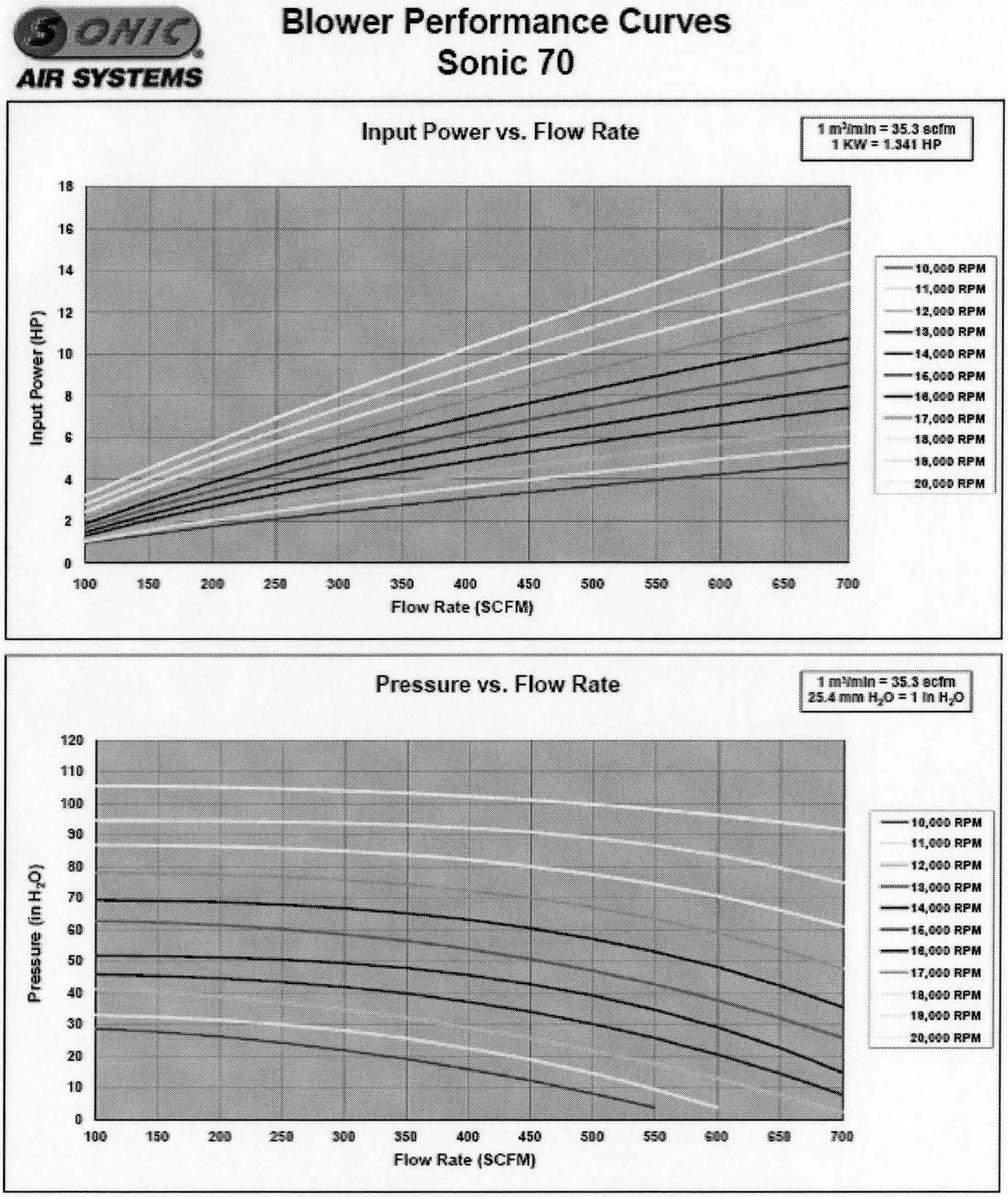

Figure A-2: Blower systems curves for Sonic Air Systems 700 Series blower. (Sonic Air Systems product support)

G.R.A.S. ½" PREAMPLIFIER - TYPE 26CA

Frequency response (cable load 4.7 nF):
2 Hz - 200 kHz .... ±0.2 dB

Input impedance:
20 GΩ, 0.4 pF

Output impedance (Cs = 20 pF, f=1000Hz):
<50 Ω

Noise (measured with 20 pF ½-inch dummy mic.):
A-weighted: ≤2.2 µV rms
(typically 1.8 µV rms)
Linear (20 Hz - 20 kHz): .... ≤6 µV rms
(typically 3.5 µV rms)

Gain:
Typically: .... -0.25 dB

Power-supply:
2 mA to 20 mA (typically 4 mA)

Maximum signal-output voltage (peak):
±8.0 V

Temperature:
Operation: .... -30°C to +70°C
Storage: .... -40°C to +85°C

Relative humidity:
Operation: .... 0 to 95%
Storage: .... 0 to 95%

Connector type:
BNC

Dimensions and weight:
Diameter: 12.7 mm (½-inch)
Length: .... 73 mm (2.9 inches)
Weight: .... 26 g (0.9 oz)

Figure A-3: Specifications for G.R.A.S. Type 26CA ½" preamplifier. (http://www.grasinfo.dk/documents/pd_26CA_ver_28_06_06.PDF)

G.R.A.S. ½" PREPOLARIZED PRESSURE MICROPHONE – TYPE 40AD

Frequency response:
3.15 Hz - 10 kHz: ±2.0 dB
12.5 Hz - 7.5 kHz: +1.0 dB

Nominal sensitivity:
at 250 Hz: 50 mV/Pa

Polarization voltage:
0 V

Temperature coefficient (250 Hz):
−10 °C to +50 °C: −0.01 dB/°C

Static-pressure coefficient:
250 Hz/25 °C: −0.01 dB/kPa

Humidity range:
0 - 100 % (non-condensing)

Influence of humidity (250 Hz):
<0.1 dB (0 - 100 % RH)

Influence of axial vibration, 1 m/s²:
62 dB re. 20 µPa

Venting:
Rear vented

IEC 1094-4 type designation:
W2SP

Upper limit of dynamic range:
3% distortion: 148 dB re. 20 µPa

Lower limit of dynamic range:
Thermal noise: 16 dB re. 20 µPa

Capacitance:
Polarized: 20 pF

Temperature range:
−40 °C to +120 °C

Dimensions (with protection grid):
Length: 16.2 mm
Diameter: 13.2 mm

(without protection grid):
Length: 15.3 mm
Diameter: 12.7 mm

Diameter (diaphragm ring):
12.1 mm

Threads:
Protection Grid: 12.7 mm - 60 UNS
Preamplifier Mounting: 11.7 mm - 60 UNS

Weight:
9 gm

Figure A-4: Specifications of G.R.A.S. Type 40AD ½" microphone. (http://www.grasinfo.dk/documents/pd_40AD_ver_28_06_06.PDF)

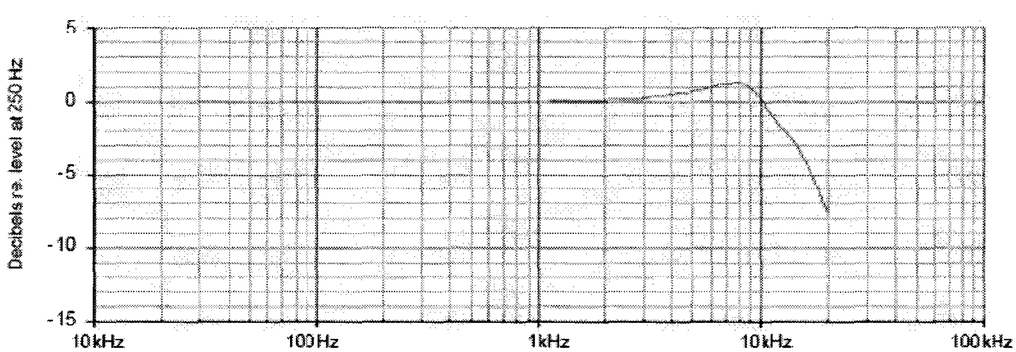

Figure A-5: Frequency response plot of G.R.A.S. Type 40AD ½" microphone. (http://www.grasinfo.dk/documents/pd_40AD_ver_28_06_06.PDF)

G.R.A.S. Sound Calibrator – Type 42AB

Output signal:
Specified on the calibrator for reference conditions.

Reference conditions:
Ambient temperature: .... 20 °C
Ambient pressure: .... 101.3 kPa
Humidity: .... 65% RH
Effective load volume: .... 250 mm³

Accuracy:
SPL: .... 114 dB ±0.2 dB re. 20 μPa
Frequency: .... 1000 Hz ±0.2%
Complies with IEC 942-1988 Class 1.

General:
Typical sensitivity to change in load
volume: .... 0.0003 dB/mm³ at 1000 Hz
Time for level to stabilize: .... max. 2 sec.

Microphone sizes:
According to IEC 1094-4
With adapters removed: 1-inch
With adapter(s): .... ½-inch and ¼-inch

Harmonic distortion:
Maximum: 1%

Controls:
Push-button start. Automatic switch-off.

CE classification:
EMC: .... EN 50081-1, EN 50082-1
Safety: .... EN 61010-1, 1993
For portable equipment, pollution category 2.

Ambient requirements for specified operation:
Temperature: .... −10 °C to +50 °C
Ambient pressure: .... 65 kPa to 108 kPa
Humidity: .... 10% to 90% RH

Battery:
Type: .... 6LR61, 9 V
Life: .... ≈ 30 hours
Battery type 6F22G has a shorter life, whereas a 9 V lithium battery gives an extended operating time.

External supply voltage:
7.5 V to 15 V
Automatic shut-off when voltage drops below 7.5 V

Overall weight and dimensions:
Weight: .... 185 gm with battery
Length: .... 109.5 mm
Diameter: .... 40 mm

Accessories included:
Delivered fitted with a removable adapter for calibrating ½-inch microphones. Remove this for calibrating 1-inch microphones.
Adapter for ¼-inch microphones: RA0049
9 V alkaline battery: EL0003

Accessories available:
Adapter for ⅛-inch microphones: RA0069

Figure A-6: Specifications of G.R.A.S. Type 42AB sound calibrator. (http://www.grasinfo.dk/documents/pd_42AB_ver_08_07_02.PDF)

ROXUL® ENERWARP 80 – ACOUSTICAL PERFORMANCE

Acoustical Performance:

ASTM C 423 CO-EFFICIENTS AT FREQUENCIES							
Thickness	125 Hz	250 Hz	500 Hz	1000 Hz	2000 Hz	4000 Hz	NRC
1.5"	0.17	0.53	1.06	1.07	1.00	0.99	0.95
2.0"	0.39	0.84	1.08	1.01	1.02	1.01	1.00
3.0"	0.68	0.92	1.08	1.03	1.03	1.03	1.00
4.0"	1.00	0.95	1.06	1.04	1.06	1.08	1.05

Figure A-7: Acoustical performance of mineral fiber insulation used in the acoustic baffling system. (http://www.roxul.com/graphics/RX-NA/Canada/products/AFB/AFB-6-1-07.pdf)

APPENDIX B – ADDITIONAL RESULTS

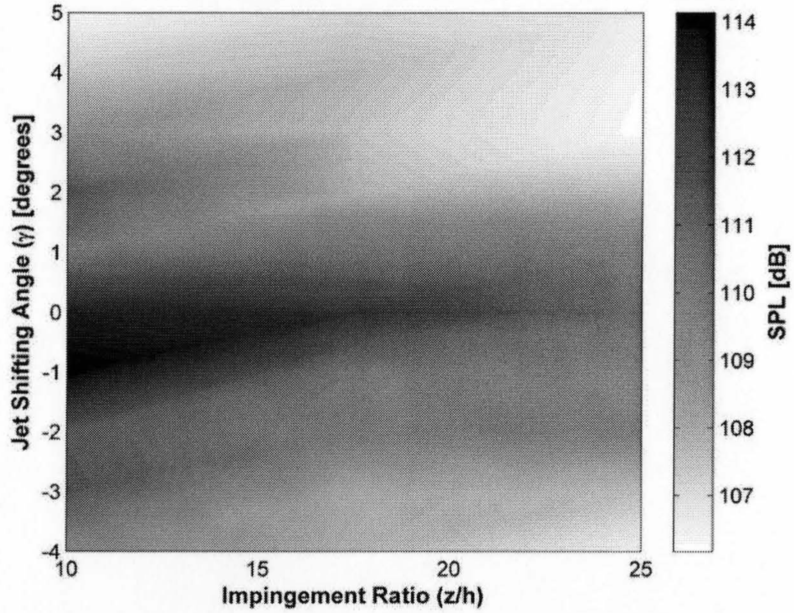

Figure B-1: Averaged overall SPL for jet-jet impingement as a function of impingement ratio and jet shifting angle, γ.

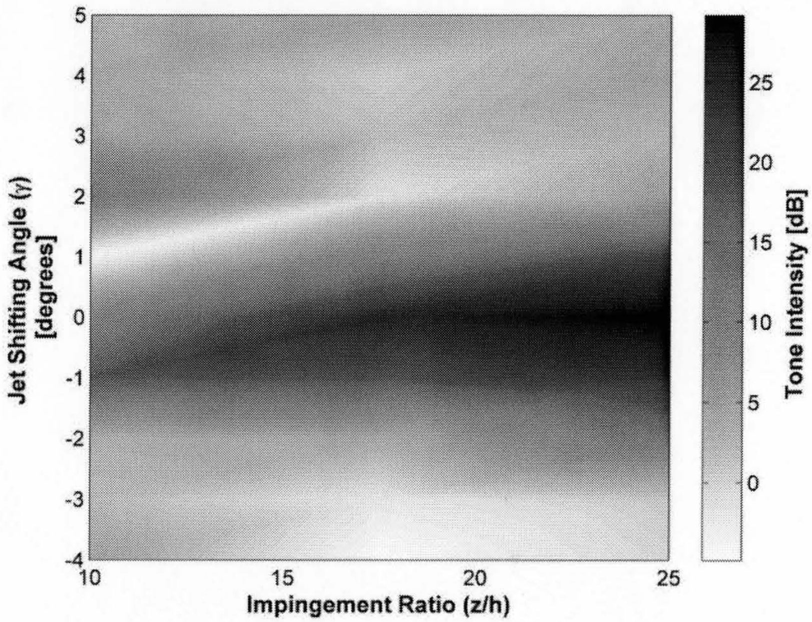

Figure B-2: Tone intensity for jet-jet impingement as a function of impingement ratio and jet shifting angle γ.